Vaccine responses in the context of impaired self-tolerance

HARVARD UNIVERSITY
Graduate School of Arts and Sciences

DISSERTATION ACCEPTANCE CERTIFICATE

The undersigned, appointed by the

Division of Medical Sciences

Committee on Virology

have examined a dissertation entitled

Vaccine responses in the context of impaired self-tolerance

presented by Marshall Emmanuel Karpel

candidate for the degree of Doctor of Philosophy and hereby certify that it is worthy of acceptance.

Signature: Benjamin Gewurz
Benjamin Gewurz (Apr 30, 2021 09:09 EDT)

Typed Name: Dr. Benjamin Gewurz

Signature: Todd Allen

Typed Name: Dr. Todd Allen

Signature: Michael Carroll
Michael Carroll (Apr 30, 2021 10:45 EDT)

Typed Name: Dr. Michael Carroll

Signature: Ann Rothstein

Typed Name: Dr. Ann Rothstein

Date: April 29, 2021

Vaccine responses in the context of impaired self-tolerance

A dissertation presented

by

Marshall Emmanuel Karpel

to

The Division of Medical Science

in partial fulfillment of the requirements

for the degree of

Doctor of Philosophy

in the subject of

Virology

Harvard University

Cambridge, Massachusetts

April 2021

Dissertation Advisor: Dr. Shiv Pillai Marshall Emmanuel Karpel

Vaccine responses in the context of impaired self-tolerance

ABSTRACT

In the context of HIV vaccine design, broadly-neutralizing antibodies (bnAbs) are those which are able to neutralize a diverse population of HIV variants. The existing global diversity of HIV necessitates that any traditional vaccine intending to generate humoral immunity must elicit these bnAbs, making them an important metric in the development of HIV vaccine design strategies. BnAbs have not, to date, ever been isolated from an individual following an HIV vaccine trial. As a group, bnAbs have been shown to exhibit a number of unusual traits, including poly- and auto-reactivity, as well as a years-long delay in development, when they arise during persistent HIV infection at all.

Interestingly, persistent HIV infection can erode self-tolerance, permitting the production of autoreactive antibodies. Conversely, when autoreactive bnAbs are expressed in mouse models, they are usually constrained by immune tolerance. To establish if the erosion of self-tolerance and the development of autoreactive bnAbs were related, we utilized immunogens that had been rationally designed to stimulate VRC01-like bnAb precursor B cell receptors (BCRs), mice that featured VRC01-like precursor BCRs, and Lymphocytic choriomeningitis mammarenavirus (LCMV), a paradigmatic model of persistent viral infection that impairs humoral self-tolerance. Here, we demonstrate that impaired self-tolerance does not permit the development of

greater neutralization breadth. During these experiments, an unexpectedly lethal phenotype developed in the experimental animals. We identified two elements which mediated the effect: an adjuvant, and the BCR expressed in the mice. The latter was a variation of a bnAb-precursor not previously thought to be constrained by tolerance, though our data suggest that the effect was antibody-mediated.

Lastly, we utilized the antigen-specificity of the same mouse model to assess the transcriptome of naïve, germinal center, memory, and antibody-secreting B cells, before pairing that dataset with a transcriptomic and proteomic analysis of the same B cell populations in humans. This permitted hypothesis-generating comparisons between molecule types, cells, and species. We were able to identify specific hits that are both meaningful and feasible to follow up on, as well as unexpected trends, including the unusual association between memory B cells and gene ontology terms associated with neuronal development.

TABLE OF CONTENTS

ACKNOWLEDGEMENTS

Having worked in research settings for the better part of a decade before starting graduate school, I thought I had learned most of what I needed to know to navigate an independent research project. As it turns out, navigating grad school isn't the same thing at all. If it weren't for a handful of mentors, a bunch of friends, and an army of collaborators, this work would not exist.

First and foremost, thank you to my mentors, Drs. Pillai, Gewurz, and Allen. Roughly five years ago, Dr. Shiv Pillai, an immunologist's immunologist, agreed to take in a virology student who had an inexplicable interest in B cell biology and a tendency to never let well enough alone. I haven't been an easy student to mentor, and Dr. Pillai deserves particular acknowledgement for his patience, understanding, patience, wisdom, and patience. He never once forbade me from performing an experiment if the result would be interesting, even if he firmly disagreed with its premise. "Do the experiment!" is as close to a professional mantra as I have, and I'll always hear it in Shiv's voice. That being said, Shiv at least had an excuse: I applied to his lab. Dr. Ben Gewurz, on the other hand, volunteered out of the blue to join my Dissertation Advisory Committee, more or less on the basis of "B cells? That sounds interesting, may I join?" Later assuming the position of Chair of my DAC, he has gently (and diplomatically) guided me around the few potholes I've encountered during grad school, and has always done so with kindness and good grace, even when they were potholes of my own making. None of those potholes would have existed, however, if it weren't for Dr. Todd Allen, who made an offhand comment, several months after I was hired to work in his lab, that began a Rube-Goldberg-like series of events that culminated in my applying

to grad school. I had been assigned the task of sequencing BCRs in B cells of humanized mice, and so I asked him to explain a particular aspect of B cell biology. He did, but then said, “You know, though, the idea is that *you’re* going to be the B cell expert soon and that *I’ll* be asking the questions.” This one remark changed how I thought of the relationship between myself and my work. High expectations are a mark of respect and a gift, and Todd’s aimed me firmly at graduate school.

Once I got there, I was lucky enough to find a number of others who helped advise me along the way. Thank you to Maria Bollinger for bushwhacking a path for me through red tape, paperwork, and, on one memorable occasion, a Harvard website that was malfunctioning after running new software and that would otherwise have prevented me from graduating. Thank you to the other members of my DAC: Dr. Arlene Sharpe, Dr. Alex Balazs, and Dr. Daniel Lingwood. Your advice and feedback were crucial to shaping how and when I switched back and forth between my various topics.

Because of the nature of the projects I chose to work on, this dissertation represents a mostly solitary enterprise, removed from the major ongoing projects within the Pillai Lab. Of course, it’s always the exceptions that prove the rule. Exceptions like Dr. Vinay Mahajan, who introduced me to Unix and allowed me to carve out a small portion of computational space to call my own in the O2 cluster; or like Dr. Kelsey Finn, who bled a ludicrous 120 mice, not once, or twice, but several times. Her contribution can’t be overstated; I loathed this aspect of the work, and these days were indubitably my worst in grad school. Thank you. And thank you to those who provided their expertise, like the MGH Histopathology Research Core, who essentially took me on as a trainee for a year, and the Ragon Flow Cytometry Core, without whom most of the

work could not have happened. That I was lucky enough to get this far in grad school without having the flow sorter break in the middle of a 4 a.m. flow sort is a testament to how well they maintain their instruments.

Thank you very much to those who contributed indirectly to the completion of this work. I was lucky enough to have three taskmasters: Dr. Rawlings, Dr. Liu, and Catherine Baron, Esq. Their motivational efforts were profoundly helpful.

However, no one contributed more to the completion of this work than my partner, Gray. Armed with patience, understanding, and a Master's degree in Library Science, she's been an invaluable research collaborator: editing, spreadsheeting, hunting down references, spotting typos, and more. She did it all, as she always does. Thank you.

Last, but not least, I would like to thank my family. I was probably as easy to raise as a child as I have been to mentor as a graduate student, so for their everlasting patience, generosity, and caring, my parents (and sister) deserve all the praise in the world. In the quotation below, from a charming work of fiction, a mother is chatting with her partner as they watch their six-year-old son begin to assert his independence. She begins with an anecdote about growing up with her own father.

> "…we made model gliders together. Two things were required to get them to fly. First we had to give them a running start. Then we had to let them go." She sighed. "Learning just when to let go was the hardest part."[1]

Thank you for the perfect launch.

DEDICATION

This work is dedicated to my breath of fresh air.

GLOSSARY OF TERMS

AIDS: acquired immunodeficiency syndrome
ASC: antibody-secreting cell
AUC: area under the curve
B6: murine model C56BL/6
BCR: B cell receptor
BnAbs: broadly-neutralizing antibodies
CD4bs: cluster of differentiation 4 binding site
CDR: complementarity-determining regions
CDR3: third complementarity-determining region
CDRL1: first light chain complementarity-determining region
CSR: class-switch recombination
DPI: days post-injection
EAE: experimental autoimmune encephalomyelitis
eOD: engineered outer domain
ES: embryonic stem
Fab: antigen-binding fragment
FACS: fluorescence assisted cell sorting
FDC: follicular dendritic cell
FMO: fluorescence minus one
GBM: glomerular basement membrane
GC: germinal center
HAART: highly active antiretroviral therapy
HIV: human immunodeficiency virus
ID: incidence density
ID50: half maximal inhibitory dilution
IGV: integrated genomics viewer
IP: intraperitoneal
LCMV: lymphocytic choriomeningitis mammarenavirus
MBC: memory B cell
MFI: mean fluorescence intensity
MPER: membrane proximal external region
NP: nitrophenyl
RDBC: Rag2-deficient blastocyte complementation
SAS: Sigma Adjuvant System
SEC: size exclusion chromatography
SHM: somatic hypermutation
SLE: systemic lupus erythematosus
SLO: secondary lymphoid organs
T/F: transmitted/founder
TLR: toll-like receptor
UCA: unmutated common ancestor
VL: viral load
VRC: Vaccine Research Center, National Institute of Allergy and Infectious Diseases
WPI: weeks post-infection

DIAGRAMS, FIGURES, and TABLES

CHAPTER 1: INTRODUCTION

Overview

This dissertation describes research that explored two broad topics of relevance to vaccine immunology. The first topic pertains to the difficulty in developing vaccine-induced bnAbs against human immunodeficiency virus (HIV), while the second addresses the fundamental nature of memory B cells. Chapter 1 introduces concepts and literature that form the basis of the hypotheses explored in this work, as well as explaining key developments in the field that shaped the work itself. The first section of chapter 1 introduces the virology, immunology, and vaccinology relevant to this work, while the second section of chapter 1 introduces the complexity of B cell development and memory B cell characterization. Chapter 2 presents data collected while investigating whether impaired immune tolerance, arising from persistent viral infection, permits the production of autoreactive bnAbs. Chapter 3 presents data from a stepwise immunization experiment intended to test the function of novel immunogens, as well as data collected after the discovered of an unexpected immune response to the immunizations. Chapter 4 reports the findings of an observational study of memory B cells in both humans and mice, consisting of both transcriptomic and proteomic analyses. Chapter 5 discusses the limitations, alternative interpretations, and possible future work of each chapter, as well as the broad caveats and implications of the data as a whole.

Section I: HIV

1.1.1 Virology and pathogenesis of HIV

HIV-1 is a retrovirus that infects human CD4+ T cells, causing immune dysregulation and dysfunction, eventually culminating in acquired immunodeficiency syndrome (AIDS). HIV can be transmitted by bodily fluids such as semen, vaginal fluids, blood, and breastmilk, and as such is often a sexually transmitted infection, with infections taking place at various mucus membranes. As a retrovirus, its genome is made up of RNA, which is retrotranscribed to DNA and integrated into the host cell's genome as a necessary prelude to HIV replication. This integration step contributes significantly to the difficulty in eradicating HIV in infected individuals. Treatment with antiviral drugs capable of reducing plasma viral loads (VLs) to undetectable levels does not remove the infection entirely; integrated viral genomes present in latently infected T cells can serve as a reservoir for the emergence of new virus at a later date.

Acute infection is often characterized by flu-like symptoms, during which individuals display high VLs.[2] Within weeks, the progression of the immune response will dramatically lower the individual's VLs and symptoms, if any existed, will resolve.[3] Over time, as the virus further infects CD4+ helper T cells and the ability of the immune system to cope becomes impaired, CD4+ T cell counts begin to decrease and viral load begins to increase. Once an individual's CD4+ T cell count has been depressed below 200 cells/mm^3 of blood, they are said to have AIDS.[4] Death in individuals with AIDS is almost exclusively caused by opportunistic pathogens, and a typical time course for HIV infection is roughly ten years from acquisition to death.[5]

The virus itself is a small particle, roughly 120nm across, and consists of two copies of an RNA genome, an icosahedral capsid and a conical nucleocapsid, wrapped in an envelope derived from the host cell's plasma membrane.[6] The genome is roughly 10kb in size, and codes for 19 proteins across nine genes. Of note for this work are the proteins generated from the Env gene, which is translated as a 160kDa precursor known as gp160. Gp160 is cleaved by proteases to form gp120, a soluble attachment subunit, and gp41, a transmembrane subunit,[7,8] each of which function as non-covalently associated trimers in the eventual viral membrane. As the mediator of cellular attachment and entry, this spike protein has been the focus of considerable interest to the HIV vaccine field for decades, with a multitude of variations having been produced for research and vaccine purposes.

1.1.2 HIV vaccine progress

HIV vaccine development has not proceeded according to the same timeline as that of other vaccines. In the last decade alone, multiple vaccines have been generated against viruses within years of their emerging on the global stage, including Ebola, Zika, and SARS-CoV-2. But despite the tens of millions of deaths caused by HIV, effective vaccines have not yet been made.

There are a number of reasons why HIV vaccine design has proven so difficult. While too nuanced and numerous to meaningfully review here, the simplest pertain to viral diversity and the subsequent necessity for neutralization breadth. HIV mutates at an incredibly rapid rate; the average rate across the genome is approximately one mutation per 1700 bases, rising in hotspots to nearly one in 70.[9] While sexual

transmission of HIV typically imposes a profound bottleneck on viral diversity,[10,11] subsequent mutation during viral replication quickly restores diversity and creates a pool of viruses available to infect a subsequent individual.[12] This diversity is compounded by the pool of global diversity, with its various groups, subtypes, and circulating recombinant forms. The end result is that for a traditional HIV vaccine to have long-term global utility, it must raise an immune response that will be effective against a wide range of possible HIV variants. A vaccine that fails to do so would likely provide selective pressure against targeted strains while providing a selective advantage to non-targeted strains, permitting the non-targeted strains to proliferate throughout the vaccinated population. In designing HIV vaccines in an attempt to elicit these broad immune responses, the attention of the scientific community has periodically alternated between T cell and B cell targeting vaccines, with reasonable justifications for both approaches. A considerable amount of that attention has focused on what are known as broadly-neutralizing antibodies (bnAbs), so-called because they are able to neutralize a wide range of HIV variants. This neutralization is in addition to their non-neutralizing functions, and the advantage of neutralization is that it holds the potential to inactivate free virus during the earliest timepoints of infection, ideally before free virus has ever entered a cell. This could provide a critical advantage, as it would prevent the establishment of a reservoir of HIV, undetectably integrated into the genomes of T cells located at the site of infection. However, reproducibly eliciting these bnAbs has proven difficult.

1.1.3 Broadly neutralizing antibodies

Antibodies that can neutralize a broad range of HIV clades tend to be unusual in both their origins and physical properties. Physically, bnAbs often exhibit unusual features such as extensive somatic hypermutation (SHM) and elongated complementarity-determining regions (CDR), often displaying extended hydrophobic loops characteristic of autoreactive antibodies.[13-15] These physical properties are reflected in the activity of the bnAbs as well, as bnAbs tend to be polyreactive and autoreactive.[16,17]

Antibody responses during acute HIV infection are usually poor, targeting immunodominant but non-neutralizing viral epitopes, allowing the virus to escape.[18] Neutralizing antibodies often arise later in infection, and are typically restricted to epitopes of autologous virus, as might be expected. Roughly 10-30% of individuals with persistent, untreated HIV infections go on to eventually generate bnAbs, often able to neutralize >80% of cross-clade viral quasispecies and function prophylactically,[19] a benefit unfortunately not provided to the individuals who generated them; individuals who express bnAbs do not spontaneously clear endogenous virus, for example.[20] One of the few near-universal features of HIV bnAbs is that they are all subject to a profound developmental delay, arising only years after initial infection.[21] The few bnAbs which have been isolated earlier than several years after infection have still been delayed by a year or more, with the notable exception of several bnAbs isolated from infants.[22-25] A number of different hypotheses have been put forth to explain this, but have not yet enabled the development of a predictive model that can reliably approximate the mechanics or kinetics of bnAb development in an individual, and our current

understanding of the processes involved clearly remains incomplete. These hypotheses include, but are not limited to, linking the time to bnAb development to: the degree of SHM,[26] Env diversity within the individual,[27] and total viral load.[20,21,28] These hypotheses, despite doing an admirable job of explaining the observations made by the field in general, are supported by solid—but often contradictory—data. For example, it has been claimed that the years-long delay in the development of highly-mutated bnAbs is due to the length of time it takes to acquire their extensive SHM. However, structural studies have shown that the majority of those mutations are unnecessary to achieve an equivalent degree of binding.[29] Furthermore, antibodies which bind to gp41 during acute infection are already highly mutated.[30] These pre-existing, mutated, HIV-specific antibodies also displayed cross-reactivity to the bacteria present in the digestive tract of the individuals in which they were identified.[31] If partially mutated bnAb precursors already exist, or can already exist, as early as during acute infection, then that considerably abbreviates the affinity-landscape a bnAb's unmutated common ancestor (UCA) has to traverse over the course of its development. Taken in combination, these data suggest that while highly mutated bnAbs certainly do take years to develop, the time required to accumulate those mutations is unlikely to be the only constraint.

A different metric that does appear to trend with the acquisition of neutralization breadth is the autoreactivity of many (but not all) bnAbs. Interestingly, this autoreactivity often is not coincidental, but is rather a fundamental property of the mechanism by which the bnAbs perform their neutralization activity.[17] In some cases, the autoantigens in question are relatively generic, as in the case of several HIV gp41-MPER-binding bnAbs such as 2E5 and 4E10. In these and other cases, the mechanism of

neutralization consists of binding to both the membrane proximal external region (MPER) on the virion as well as to human plasma membrane lipids, thereby preventing membrane fusion.[32,33] The effect is the demonstration of neutralization and autoreactivity, simultaneously.[34]

In other cases, the autoantigen is a much more specific molecule, as in the case of 21c, a bnAb which binds a complex epitope made up not of a HIV protein or a sole host protein, but rather by their combination. 21c binds to an epitope made up of HIV gp120 in complex with CD4. Binding and structural assays performed using mutated CD4 demonstrated that while 21c could bind the autoantigen alone, Fab-binding to the viral gp120 required association with the autoantigen CD4.[35]

This dovetailing of neutralization and autoreactivity has even been observed and recorded longitudinally, during bnAb development. A study that observed an HIV-infected individual over a 144-week period who went on to develop bnAbs showed that the acquisition of neutralization breadth, potency, and autoreactivity all coincided, and were substantially delayed, emerging after two years.[36] Further, the same study expressed antibodies in the lineage of the isolated bnAb (some directly sequenced at earlier timepoints, others inferred) and evaluated their binding to a variety of autoantigens. The delays between the acquisition of neutralization breadth and autoreactivity were similar.

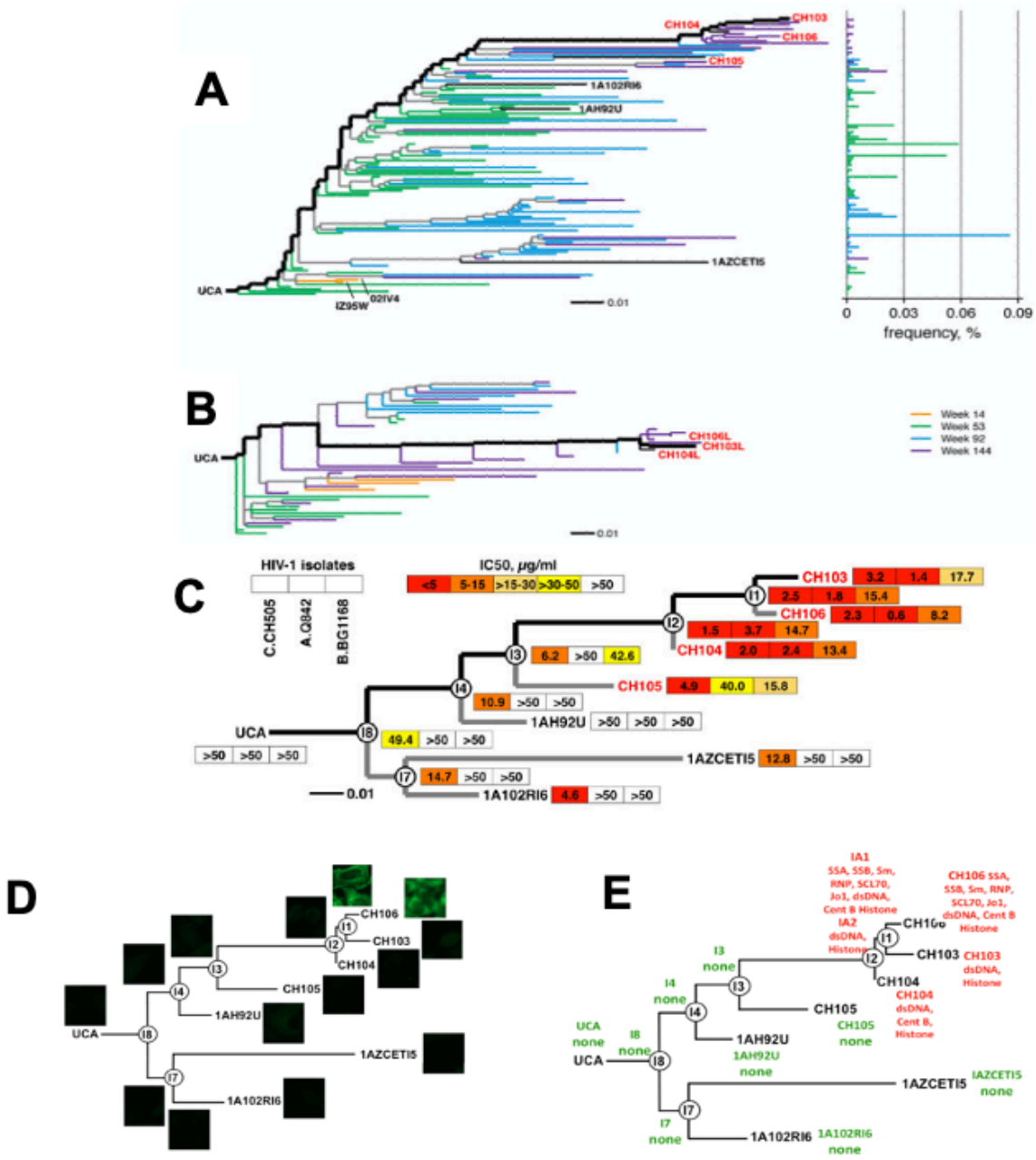

Figure 1.1.3. Development and autoreactivity of bnAb CH103. Phylogenies of VHDJH (A) and VLJL (B) sequences from sorted single memory B cells and pyrosequencing. The phylogenetic trees themselves were computed using neighbor joining on the complete set of DNA sequences to illustrate correspondence of sample date and read abundance in the context of the clonal history. Phylogenetic CH103 clonal lineage tree showing the IC50 (ug/ml) of neutralization of either autologous transmitted/founder (T/F) (C.CH505), heterologous tier clades A (A.Q842) and B (B.BG1168) viruses as indicated. Isolated mature antibodies are red, pyrosequencing-derived sequences are black. The inferred evolutionary paths to observed matured antibodies are bold. Reactivity to antibodies in CH103 clonal lineage assayed by (D) indirect immunofluorescence HEp-2 staining and (E) ANA assays. Figure and figure legend adapted from Liao et al., Nature, 2013. [36]

The concurrent acquisition of neutralization breadth and autoreactivity takes place not merely over time, but over time in a specific context: persistent HIV infection.

BnAbs have only ever been identified within this context, with the exception of experimental animal models. To the best of this author's knowledge, no bnAb has ever been isolated from a healthy individual during any human vaccine trial, making the context of persistent viral infection a possible factor in the development of bnAbs.

1.1.4 Persistent viral infection

Viral infections that are not cleared by the immune system and that endure for a period of months or years are commonly referred to as chronic infections. These can be either latent or persistent. In latent viral infections, both the symptoms and the production of viral antigens can come and go with time. Herpes simplex virus (HSV), for example, utilizes chromatin control and a nucleic-acid-based latency associated transcript (LAT) to maintain a latent infection within sensory neurons without detectable protein expression.[37] On the opposite end of the spectrum are persistent viral infections that are characterized by the continuous production of high titers of antigens, such as Hepatitis C and HIV. In these cases, the constitutive stimulation of the immune system by cell death, pathogen-associated molecular pattern (PAMPs), danger-associated molecular patterns (DAMPs), and antigens, over months or years of constant inflammation, take a toll on the immune system. Interestingly, after years of persistent viral infection, regardless of the specific pathogen, the resulting immune disruptions often display convergent motifs. Lymphocyte exhaustion is one such theme, with the expansion of functionally-impaired adaptive immune cells that express high levels of

inhibitory receptors.[38] Impaired humoral immune tolerance is another. Persistent viral infections often result in the production of autoantibodies. It is unlikely that this eventual breach of humoral self-tolerance is mediated by the precise interaction of a single viral protein and a specific host factor, given the wide range of viruses that can induce this effect: Hepatitis A,[39] B,[40] and C,[41] which in the Baltimore classification system represent group IV picornaviruses, group VII hepadnaviruses, and group IV flaviviruses, respectively; HIV,[42] a group VI retrovirus; LCMV,[43] a group V arenavirus; and others. This effect isn't limited to persistent viral infection, in fact, and is also observed in some persistent bacterial infections as well, including *Borrelia burgdorferi,*[44,45] the spirochete that can cause Lyme disease, and *Mycobacterium leprae,*[46,47] which can cause leprosy. The activation of autoreactive B cells by the combination of toll-like receptor (TLR) signaling and specific autoantigen binding is likely one of several common mechanisms by which this wide variety of persistent infections gradually impair B cell tolerance.[48,49]

1.1.5 HIV and autoimmunity

HIV is often thought of as causing immune deficiency; while this is accurate, it is also incomplete. Persistent HIV infection causes not merely immune deficiency but immune dysregulation, an aspect of AIDS that is often overlooked.

Specifically, while HIV infects CD4+ and CCR5+ T cells and macrophages, it dysregulates a far greater variety of immune cells than it can infect directly, including B cells, in which it causes a counterintuitive combination of hyperactivation and exhaustion that can alter B cell subpopulation frequencies, phenotypes, and functions. As lymphopenia develops over time, frequencies of immature transitional B cells

increase, and peripheral B cells lose expression of CD21.[50] Traditional memory B cell (MBC) frequencies decline while altered MBCs arise, which display unusual CD20, CD27, CD21, and FcRL4 expression.[51,52] Other B cell inhibitory factors besides FcRL4 are also upregulated, including CD22, CD72, CD85j, CD11c, and Tbet.[51,53,54] Polyclonal B cell activation[55-58] alters B cell survival[59,60] and differentiation into short-lived plasmablasts.[56,59,61,62] Most importantly, as expected from a persistent viral infection that constitutively stimulates the immune system with high titers of antigen, hypergammaglobulinemia[56,63-65] and autoreactive antibodies also increase over time.[57,42]

It is important to note that, in many cases, the appearance of these autoreactive antibodies during persistent HIV infection represents a true breach of self-tolerance and not a mere increase in autoreactivity. Autoreactivity itself is not pathogenic; there are a number of constructive purposes for low-affinity autoreactive antibodies, such as wound clearance and healing.[66,67] Autoreactive antibodies are not uncommon in healthy individuals. What can develop during untreated persistent HIV infection is not mere autoreactivity, but genuine autoimmunity, as it often results in pathogenic autoimmune disease. If self-tolerance is a property of a normally-functioning immune system, and the failure of self-tolerance results in autoimmunity,[68] then the pathogenic autoimmunity that often develops after years of persistent HIV infection represents a true failure of self-tolerance.

These breaks in self-tolerance do not appear to be universally targeted to a single organ, tissue, or cell type, but are instead fairly diverse. Small studies going back decades have assessed cohorts of HIV positive individuals and shown increased rates

of autoimmune sequelae.[69] A tremendously well-powered study, performed in 2017, leveraged the National Health Insurance Research Database of Taiwan, which can link to the healthcare data of 99% of the Taiwanese population.[70] In this study, the autoimmune disease rates of more than 20,000 individuals with persistent HIV infection, treated and untreated, were compared with two million matched uninfected individuals.[71] For almost every autoimmune disease assessed, HIV+ individuals had greater, not lesser, rates of autoimmune diseases than their uninfected counterparts. In the case of some autoimmune diseases like Systemic Lupus Erythematosus (SLE), the standardized incidence ratio was a modest three times higher than expected. In others, as in the case of autoimmune haemolytic anemia, the increased risk was anything but modest—more than thirty-five times greater after HIV infection. There have long been questions concerning whether the immune system rebound observed during highly active antiretroviral therapy (HAART) might increase the rates by which autoimmune diseases develop. In 12 of the 13 autoimmune diseases assessed in this study the standardized incidence rate (SIR) was greater in untreated individuals than in those on HAART, suggesting that persistent HIV infection, with its attendant high titers of viral antigens and immune stimulation, predisposes one to developing autoimmune diseases more than suppressed HIV infections, in which VLs have been diminished by HAART. This and other studies demonstrate that the autoreactive antibodies often observed during persistent HIV infection can be indicative of true breaks in self-tolerance and of an immune system that is no longer capable of constraining the development of autoreactive antibodies as it once (presumably) was. In summary, persistent viral

infection can permit the production of autoreactive antibodies that would otherwise be constrained in the context of functioning immune tolerance.

The importance of this phenomenon is supported by a number of observations concerning the elicitation of bnAbs, though it is prudent to point out that these can only be said to apply to those bnAbs for which realistic autoreactivity has been demonstrated. First and simplest, it is in keeping with the observation that bnAbs have not been isolated from individuals unless years of persistent viral infection have occurred, implying that impaired self-tolerance may be one of several prerequisites for their elicitation. Second, it is in keeping with the observation that nearly all of the most-rapidly-elicited bnAbs isolated to date have been isolated from HIV-infected infants. This is relevant because an infant's immune system is disrupted much more rapidly during persistent HIV infection than an adult's.[72,73] Median infant progression to AIDS is roughly one year.[74] Not only do the bnAbs isolated from infants acquire their breadth extraordinarily rapidly, but can also do so with quite limited SHM.[25] This demonstrates that high degrees of SHM, and the long years proposed to be necessary to achieve that, may not be strictly required, per se, but that some other factor—in this example, breach of self-tolerance—is. Third, it suggests why bnAbs have never been isolated during acute HIV infection or by vaccination; functional self-tolerance may have been constraining their development. If this were the case, one might expect to see anecdotal evidence of improved neutralization from, for example, vaccine trial participants who happened to have autoimmune conditions or other persistent viral infections. In fact, cases like this have been reported. A 2014 study described bnAbs isolated from an individual who suffered from both lupus and HIV, who controlled VLs despite

possessing a non-controlling HLA genotype.[75] A 2009 study of the neutralization breadth of 39 persistently infected individuals discovered that the only individual who neutralized the entire panel of tested HIV strains was also the only individual who was persistently infected with HCV and HBV as well.[76] Finally, large-scale human studies have shown links between autoreactivity and neutralization breadth. One study of the B cell receptor (BCR) repertoires of 96 HIV+ patients, roughly half of whom displayed neutralization breadth and half of whom did not (as well as of 43 HIV- patients), showed that long CDRH3 regions, previously shown to be overrepresented in autoreactive and polyreactive antibodies,[77] were enriched in HIV-infected individuals. They also showed that inherently autoreactive IGHV genes like IGHV4-43 were overrepresented in HIV+ individuals compared to HIV- individuals, and within the HIV+ group were overrepresented to a greater extent in those individuals with neutralization breadth than without.[78] Further, a study published in 2016 assessed the neutralization breadth and autoreactivity of the plasma of 239 people, and showed that 33 of 51 of the neutralizers with the greatest breadth also produced autoreactive antibodies, compared to 16 of 51 individuals who did not generate HIV neutralizing antibodies.[79] However, it should be noted that gradual erosion of self-tolerance by persistent viral infection does not, in and of itself, explain the difficulty of eliciting bnAbs by immunization. For example, a number of bnAbs exist for which no autoreactivity has ever been shown. Likewise, many highly mutated bnAbs bind antigens that have difficulty activating their own UCA. To overcome these and other barriers, a number of immunization paradigms have been developed, including longitudinal, or stepwise, immunizations.

1.1.6 Stepwise immunization and germline-targeting immunogens

The rationale behind stepwise immunizations is to provide the immune system with a series of immunogens which guide the affinity maturation of B cells in an iterative process. The starting point is the activation of the putative UCA of a particular bnAb, and the end goal is a BCR with the same affinity and neutralization breadth as the original bnAb. A difficulty in both studying and eliciting bnAbs is that in many cases, the mature bnAb displays little to no affinity for the antigens bound by its UCA.[80-82] Stepwise immunization strategies aim to overcome that impasse.

The immunogens used in this work began as a rationally-designed minimal antigen of the HIV CD4 binding site (CD4bs), but lacking the inner domain, V1, V2, and V3 regions.[13] This was referred to as an eOD, or engineered outer domain. Early modeling of a homology model of the putative UCA of VRC01 bound to gp120 predicted a steric clash between the BCR CDRL1 and an N-linked glycan at position 276 (re HIV group M reference strain HXB2). This predicted conflict, or lack thereof, is referred to in chapter 3 as the N276 blockade. The authors modified their eOD to accommodate that perceived hindrance, and sought to present these antigens as multimers on a virus-like nanoparticle. The 6,7-dimethyl-8-ribityllumazine synthase enzyme from *Aquifex aeolicus* was selected as the base of each protein, and when expressed in mammalian cells, the monomers self-assembled into 60-mers with greater ability to activate B cells.[83] Iterative design changes led to the creation of eOD-GT6 and eOD-GT8,[84] which was used as the base design for the studies outlined in chapter 3. eOD-GT8, a modified GT6 with greater affinity for the putative UCA of VRC01, can be expressed either as a 60mer (consisting of a 154 amino acid tail, a 15 amino acid linker, and a 172 amino acid cap),

or as a 24mer on ferritin-based nanoparticles. Ferritin is ideal for nanoparticle applications as the monomers are simple, consisting of five helices, four of which are parallel with the fifth more or less perpendicular, which arrange into 24mers with four-fold axes of symmetry arranged around the perpendicular helices. The resulting nanoparticles are incredibly robust and have been used for decades, including by this author in previous work.

Section II: Memory B cells

1.2.1 Synopsis of canonical B cell development

B cells develop from HSCs (hematopoietic stem cells) in bone marrow, going through sequential steps of immunoglobulin gene rearrangement and selection at specific checkpoints. Early B cells that productively rearrange their Ig heavy chain gene utilize a surrogate light chain[85] and are driven by pre-BCR signaling that mediates survival, expansion, and allelic exclusion. Each selected pre-B cell then rearranges its Ig κ light chain gene and the resulting immature B cell, if strongly autoreactive, typically undergoes apoptosis or receptor editing. This can take the form of a modified Ig κ light chain or an Ig λ light chain. Immature B cells that depart the bone marrow are referred to as transitional B cells, and progress through T1, T2, and T3 transitional B cell stages before migrating to secondary lymphoid organs (SLO) and maturing into naïve follicular B cells. Within the SLO resides a complicated milieu of lymphocytes and stromal cells, arranged in highly-organized fashions and forming dynamic, often-transient anatomical structures. CXCL13, secreted by follicular dendritic cells (FDCs), recruits late

transitional and naïve B cells into follicles, loosely organized clusters of B cells which serve as the primary sites for naïve B cell activation.

During the canonical immune responses to protein antigens, T-dependent B cell activation and T/B collaboration involve helper T cells, recognizing a linear epitope, and B cells, recognizing a conformational epitope. Previously activated CD4+ T cells help B cells, initially driving an extra-follicular focus; B cell triggering of T cells then generates T follicular helper cells, which catalyzes the creation of a germinal center (GC) within the follicle. One purpose of a germinal center, in the canonical view, is the establishment of an iterative process of BCR mutation, guided by both positive and negative selection, to enhance affinity for a particular antigen; this process is known as affinity maturation. Another purpose is the creation of long-lived B cells that preserve the BCRs created within the germinal center, in the form of MBCs and plasma cells.

Naïve and GC B cells are profoundly different. While naïve B cells persist in a quasi-resting state for weeks to months, waiting to encounter their cognate antigen, GC B cells are metabolically hyperactivated, undergoing cell division as rapidly as once every four to six hours.[86] With each division, SHM introduces mutations in the BCR, each of which has the potential to modulate the BCR's affinity for its cognate antigen. These changes in affinity are what form the basis for selection within a GC, though they do so within an important context: as naïve B cells become GC B cells, they become inherently pro-apoptotic, and require survival signals provided by other cells to survive. Not long after it develops, the germinal center takes on a polarized structure, loosely consisting of a light zone and a dark zone. GC B cells proliferate within the dark zone, then migrate to the light zone where they compete with sister GC B cells with similar

BCRs for antigen that is sequestered and retained on FDCs. B cells that are able to capture antigen from FDCs can present them to helper T cells, receive pro-survival signals, and re-enter the dark zone. The ability to successfully navigate this process relies to a large extent on the affinity of the BCR to the antigen retained by the FDC, and forms the basis for the positive selection within the GC reaction: B cells with BCR mutations that improve affinity for the target antigen are more likely to out-compete B cells with lower affinity, and thus re-enter the dark zone. The loss of lower affinity B cells within the GC response results from the failure to compete for antigen in conjunction with the GC B cells' baseline predisposition to apoptosis. This is crucial, or affinity maturation would generate huge numbers of low-affinity BCRs; it is the combination of these mechanisms (the competitive element, the iterative element, and the active culling of the low-affinity BCRs) that drives affinity maturation to produce a pool of high-affinity BCRs.

Memory B cells (MBCs) undergo limited affinity maturation and emerge early in the course of a germinal center response. Late in the germinal center response, antibody secreting cells (ASCs) emerge initially as plasmablasts, which traffic to the bone marrow and differentiate into long-lived plasma cells that can secrete antibodies for years or decades. Plasmablasts express detectable levels of the BCR, but fully differentiated plasma cells no longer express the BCR. Memory B cells, on the other hand, express their BCRs at high levels in order to detect the presence of their cognate antigen. Upon reactivation, memory B cells can be rapidly activated, proliferate, reenter a GC, and reinitiate SHM, affinity maturation, and further memory B cell and long-lived plasma cell generation.

The definition of what constitutes a memory B cell has changed dramatically over the past several decades. Once thought to consist purely of B cells that emerged from a GC having undergone class-switch recombination and extensive SHM,[87] it is now recognized that those elements, while certainly features of canonical switched memory B cell populations, are by no means prerequisites. A more functional definition has been proposed: a memory B cell is a B cell that has responded to antigen, returned to a quiescent state, remains present for a period of time, and is responsive to a subsequent encounter.[88]

1.2.2 Memory B cells in humans

CD27 has long been used as the defining marker for memory B cells in humans, and for good reason. A number of functional studies support this,[89-91] and traits like class-switching and SHM certainly trend with CD27 expression.[92,93] Early B cells express no CD27, while ASCs and memory B cells typically do; in canonical B cell development, it is during the GC response that the expression of CD27 begins. Other markers traditionally used to define memory B cells in humans include CD19+, CD20+, CD24+, CD38-, CD44+, and CD80+.[94] However, exceptions exist in almost every case. CD80 is not expressed on all CD27+ B cells, both IgG and IgA B cells can be CD27-,[95,96] and unusual CD27- CD21- B cells, expanded in conditions like HIV infection and Common Variable Immune Deficiency (CVID), which overexpress inhibitory receptors and appear hyporesponsive,[52,97-99] further complicate the picture. This is on top of well-accepted B cell populations such as marginal zone B cells, which are

CD27+;[100] unswitched IgM memory B cells;[101] and CD27+ B cells found in umbilical cord blood.[102]

1.2.3 Memory B cells in mice

The portrait of MBCs in mice is more complicated that it is in humans for two reasons. First of all, it is more complex because most of what is known about memory B cells is derived from studies performed in mice. Secondly, CD27 is ineffective in mice at discriminating between MBCs and other cell types. It doesn't even distinguish between post-germinal center B cells and pre-germinal center B cells as it does (to some extent) in humans. A number of different phenotypic definitions have emerged over the years, but none is widely agreed upon; most studies and research groups use different combinations of phenotypes and functional definitions to define MBCs in mice for the purpose of completing their studies. For the purpose of this chapter, discussion of murine "MBCs" should be presumed to imply memory-like B cells, and examples of murine MBCs across different studies should not be assumed to have been defined according to the same criteria.

The use of an activation-induced cytidine deaminase (AID) promoter-driven Cre to mark cells with an EGFP reporter is one method which has been used to identify putative murine MBCs[103] of varying isotypes. Another approach has been a simple but elegant experimental framework using cell transfers and BrdU labeling. In this latter approach, B cells from B1-8i$^{+/-}$ mice (expressing a BCR knock-in with affinity for nitrophenyl) were adoptively transferred to recipient AM14 Tg Vk8R KI mice (with an irrelevant monoclonal BCR knock-in), some of which were then immunized with

nitrophenyl (NP). Eight weeks later, NP-specific B cells were present only in the NP-immunized animals; without immunization, the transferred B cells did not persist (or rather, appear in the spleen). This framework has been used in conjunction with BrdU labeling to study both the development of MBCs[104] as well as to establish alternate and surrogate markers for murine MBCs.[105] These authors identified CD80, CD95, CD73, MHC II, and CD62L either by proportion of memory vs naïve B cells expressing them, or by mean fluorescence intensity (MFI) during flow cytometry.[106] However, none of these markers is ideal. CD80, while expressed on 63% of MBCs, was also expressed on 24% of naïve B cells. MHC II, with an MFI of 206 in MBCs and only 131 in naïve B cells, was expressed on 99% and 98%, respectively. That said, somatic hypermutation did appear to be restricted to the CD80+ CD35- memory B cells, and CD80 has been highlighted in conjunction with CD73 and PD-L2 in other studies as well.[105,107] Even without a universally-agreed upon consensus on how to identify murine MBCs, these and other studies have permitted the investigation of their origins and development.

Just as the phenotypic descriptions of MBCs discussed in section 1.2.1 have become increasingly complex over time, so too have their origins. Although commonly thought to develop towards the end of a germinal center response, antigen-specific memory-like B cells were once identified emerging ten days after immunization,[108] and more recently have been shown by two different groups to emerge early in the GC reaction.[109,110] More BrdU pulse experiments have likewise shown that roughly 25% of IgM MBCs present eight weeks post-immunization were formed in the first two days after immunization,[111] which, canonically, would be prior to the formation of a typical GC. MBCs have been observed under conditions in which elements once thought to be

critical to their formation have been removed, including antigen presented on FDCs within GCs,[112] and even GCs themselves.[106-109] SHM can even occur outside of GCs.[113] Lastly, not only can MBCs arise unexpectedly, but when they do, they sometimes forgo yet another hallmark of canonical MBCs: extensive SHM. A number of studies in different systems have demonstrated that MBCs of various types sometimes exhibit dramatically less SHM than other subsets.[114-116] Some aspect of this may be due to the differing criteria by which each study was performed, but the end result is the same: not only are MBCs phenotypically diverse, the pathways by which they develop are similarly diverse.

1.2.4 Trends in MBC differentiation

While MBC subset discrimination complicates the picture when comparing findings between studies, recent work has begun to shed light on the process by which GC B cells differentiate into MBCs; less is known about the differentiation of extrafollicular MBCs. Many of the factors in these pathways are discussed in greater depth in section 4.1.

In the canonical view, GC B cells that fail to receive BCR or CD40 stimulation, as well as T cell help in the light zone due to their low affinity BCRs, undergo apoptosis.[86,117] Those which receive weak BCR stimulation and weak T cell help may differentiate into MBCs, mediated to a large extent by BCL-6, HHEX, and SKI.[118-121] Lastly, those which receive strong T cell help are more likely to differentiate into plasma cells, mediated in part by factors like BLIMP1[122*123] and IRF4.[124] These trends were supported recently with the publication of a single-cell and bulk RNAseq dataset which

showed that cMyc+ GC B cells diverged in the light zone based on their BCR affinity, with high-affinity clones featuring plasmablast precursors, and low-affinity clones featuring MBC precursors or future dark zone entrants.[121]

Generally speaking, hypotheses of MBC development can be binned into four models.[125] The asymmetric fate model holds that the differentiation of MBCs or plasma cells from GC B cells is stochastic, resulting from asymmetric distribution of cell-fate-factors like BCL-6 and IRF4.[126,127] However, limited *in vitro* data do not appear to support the phenomenon of asymmetric cell division,[110] calling this model into doubt. The instructive fate model holds that factors outside the GC B cell control its fate, specifically cytokines and cell-to-cell contacts. The cascade of events that occurs after BCR/antigen binding is central to the instructive fate model, but it remains a stochastic model at heart, as it permits B cells with identical BCRs to differentiate along different paths.[128,129] The decreasing-potential fate model holds that the fate of the GC B cells is determined by the signals received during the iterative rounds of light and dark zone migration, with a particular emphasis on their progressive impact on the cell over time. According to this model, a GC B cell bearing a low-affinity BCR will experience fewer rounds of less-powerful T cell stimulation, and that it is this accrual—or lack thereof—that, over time, predisposes a GC B cell to emigrate early as an MBC. High-affinity BCRs, on the other hand, will receive stronger T cell help, leading to more iterations of selection and predisposing B cells bearing those BCRs to emerge later as plasma cells. This model is supported for the most part by data demonstrating the relative timing with which MBCs and plasma cells emerge from the GC.[111] Lastly, the integrative fate model incorporates elements of the others, holding that a GC B cell's fate is determined by a

combination of two elements: whatever predisposition it may have acquired as a result of an accumulation of signals during earlier rounds of SHM, in combination with the quality of signaling received at the time of differentiation. Data in favor of this include murine cell transfer experiments in which T follicular helper cells (T_{FH}) were found to engage in transcriptomically-discrete stages of differential signaling to GC B cells, secreting IL-21 first (in order to induce BCL-6 expression in GC B cells), then later secreting IL-4, in order to induce BLIMP-1 (in order to induce BLIMP-1 expression in GC B cells).[130]

CHAPTER 2: Vaccine responses in the context of impaired tolerance

2.1 INTRODUCTION

2.1.1 LCMV

LCMV, or lymphocytic choriomeningitis mammarenavirus, is an arenavirus that can infect both humans and mice. The virus itself is roughly 100uM in diameter, enveloped, and features a helical nucleocapsid containing two ambisense RNA genetic elements.[6]

LCMV infections in humans can cause non-specific symptoms including headache, nausea, cough, fever, and vomiting, though as many as one-third of infections are asymptomatic.[131-134] In rare cases, more complex neurological symptoms can result, including meningitis, meningoencephalitis,[132,135] paralysis, hearing loss, and Guillain-Barre syndrome.[131,132,135] The outcome of congenital LCMV infection in humans depends on the timing of infection during fetal development, but can include hydrocephalus, intellectual impairment, chorioretinitis, cerebral palsy, seizures, visual impairment, or spontaneous abortion.[131,133,135-137]

Infections in mice depend on the strain of LCMV used—which is not to say that the same might not likewise be true in humans. Two strains of LCMV, Armstrong and Clone 13, are commonly used for research purposes, and have both been used for decades. Armstrong causes a strong cytotoxic lymphocyte response and is rapidly cleared by the host, while Clone 13 can be used to induce a less acute, more chronic infection.[138,139] CD4+ T cell depletion prior to infection with Clone 13 can produce a chronic infection lasting for many months.[140] Clone 13 features several mutations that differentiate it from Armstrong, including A603G, U856C, U1298C, and A3953C,[141] though the second is more responsible for mediating persistence, as it results in a

mutation in the viral glycoprotein thought to modify binding affinity to its receptor, a-dystroglycan.[142]

2.1.2 Use of LCMV in research

LCMV has most often been used not as a model in and of itself, but rather as a way to perturb other model systems. It has played a pivotal role in studies that have elucidated underlying mechanisms of immunology, including MHC restriction,[143] tolerance,[144] and T cell exhaustion.[145,146] Most relevant to this work, however, are the effects of LCMV as pertains to immune tolerance and persistent viral infections.

While HIV and LCMV are categorically different viruses, the outcomes of their respective infections share some superficial similarities. Both can produce persistent infections in which early T cell responses, unable to clear the infection, lead to the expansion of functionally exhausted CD8+ T cells,[147,148] with similar transcriptional profiles being induced in these cells in humans and mice, respectively.[149] And most importantly, both infections cause both hypergammaglobulinemia[43 150] and the production of autoreactive antibodies.[43,151] It is these last two phenotypic changes that make LCMV a reasonable model system for the experiments presented below. This induction of autoreactive antibodies during HIV infection is unlikely to be the result of the interaction between a specific HIV protein and a corresponding host factor, given that the effect is observed across a wide range of viral and bacterial infections. It is more likely due to the constitutive stimulation of the immune system by high titers of antigen. This effect is reviewed in greater depth in section 1.1.6.

2.1.3 Experimental framework

The notion that immune tolerance might be playing a role in constraining the development of autoreactive bnAbs is not novel in 2021. It remains, however, difficult to test. An interesting study was published in 2017 titled “Breaching peripheral tolerance promotes the production of HIV-1-neutralizing antibodies.”[152] In this work, the authors assessed the HIV-1 neutralizing capability of murine serum after immunization with HIV-like antigens, comparing that of wild type (WT) mice with that of autoimmune-prone mice. To this end, they used three lines of mice: WT C57BL/6 (B6) mice, autoimmune-prone B6.SLE123 mice, and MRR/lpr mice. They also used an agent known as pristane that was injected into the B6 mice. Pristane is a short hydrocarbon that, when injected intraperitoneally, induces autoimmunity in non-autoimmune-prone mice. In short, it impairs B cell tolerance, or permits autoreactive antibodies to be produced, and is reviewed in greater depth in section 3.1.5. Among their findings were that B6 mice, treated with pristane to breach immunological tolerance and immunized with gp140, developed greater HIV-1 neutralization breadth, and that histone H2A-reactive antibodies isolated from B6.Sle123 mice were HIV-neutralizing.

Our aim was to assess whether the increase in neutralization and breadth of neutralization observed by these authors with pristane treatment would likewise extend to a breach of tolerance mediated by a different perturbation, namely, persistent viral infection in the form of LCMV.

Subsequent experimental design was complicated by the unexpected results. In order to generate data responsive to the hypothesis, the more-autoimmune-prone mice (MRL/lpr and MRL) would have to generate substantially greater neutralization breadth,

above background, than the B6 mice. However, B6 serum, at baseline, features HIV-1 neutralization capability at a frequency far greater than that of non-human primates (Dr. Michael Seaman, Beth Israel Deaconess Medical Center, unpublished communication). Further, there is no reasonable expectation that a standard B6 mouse, immunized with gp140, would generate high neutralization breadth. Therefore, to test our hypothesis, a more-HIV-specific experimental framework was sought, which paired two elements: mice that might reasonably be expected to generate a high number of bnAb-precursor B cells, and an immunogen that might reasonably be expected to stimulate those B cells.

Our experimental framework consisted of several types of mice including B6, MRL, MRL/lpr, and V_H1-2/LCL, the latter of which are described in depth in section 2.1.4. MRL mice, or Murphy Roths Large, are an autoimmune-prone lineage that is often used in lupus research, while MRL/lpr mice are homozygous for the *FAS*^{lpr} mutation, impairing the function of the death receptor FAS, a.k.a. CD95, which results in lymphoproliferation and dramatic autoimmunity as the mice age. Our immunogens consisted of a mosaic HIV gp140, a soluble Env protein designed to mimic the epitopes of a variety of clade M viruses,[153] and eOD-GT8, an immunogen that is described in greater depth in section 1.1.6. Our immune-tolerance-related perturbations consisted of the use of genetically-autoimmune-prone mice lineages as well as LCMV infection, and our final endpoints were neutralization breadth as determined by TZM-bl neutralization assay, as well as single-cell BCR sequencing.

2.1.4 The V_H1-2/LC mouse model

The V_H1-2/LC model was first published in 2016, [154] and was intended to serve as a model in which to test the efficacy of immunogens designed to stimulate VRC01-like precursor B cells. To create it, Tian et al. [154]replaced the murine V_H81X gene with the human IGHV1-2*02 gene, which is the human V gene used by the UCA of the VRC01 bnAb, and deleted an intergenic control region on one IgH allele in murine embryonic stem (ES) cells. This deletion causes the D-proximal V-gene (in these mice, the knocked-in human IGHV1-2 gene) to be preferentially used during recombination. These modified ES cells were utilized in a Rag2-deficient blastocyst complementation (RDBC) approach to create chimeric mice.

To create V_H1-2/LC mice from VH1-2 mice, Tian et al. modified the BCR light chain as well. Given the published requirement for VRC01-like antibodies to feature an unusually short, five amino acid-long light chain CDR3, and the rarity with which such an event might be expected to occur naturally, the authors knocked-in a rearranged version of the VRC01 Igκ variable region exon and did so in the murine *J*κ locus of already-modified IGHV1-2*02/IGCRI ES cells. Note that while the human IGHV1-2 gene knocked into the heavy chain was the unmutated, germline version of the gene used by VRC01, this light chain modification consists not of the UCA of the VRC01 light chain, but rather a combination of the unmutated IGKV gene used by VRC01 (IGKV3-30*01) and the mutated, five amino acid VRC01 CDRL3. This provides the short CDRL3 required for VRC01/CD4bs binding, as well as other advantages including a key glutamic acid residue conserved across VRC01-like bnAbs.[154-156] Lastly, the authors also deleted the J_H region from the unmodified murine *IgH* allele, to limit gene

expression to their modified chromosome. After applying these modifications to formerly VH1-2 ES cells, the authors used those cells for RDBC and immunized the chimeras in their immunization experiments. These mice express BCRs that utilize the human IGHV1-2 gene roughly 40% of the time, but which can draw from the entire murine complement of heavy-chain D and J genes, providing tremendous variability to their HCDR3s (Fig. 2.1.4). These mice can likewise undergo class-switch recombination, somatic hypermutation, and affinity maturation, all within the context of a light chain that is capable of binding to CD4-binding site-like antigens.

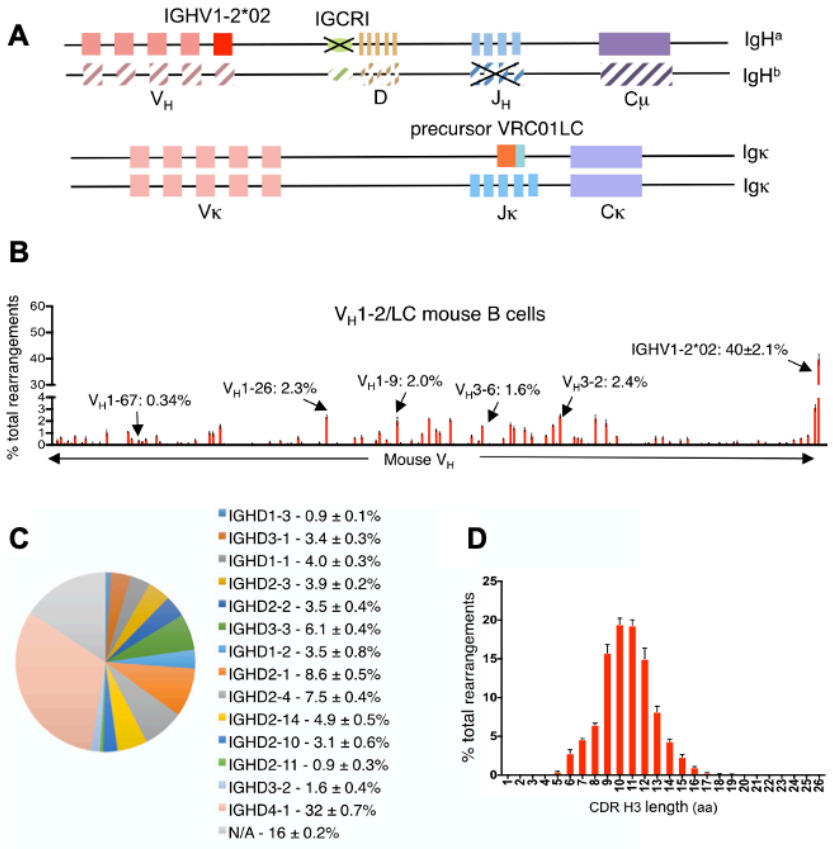

Figure 2.1.4: Characterization of the VH1-2/LC model. (A) Illustration of genetic modifications involved in the V_H1-2/LC model. (B) Analysis of V_H gene usage in splenic B cells from V_H1-2/LC mice. (C) D segment usage in productive IGVH1-2*02 rearrangements in V_H1-2/LC mouse model. (D) Length distribution of IGHV1-2*02-associated CDRH3s in V_H1-2/LC mice. Figure and legend adapted from Tian et al., Cell, 2016. [154]

2.2 RESULTS

2.2.1 V_H1-2/LCL mice display key features of the V_H1-2/LC model

Two mice were obtained from Dr. Frederick Alt, Children's Hospital Boston, each with some but not all of the features of the V_H1-2/LC mouse model. These were each crossed with C57BL/6 mice, and their resulting F1 pups crossed until the knocked-in light chains had been bred to homozygosity. These mice are referred to here as V_H1-2/LCL ("light chain-like") mice. Prior to any immunization or intervention, they possess a BCR repertoire in which roughly 40% of all naïve B cells are specific for eOD-GT8 (Fig. 2.2.1). These data match our expectations, as the deleted intergenic control region predisposes the rearranging BCRs to select the human IGHV1-2 gene roughly 40% of the time, and with the light chain bred to homozygosity, it follows that roughly 40% of the naïve B cell pool should be specific for eOD-GT8 and similar antigens. These data suggest that these mice, which bear knock-in BCRs in their germlines (as opposed to being created by blastocyst reconstitution in the Rag knockout background) were suitable for our subsequent HIV-immunogen and bnAb studies.

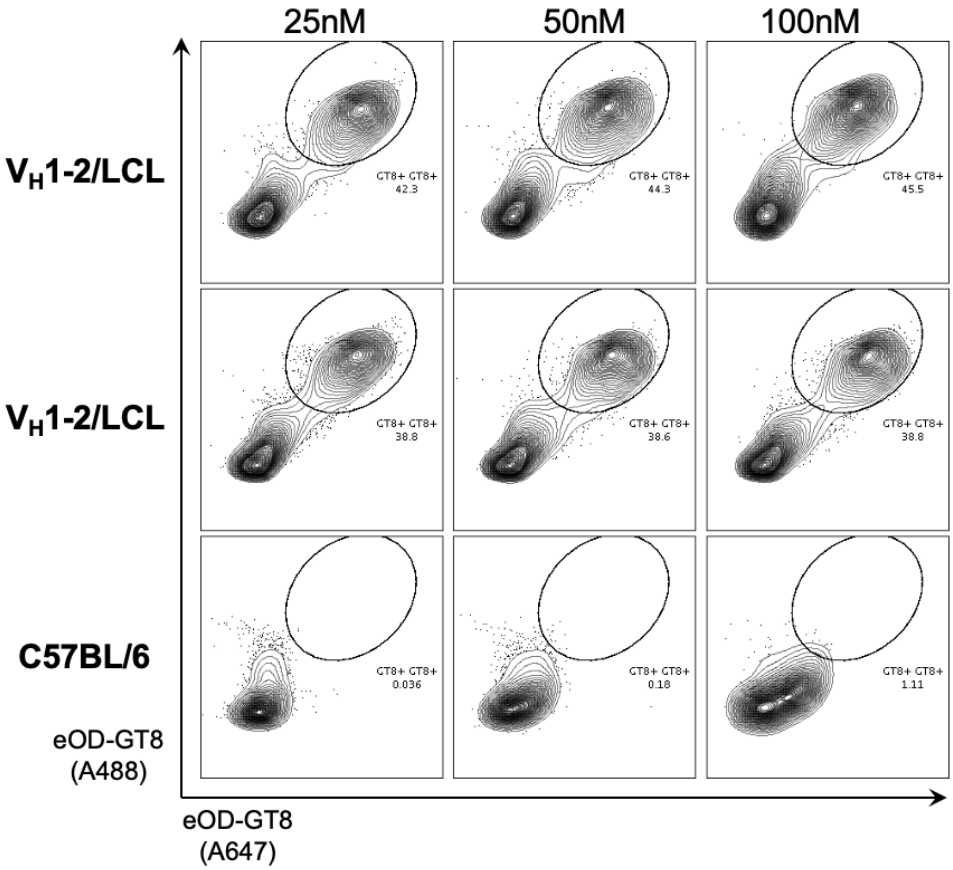

Figure 2.2.1: Frequency of antigen-specific B cells in the V_H1-2/LCL mouse model reflects human V gene use frequency of the V_H1-2/LC mouse model. V_H1-2LCL and C57BL/6 mice were euthanized, and their spleens were processed, cryopreserved, thawed, and stained with a flow cytometry panel that included dual-color (A488 and A647) eOD-GT8 tetramers across a range of staining concentrations. Upstream gating included size, granularity, viability, and CD19. Roughly 40% of the naïve B cell pool demonstrated affinity for eOD-GT8. Flow profiles were representative of naïve mice from three different experiments.

2.2.2 LCMV infection validated by demonstration of T cell exhaustion phenotypes, hypergammaglobulinemia, and autoreactive antibody production

Prior to utilizing LCMV as an experimental tolerance perturbation, validation was required of its capabilities to perform this function as published. We began by generating our own virus in-house, from stocks generously provided by Dr. Arlene Sharpe. We began by confirming the strain of both in-house batches of virus by

sequencing their genomes using next-generation sequencing (NGS). This allowed us to positively identify each strain we had generated and to monitor the acquisition of unexpected mutations that might have appeared at any appreciable frequency within the viral pool. In doing so, we confirmed the presence of key mutations often used to identify Armstrong and Clone 13 strains of LCMV, including A603G, U856C, and U1298C (Fig. 2.2.2a).

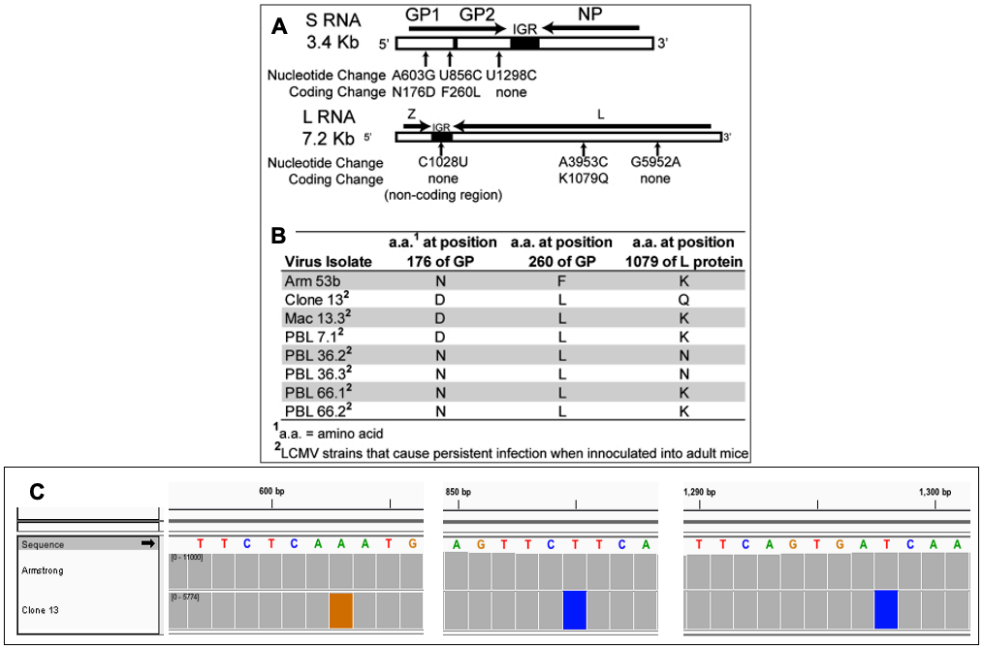

Figure 2.2.2a. Genome sequencing of personal stocks of LCMV.
(A) Nucleotide changes between the LCMV Armstrong and Clone 13 strains. (B) Several key amino acid differences between strains causing acute or persistent infections. A and B adapted from Sullivan et al., 2011, Proc Natl Acad Sci.[141] (C) Integrative Genomics Viewer display of high-throughput sequencing performed on batches of virus replicated in-house. Viral stocks were lysed, viral RNA was isolated, fragmented, retrotranscribed by random priming, and prepared as libraries for Illumina Nextseq sequencing. Donated and in-house stocks were both sequenced; both showed expected mutational profiles.

Batches of high-titer LCMV, when replicated in-lab, are sometimes plagued by the overproduction of defective-interfering viruses which can alter the infectivity, chronicity, and lymphocyte-exhaustion profile of the viral stock when used *in vivo*. Oftentimes roughly 1/3 of injected mice will demonstrate subpar infection, either in

terms of chronicity or viral load (unpublished communications). To address this frequency in our own hands, a longitudinal *in vivo* assessment was performed to validate the utility of the in-house viral stocks. Four groups of mice were injected with PBS, Armstrong, or Clone 13 virus; in the latter case, both in the context of CD4+ T cell depletion and without depletion. Each mouse was bled once a week for 10 weeks, plasma VLs were quantified by plaque assay (Fig 2.2.2b), and mice were reinfected at nine weeks post-infection (wpi). Mice injected only with PBS were LCMV negative, as expected, but that they remained so for 10 weeks while housed and handled alongside LCMV-infected cages served as a confirmation of the efficacy of the infection control measures adopted for this and other LCMV experiments. The Armstrong virus was detectable at 1wpi and was undetectable thereafter, implying that the virus had been cleared or nearly cleared as early as 2wpi, matching expectations yet again. The Clone 13-virus-infected mice also behaved as expected, with mice demonstrating a 10- to 100-times greater initial viral load (VL) than the Armstrong mice, one mouse clearing the infection early while another displayed the characteristic chronic infection profile desired from Clone 13 infections; namely, extraordinarily high initial VLs that came down over the course of roughly five weeks, leading to eventual control. The mice which were depleted of CD4+ T cells one day prior to and one day after infection also matched expectations, with roughly 1/3 of the mice managing to maintain borderline undetectable VLs over the course of the 10 weeks, while the other two mice went on to develop the characteristic high-titer long-term infection expected following CD4+ T cell depletion in this model system. Reinfection at week 9 did not appear to result in runaway infections in any mice, indicating that an immune response was capable of controlling VLs and

suggesting that LCMV would be best utilized as an immune tolerance perturbation only once per mouse.

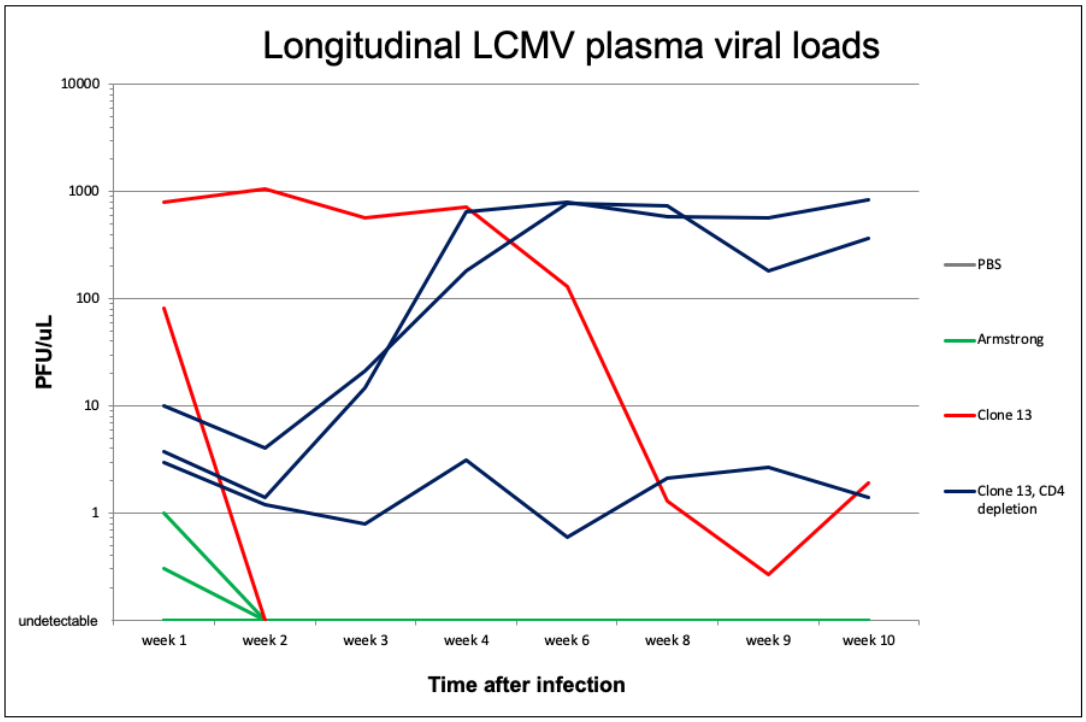

Figure 2.2.2b. Chronicity and infection profile of personal stocks of LCMV. Six-week-old female B6 mice were infected with $2x10^5$ PFU LCMV Armstrong (IP) or $4x10^6$ PFU LCMV Clone 13 (RO), and reinfected 8wpi. Three mice were depleted of CD4 T cells by injection of anti-CD4 antibodies one day pre- and one day post-infection. Weekly blood draws were assessed for virus by plaque assay in Vero cells.

To confirm that the persistent LCMV infections were inducing T cell exhaustion, flow cytometry analysis was performed on PBMCs isolated concurrently with the serum used above. After gating to exclude doublets, debris, and dead cells, these data confirmed the efficacy of the CD4+ T cell depletion, as at 2wpi, CD4+ T cell counts were strongly reduced in CD4+ T cell-depleted mice (Fig. 2.2.2c). At 4wpi, PBS-treated and CD4+ T cell-depleted mice showed no strong elevation in CD8+ T cell counts, while in mice infected with Armstrong and Clone 13 the CD8+ T cell numbers do appear slightly elevated. Most importantly, however, the CD8+ T cell flow cytometry demonstrated

markers of exhaustion where expected. Armstrong-infected mice with higher VLs exhibited greater CD44 expression than those with lower VLs or PBS-only mice, with Clone 13-infected mice demonstrating even greater CD44 expression, particularly within the CD8/CD44/PD-1 gate. The Clone 13-infected mouse, which at 4wpi had failed to control its VL (depicted in red, bottom-middle), displayed by far the highest frequency of PD-1 expression, while the Clone 13-infected mouse, which at 4wpi had already controlled its VL (depicted in blue), had begun to resolve its T cell exhaustion.

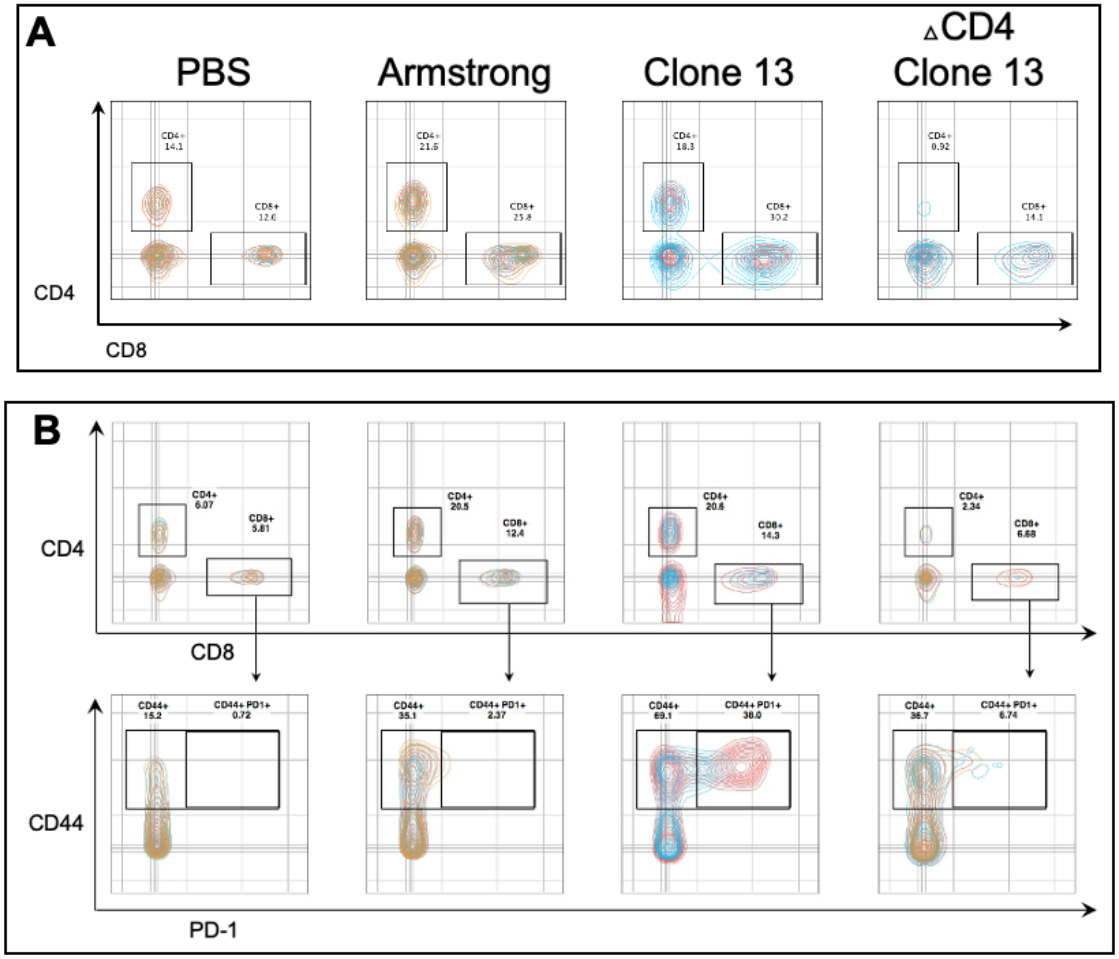

Figure 2.2.2c. Personal stocks of LCMV induced T cell exhaustion phenotype. Flow cytometry assessment of T cell depletion and indicators of T cell exhaustion. (A) Mice were bled two weeks after infection and CD4 T cell depletion, and PBMCs were analyzed. Upstream gating included size, granularity, viability, and excluded debris. (B) Analysis of PBMCs collected four weeks after infection and CD4 T cell depletion, with similar gating. Exhausted T cells typically co-express PD-1 and CD44.

In order to confirm the capacity of the in-house LCMV batches to induce hypergammaglobulinemia, anti-murine-IgG ELISA assays were performed using plasma from the same timepoints as those used above. As expected, bulk IgG concentrations were dramatically elevated in the Armstrong and Clone 13-infected mice, with the exception of those which were depleted of CD4+ T cells prior to infection (Fig. 2.2.2d). As the effects of the CD4+ T cell depletion wear off with time, the plasma IgG concentrations of those mice increase over time. Lastly, in those mice that were reinfected at 9wpi, there was a corresponding surge of IgG at the 10wpi timepoint. While the small number of mice in each group, as well as the differing infection profiles of mice within those groups, make statistical assessment between the Armstrong and Clone 13-infected groups impossible, that was never the intended purpose of these experiments; the value of these data is derived from their demonstration that the viruses which were produced in-house are quite capable of inducing hypergammaglobulinemia during infection.

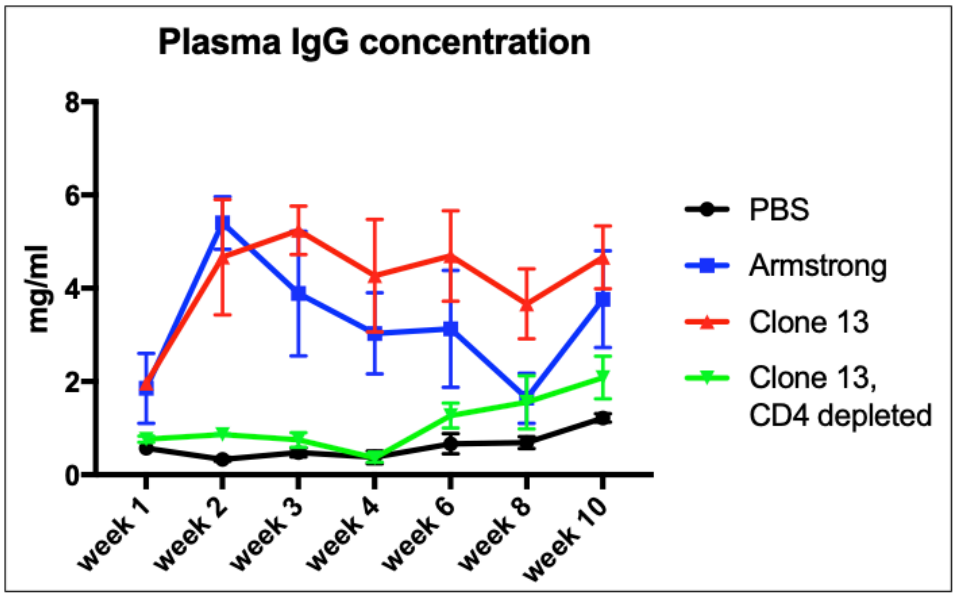

Figure 2.2.2d. Personal stocks of LCMV induced hypergammaglobulinemia. Plasma obtained from the longitudinal blood draws used in Figure 2.2.2c were assessed by ELISA for total IgG concentrations. Note that mice were reinfected at 8wpi. Plasma was diluted and the mean of each dilution within the standard curve was reported. Error bars represent mean +/- standard deviation of IgG concentrations in mice within each group at each timepoint.

Lastly, but most importantly, we sought to confirm whether LCMV infection could serve as an experimental perturbation capable of impairing humoral immune tolerance to an extent sufficient that the production of autoreactive antibodies could be reliably observed. To assess this, a human clinical assay known as the ANA HEp-2 test was modified for use in murine systems. Used to qualitatively detect the presence of autoreactive antibodies in the plasma of patients who may have SLE, the HEp-2 assay consists of plated and permeabilized human cells over which serum or plasma is laid, followed by a fluorescently-labeled anti-human-IgG antibody. Visualization is microscopy-based, and scoring is performed visually by trained technicians. Substituting the anti-human-IgG antibody for an anti-mouse-IgG antibody permits the detection of cell-specific antibodies in the plasma of LCMV-infected mice. While the assay is qualitative in nature, the modified HEp-2 assay clearly demonstrated the presence of

cell-reactive antibodies in the plasma of mice infected with LCMV, which were not observed in the plasma of uninfected mice (Fig. 2.2.2e).

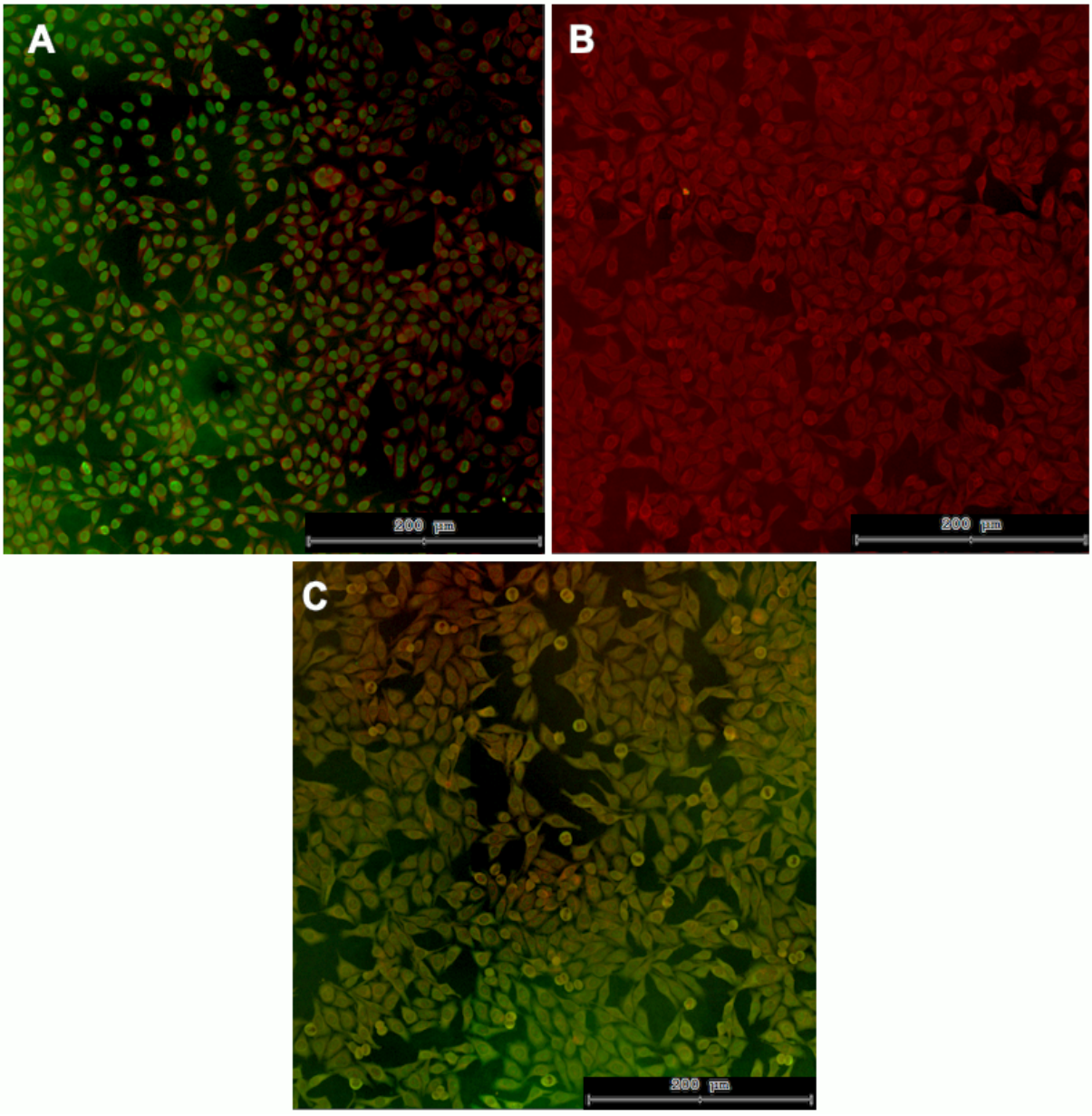

Figure 2.2.2e Personal stocks of LCMV induced the production of cell-reactive antibodies. A clinical HEp-2 autoreactivity assay, modified to assess the extent of cell-reactive antibodies present in murine plasma. (A) MRL plasma, 1:1280 dilution. (2) C57BL/6 plasma, uninfected, 1:40 dilution. (C) C57BL/6 plasma, 3wpi with LCMV Clone 13, 1:40 dilution. Light source intensity, aperture, exposure time, and gain were established using HEp-2 cells overlaid with known plasma, then each image was acquired using the same settings. Evan's blue counterstain. Murine IgG.

2.2.3 Genetic autoimmunity and neutralization breadth

While LCMV was being validated, genetic predisposition to autoimmunity was explored as another means by which the impact of immune tolerance on bnAb development might be assessed. B6, MRL, and MRL/lpr mice, discussed in section 2.1.3, were immunized with gp140 mosaic Env, adjuvanted with alum (Figure 2.2.3), and their sera were used to conduct neutralization assays against a panel of four HIV pseudoviruses (two Tier 1 and two Tier 2). Unlike similar studies,[152] no significant distinction in neutralization breadth was observed across murine lineages (Table 2.2.3).

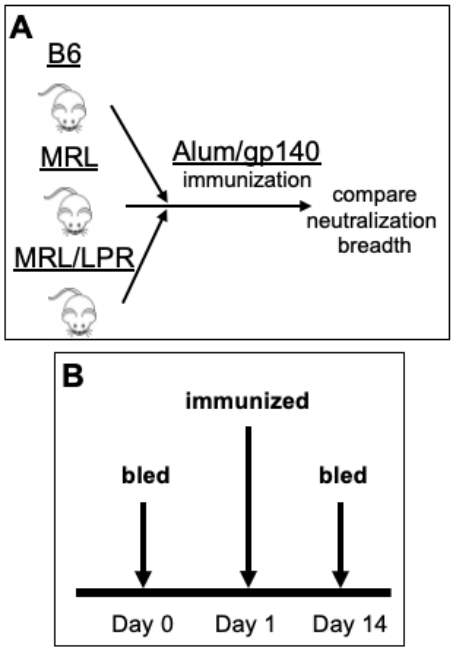

Figure 2.2.3. Experimental design of neutralization study.
(A) Experimental groups, interventions, and outcome. (B) Chronology.

Sample ID	Timepoint	BaL.26 Clade B Tier 1	YU2.DG Clade B Tier 2	TRO.11 Clade B Tier 2	ZM249M.PL1 Clade C Tier 2	MuLV Neg. Control
B6, #1	Day 0	<50	<50	<50	<50	<50
	Day 14	<50	<50	**50**	**53**	**51**
B6, #2	Day 0	<50	<50	<50	<50	<50
	Day 14	<50	<50	<50	<50	<50
B6, #3	Day 0	<50	<50	<50	<50	<50
	Day 14	<50	<50	<50	<50	<50
B6, #4	Day 0	<50	<50	<50	<50	<50
	Day 14	<50	<50	<50	<50	<50
B6, #5	Day 0	<50	<50	<50	<50	<50
	Day 14	<50	<50	<50	<50	<50
MRL, #1	Day 0	<50	<50	<50	<50	<50
	Day 14	<50	<50	<50	<50	<50
MRL, #2	Day 0	<50	<50	<50	<50	<50
	Day 14	<50	<50	<50	<50	<50
MRL, #3	Day 0	<50	<50	<50	<50	<50
	Day 14	**54**	<50	**77**	<50	<50
MRL, #4	Day 0	<50	<50	<50	NT	<50
	Day 14	<50	<50	<50	<50	<50
MRL, #5	Day 0	<50	<50	<50	<50	<50
	Day 14	<50	<50	<50	<50	<50
MRL, #6	Day 0	<50	<50	**133**	<50	**59**
	Day 14	<50	<50	**51**	<50	<50
MRL, #7	Day 0	<50	<50	<50	NT	<50
	Day 14	<50	<50	<50	<50	<50
MRL, #8	Day 0	<50	<50	<50	<50	<50
	Day 14	<50	<50	<50	<50	<50
MRL, #9	Day 0	<50	<50	<50	<50	<50
	Day 14	<50	<50	<50	<50	<50
MRL, #10	Day 0	<50	<50	<50	<50	<50
	Day 14	<50	<50	<50	<50	<50
MRL/lpr #1	Day 0	<50	<50	<50	<50	<50
	Day 14	<50	<50	<50	<50	<50
MRL/lpr, #2	Day 0	<50	<50	<50	<50	<50
	Day 14	<50	<50	<50	<50	<50
MRL/lpr, #3	Day 0	<50	<50	**72**	<50	<50
	Day 14	<50	<50	<50	<50	<50
MRL/lpr, #4	Day 0	<50	<50	<50	<50	<50
	Day 14	<50	<50	<50	<50	<50
MRL/lpr, #5	Day 0	<50	<50	<50	<50	**54**
	Day 14	NT	NT	NT	NT	NT
CH01 31	Pos.	**0.042**	**0.091**	**0.217**	**0.034**	>25

Table 2.2.3. Neutralization breadth of autoimmune-prone mice immunized with gp140 was not greater than that of C57BL/6 mice. Serum ID50 titer, as calculated by plaque assay in TZM.bl cells. 1:50 dilutions, titrated 3-fold, 7x (duplicate wells). Top row: HIV pseudoviruses. Left column: mouse ID and lineage. NT: Not Tested due to limited sample. Assay performed in the laboratory of Dr. Michael Seaman, Center for Virology and Vaccine Research, Beth Israel Deaconess Medical Center, Boston, MA.

2.2.4 LCMV infection does not support the elicitation of HIV-specific bnAbs

To assess if virally-induced breaches of humoral self-tolerance were sufficient to permit the development of autoreactive bnAbs, we combined the V_H1-2/LCL mouse model, eOD-GT8, and LCMV in a single experiment. Twenty V_H1-2/LCL mice were injected with PBS or LCMV, then two weeks later with eOD-GT8, then euthanized at 14 or 42 days post-immunization (Fig. 2.2.4a).

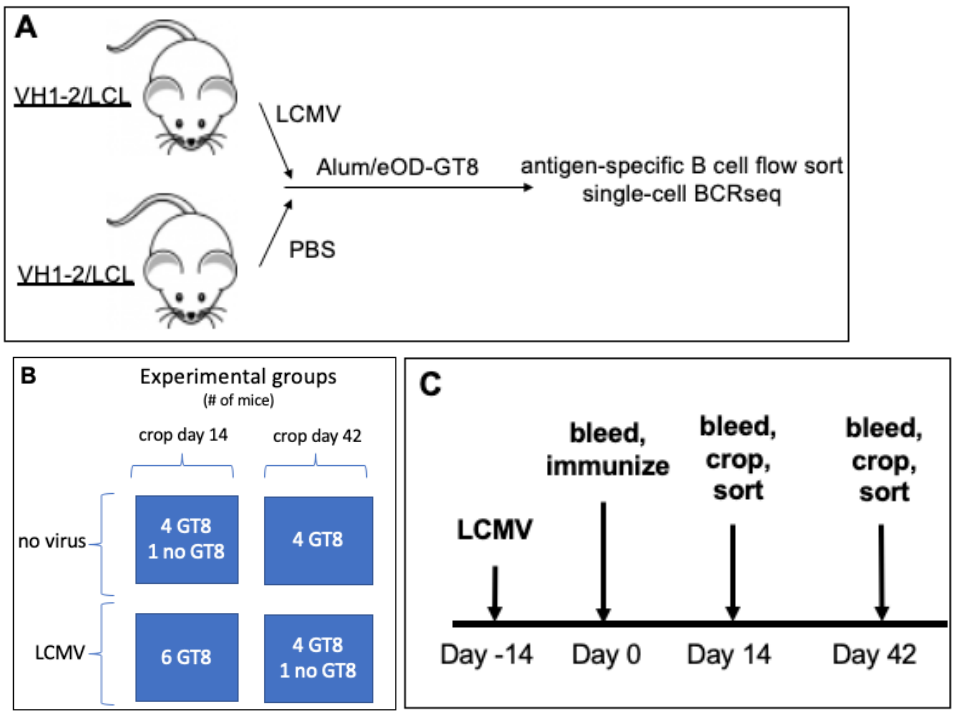

Figure 2.2.4a. Experimental design of LCMV study.
(A) Overview of experiment. (B) Breakdown of experimental groups. (C) Chronology.

In order to sort antigen-specific B cells, a three-color tetramer system was employed. Two colors (A488 and A647) were used to label separate pools of eOD-GT8 tetramers, on the basis that affinity by a B cell for a single tetramer might be due to binding either to the CD4bs, other epitopes on the tetramer, or the fluorophore itself. A B cell with affinity for both labelled tetramers is unlikely to have cross-reactivity to both

fluorophores, and would suggest that the B cell binds to the tetramers rather than the fluorophores. To discriminate between B cells specific for the CD4bs and B cells specific for irrelevant epitopes on the tetramer, a third color (A594) was used to label eOD-GT8-KO tetramers (referred to here as KO tetramers) with a mutated CD4bs. B cells capable of binding to A594-labeled tetramers as well as either of the other colors would not have affinity for the CD4bs, but would instead be specific for some other portion of the tetramers. We compared the total B cells of V_H1-2/LCL mice for CD4bs-specificity and found that virtually all of the B cells that were specific for the standard GT8-tetramers were not specific for the KO tetramer, implying that they were binding to the CD4bs specifically (Fig. 2.2.4b). Few B cells in the V_H1-2/LCL mouse model could reasonably be expected to have strong affinity for the KO tetramer (having never been exposed to it, and having no knock-in BCRs which would recognize it), which made positive controls difficult to design. However, it was observed that B cells that bound nonspecifically to the A488 tetramer (and not the A647 tetramer) also bound the A594 KO tetramer. These cells were used as an impromptu positive control for the KO tetramer's functionality, as their mean fluorescence intensity within the A594 channel was noticeably greater than that of other populations of B cells.

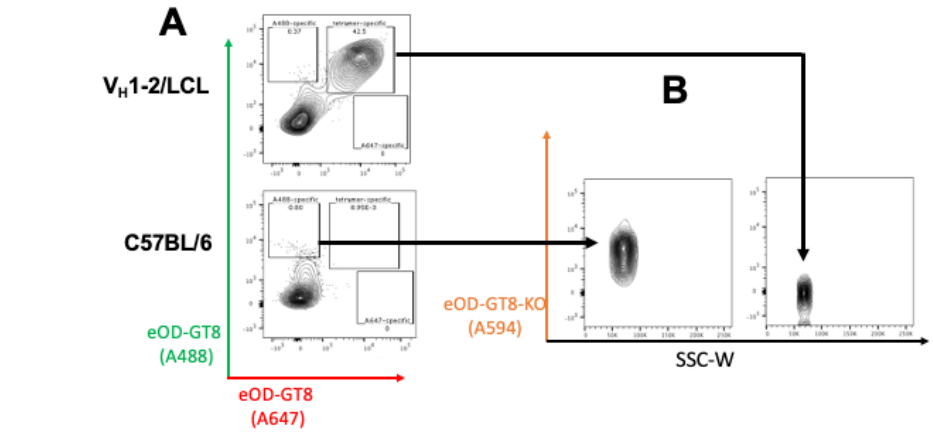

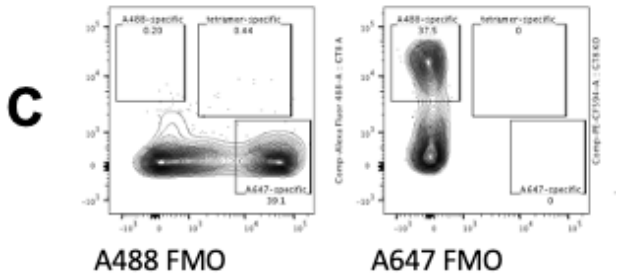

Figure 2.2.4b. Three-color tetramer fluorescence assisted cell sorting (FACS) for antigen-specific B cells. Murine splenocytes were stained for flow sorting using a combination of conventional antibody and fluorophore-labeled tetramers. Previous gating included size, granularity, viability, CD4-, and CD19+. (A) Comparison of antigen-specific B cells as a portion of total B cells from V_H1-2/LCL and C57BL/6 mice. (B) Comparison of KO-tetramer-specific B cells from previous gates: non-specific, single-color binding B cells from a C57BL/6 mouse, and specific, dual-color binding B cells from a V_H1-2/LCL mouse. (C) Single-color fluorescence minus one (FMO) demonstrating that dual-color binding B cells from V_H1-2/LCL mice reflect genuine affinity and not cell-staining artifacts.

Immunization status did little to change the frequency of antigen-specific B cells to any significant extent; this was expected, as the V_H1-2/LCL mice had so many antigen-specific B cells at baseline. While the LCMV-infected mice appeared to have greater numbers of CD4bs-specific IgG1 B cells at 14 days post-immunization than the LCMV-uninfected mice (and the reverse at 42 days post-immunization), neither timepoint was statistically significant. Interestingly, LCMV-infected mice did have significantly greater numbers of eOD-GT8-KO-specific B cells than uninfected mice, at both 14 and 42 days post-immunization (Fig. 2.2.4c). Given that neither LCMV-infected or uninfected mice had ever encountered the GT8-KO antigen, this likely represents the induction of virus-nonspecific B cells reported during persistent viral infection, and LCMV infection in particular.[43]

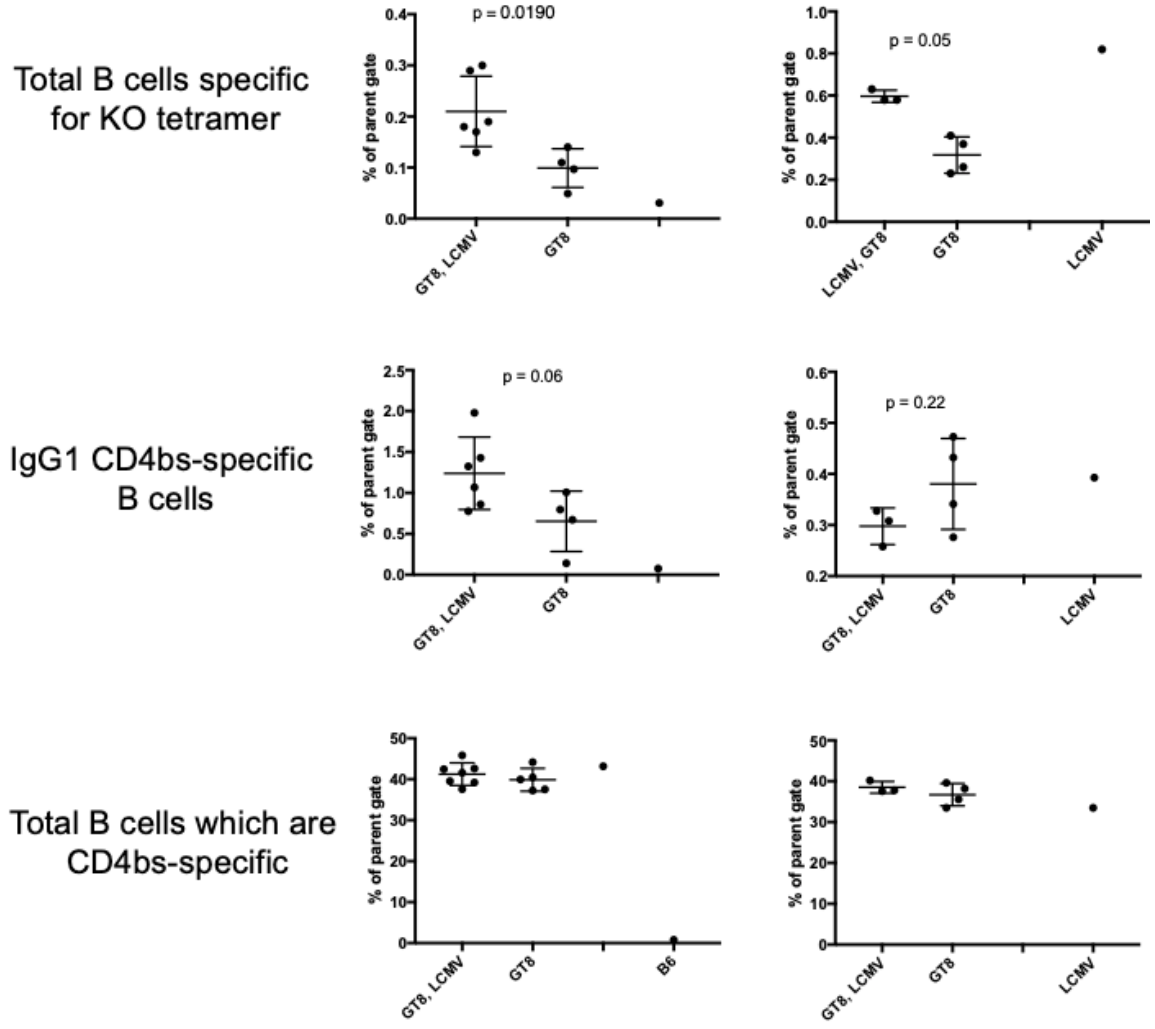

Figure 2.2.4c. Frequencies of antigen-specific B cells in LCMV-infected and uninfected mice. V_H1-2/LCL mice infected with LCMV Clone 13 and immunized with eOD-GT8 or PBS. Cryopreserved splenocytes, thawed and stained with antibodies and tetramers described above for flow cytometry. Previously gated for size, granularity, doublets, viability, and CD19 (top, bottom), or CD19+ and IgG1+/GL7-. Day 14 (left), and day 42 (right) post-immunization. All mice were V_H1-2/LCL unless specifically stated.

To assess if persistent LCMV infection had any effect on the BCRs of the immunized mice, single-cell sorting was performed (Fig. 2.2.4d), followed by single-cell BCR sequencing.

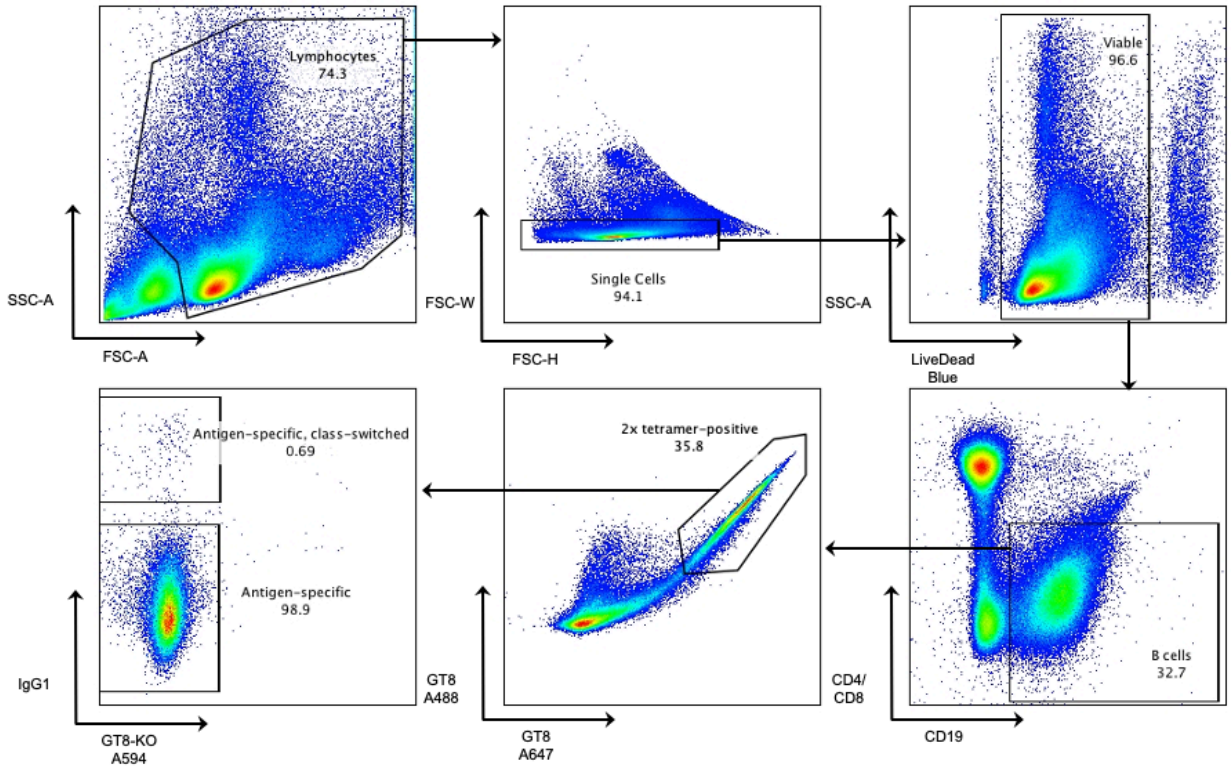

Figure 2.2.2d. Gating scheme: FACS of class-switched, antigen-specific B cells. V_H1-2/LCL mice were immunized with eOD-GT8/alum, spleens were collected 42 days later, processed, and cryopreserved,. Thawed splenocytes were stained and single-cell-sorted as depicted above. >2500 cells were sorted from 11 immunized mice, both LCMV-infected and not.

The heavy chains of each BCR were sequenced, as the light chains, given the breeding and genotyping of the mice from which these were derived, were presumed to be VRC01-like even prior to immunization.

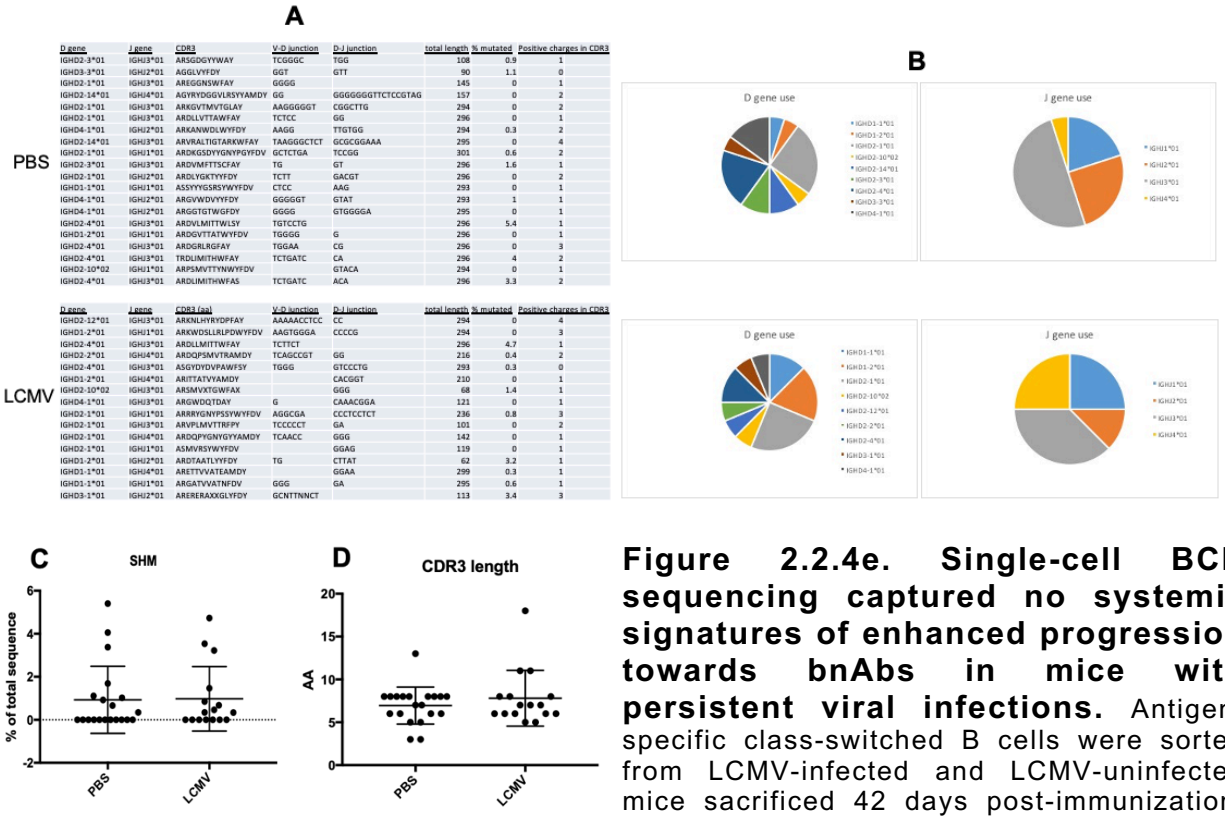

Figure 2.2.4e. Single-cell BCR sequencing captured no systemic signatures of enhanced progression towards bnAbs in mice with persistent viral infections. Antigen-specific class-switched B cells were sorted from LCMV-infected and LCMV-uninfected mice sacrificed 42 days post-immunization. The cells were lysed and their BCR heavy chain were amplified by PCR then Sanger sequenced. Sequences of sufficient length and quality were assessed by IgBlast, using custom settings in order to utilize the human IGHV1-2*02 gene in conjunction with all possible murine D and J genes as references (A). (B) Distribution of D and J gene use. (C) Somatic hypermutation, and (D) CDRH3 length. Results are mean +/- standard deviation.

The majority of the BCRs sequenced did not feature a significant amount of mutation within the human IGHV1-2 gene, though there was a wide variety of murine D and J gene use, as well as considerable variability around the V-D and D-J junctions. SHM and CDRH3 lengths were similar across conditions, as well. VRC01-like mutations did not appear in any statistically significant pattern within either the LCMV-infected group or the LCMV-uninfected group. The effect of LCMV infection was observed in one respect, however. Positive amino acid residues in CDR3 regions has often been associated with autoreactivity, and 25% of the BCRs from the LCMV-infected group fit that description, compared to only 10% of the LCMV-uninfected groups.

2.3 DISCUSSION

The data in sections 2.2.1 and 2.2.4 demonstrated cleanly and clearly that the murine aspects of the model were in good working order. Previously published data suggested that V_H1-2/LC mice utilize their knocked-in human V gene roughly 40% of the time, [154] and in the V_H1-2/LCL mice, roughly 40% of total B cells were specific for the CD4bs epitope on eOD-GT8. This was expected, as the light chain of the V_H1-2/LCL mice is homozygous. Spectral spillover between fluorophores often takes the form of diagonally-shaped false double-positive cell populations, which made relying on a double-positive flow cytometry phenotype for such a crucial element of both the system validation and the later flow sorting (eOD-GT8-A488-positive and eOD-GT8-A647-positive) less than ideal. However, the inclusion of the third tetramer, eOD-GT8-KO-A594, neatly demonstrated that affinity for both conventional GT8 tetramers represented affinity for the CD4bs itself, rather than for another element of the flow probes. Along the same lines, a diagonal flow profile is the most common artifact to result from spectral spillover between fluorophores, so the neatness of the FMOs in Figure 2.2.4b was crucial. The V_H1-2/LCL mice clearly produce large numbers of B cells with BCR specificity to the CD4bs epitope of eOD-GT8.

LCMV required particularly stringent validation. The use of LCMV here, specifically to induce or permit the production of autoreactive antibodies, was completely dissociated from any intent to elucidate the mechanism by which that occurs. While the virus has been used in research for decades and this phenomenon was well-published, batch to batch variation can be dramatic, altering titers, infectivity,

and even chronicity. The validations performed here reassured us that the viruses produced in-house were performing as expected. The kinetics of the longitudinal VLs were as reported, the chronicity of the infection following CD4 T cell depletion was better than expected, and the failure of roughly 1/3 of the mice to develop detectable VLs after infection was entirely in line with what we had been led to expect based on advice received informally from other research groups that utilize LCMV. The pronounced enhancement of CD44 and PD1 expression by CD8+ T cells in Clone 13-infected mice, while not as convincing as a functional assay in establishing exhaustion, was sufficient to confirm that the expected phenotypes were induced in these cell populations. Most important, however, were the systemic immunological perturbations which LCMV was being used for. Briefly, the hypergammaglobulinemia and autoreactive antibody production observed were entirely as expected. No assay was performed to determine if the surge in IgG being produced after infection was LCMV-specific or not; it is likely, based on published literature, that at weeks two through eight it was not. It is worth noting, however, that the adaptation of the HEp-2 assay was not flawless. In addition to being an inherently qualitative assay, a persistent edge effect was noted; the staining of cells in the centers of each well was noticeably dimmer than that at the edges. The images used in Figure 2.2.2e were selected specifically because they are representative of dozens of such images, and because the edge effect can be noted in panels A and C. In the context of a non-quantitative assay, the line between qualitative and subjective interpretation can be blurry, so confirmation of our interpretations of the HEp-2 assay was sought and was generously provided by the Massachusetts General Hospital Pathology Immunology Laboratory. Lastly, while it is clear that LCMV-infected

mice produce autoantibodies, it is important to note that because the modified HEp-2 assay depicted here utilizes murine sera incubated on human HEp-2 cells, the "autoreactive" antibodies demonstrated by this assay should instead be more accurately thought of as cell-reactive antibodies.

The data depicting the difference in neutralization breadth between autoimmune-prone mice and WT mice following gp140 immunization were clear; there was none. The MRL and MRL/lpr mice weren't in any meaningful way different in their neutralization breadth from the B6 mice, or from each other. The simplest interpretation of this data is that the original hypothesis is invalid, and when all is said and done, that is the interpretation we favor. However, these data and interpretation are in conflict with earlier studies. Schroeder et al.[152] reported that B6 mice, treated with pristane and immunized with alum and gp140, generated greater neutralization breadth than those treated only with pristane, and that this effect was magnified with a second and third immunization (Fig. 2.3).

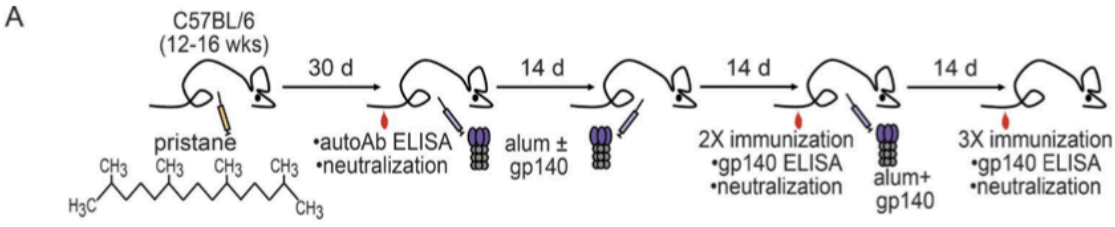

B pristane only

B6 Mouse ID	ID50 Tier 1A SF162	Tier 1B BaL.26	Tier 2 JRFL	Tier 2 YU2
P16	<30	<30	30	51
P17	NS	NS	NS	NS
P18	<30	<30	<30	30
P19	<30	<30	<30	<30
P26	<30	<30	30	<30
P29	<30	<30	<30	31
P13	<30	<30	<30	<30
P14	<30	<30	47	50
P20	<30	<30	36	36
P21	<30	<30	<30	<30
P24	<30	<30	<30	<30
P25	<30	<30	30	<30
P27	<30	<30	<30	<30
P28	<30	<30	30	<30
P31	<30	<30	<30	<30
P15	NS	NS	NS	NS
P1	NS	NS	NS	NS
P2	<30	<30	41	NS
P3	<30	<30	<30	NS
P4	<30	<30	<30	<30
P5	<30	<30	32	<30
P6	NS	NS	NS	NS
P7	<30	<30	<30	<30
P8	<30	<30	<30	<30
P9	<30	<30	88	NS
P10	<30	<30	30	33
P11	<30	<30	<30	<30
P12	NS	NS	NS	NS

C 2X alum ± Env

B6 Mouse ID	Primary Immunization and Boost	ID50 Tier 1A SF162	Tier 1B BaL.26	Tier 2 JRFL	Tier 2 YU2	muLV
P16	Alum	<30	<30	43	42	<30
P17	Alum	<30	<30	55	51	75.9
P18	Alum	<30	<30	37	30	<30
P19	Alum	<30	<30	<30	<30	<30
P26	Alum	<30	<30	44	38	<30
P29	Alum	<30	<30	35	34	<30
P13	Alum	<30	<30	<30	33	NS
P14	Alum	<30	<30	<30	<30	NS
P20	Env in Alum	<30	45	304	319	<30
P21	Env in Alum	<30	<30	54	57	<30
P24	Env in Alum	30	54	106	97	<30
P25	Env in Alum	<30	<30	90	78	56.5
P27	Env in Alum	<30	<30	36	36	56.5
P28	Env in Alum	<30	<30	36	53	52.8
P31	Env in Alum	30	30	62	59	<30
P15	Env in Alum	<30	<30	<30	<30	NS
P1	Env in Alum	<30	<30	36	35	NS
P2	Env in Alum	<30	<30	46	54	NS
P3	Env in Alum	42	<30	166	361	NS
P4	Env in Alum	35	<30	110	86	NS
P5	Env in Alum	<30	<30	<30	46	NS
P6	Env in Alum	<30	<30	<30	<30	NS
P7	Env in Alum	<30	<30	<30	<30	NS
P8	Env in Alum	<30	<30	<30	<30	NS
P9	Env in Alum	<30	<30	<30	<30	NS
P10	Env in Alum	<30	<30	30	30	NS
P11	Env in Alum	<30	<30	30	31	NS
P12	Env in Alum	<30	<30	35	33	NS

D 3X alum ± Env

B6 Mouse ID	Primary Immunization and Boost	ID50 Tier 1A SF162	Tier 1B BaL.26	Tier 2 JRFL	Tier 2 YU2
P13	Alum	32	<30	<30	<30
P14	Alum	<30	<30	<30	36
P15	Env in Alum	<30	<30	<30	<30
P1	Env in Alum	36	<30	<30	<30
P2	Env in Alum	67	33	<30	32
P3	Env in Alum	284	<30	<30	54
P4	Env in Alum	155	40	36	44
P5	Env in Alum	31	<30	<30	<30
P6	Env in Alum	37	<30	<30	<30
P7	Env in Alum	91	45	54	34
P8	Env in Alum	42	<30	<30	<30
P9	Env in Alum	61	39	33	37
P10	Env in Alum	47	<30	<30	<30
P11	Env in Alum	56	<30	34	43
P12	Env in Alum	34	<30	<30	<30

ID50
<30
30-100
>100

Figure 2.3. Wild-type mice neutralize tier 2 HIV-1 after an experimental breach in immunological tolerance. (A) Schematic of experimental protocol. Serum neutralization of tier 1 and 2 HIV-1 strains by C57BL/6 mice treated with (B) pristane alone for 30d or after (C) 2 (2x) or (D) (3x) subsequent immunizations with alum alone or Env + alum as indicated. Figure and figure legend from Schroeder et al., J. Exp. Med., 2017.[152]

Direct comparison between datasets is impossible; the exact gp140 differed between the two studies, as did the specific cause of the autoimmunity present in the mice. Despite those caveats, it is worth noting that the cutoff used in Schroeder et al. is lower than that used here. This is meaningful because murine sera, even from naïve B6 mice, tends to display some degree of HIV-1 neutralization breadth capability even at baseline—which is to say, more so than sera from primates (unpublished communications). The neutralization data reported in here in Table 2.2.3 were performed in the laboratory of Dr. Seaman at the Center for Virology and Vaccine

Research of Beth Israel Deaconess Medical Center, in its capacity as a CAVD (Collaboration for AIDS Vaccine Discovery) core facility, using methods, reagents, and standards that have been standardized across dozens of grants and publications. When their higher cutoff of $ID_{50} > 50$, (used in Table 2.2.3) is applied to the data published by Schroeder et al., the signal-to-noise ratio changes dramatically, relegating most of those results to background. In fact, the use of the higher cutoff of $ID_{50} > 50$ is supported by Schroeder's neutralization of the control virus, murine leukemia virus (muLV), at slightly > 50. That being said, several mice do stand out from the pack in their neutralization data; however, even those mice are not consistent across timepoints. The highest neutralization ID_{50} reported, 361, was achieved against YU2 (a tier 2 strain pseudotype representative of clade B) by a mouse that, two weeks later, was reported to be neutralizing YU2 at an ID_{50} of 54, barely above baseline. It is possible that if our experiment had been extended to 10 weeks (and across three immunizations), similar data may have been obtained, but what data we did observe at day 0 vs day 14 suggest otherwise, given that what examples of meaningful neutralization do appear in our datasets often appears at day 0 rather than day 14. Overall, though it does not support our initial hypothesis, we suggest that the conflict between the two studies is best resolved with the interpretation that neither dataset supports our hypothesis, rather than that both of them do. Perhaps the hypothesis is correct, but the mosaic gp140 used here was insufficient to activate the necessary B cells. Not all breaches of humoral self-tolerance are equal in magnitude or mechanism; perhaps the MRL and MRL/Lpr mice, while prone to literally lethal autoimmunity, still do not permit the type of autoreactivity often observed during bnAb maturation. Perhaps the hypothesis was correct, and one

immunization was insufficient to demonstrate improved neutralization breadth in the autoimmune-prone mice. Perhaps the hypothesis is correct and subsequent exposures to immunogens may perhaps have resulted in a break of immune tolerance, perhaps because a higher degree of SHM was required. Speculation aside, were the hypothesis to represent a generalizable and robust phenomenon, one of genuine biological relevance which might reliably be expected to be observed in settings that differ by, for example, the type of gp140 used, then such an effect would likely have been observed in the data presented above. It was not.

In the final study reported here, utilizing LCMV as the driver of the experimental breach in tolerance, the data are much the same. This study featured mice that might reasonably be expected to have VRC01-class precursor B cells, an immunogen that might reasonably be expected to stimulate those B cells, and a self-tolerance perturbation that might reasonably be expected to permit the development of autoreactive antibodies. Taken together, it could be said that one might reasonably expect to see, while perhaps not a bnAb itself, at least some evidence of maturation in that direction. We did not. What was generated was a model system which could be utilized to sort memory-like B cells (used in section 4), and further information was obtained about that model system.

A group of V_H1-2/LCL mice were injected with either PBS or LCMV Clone 13, immunized with eOD-GT8, then sacrificed at 14 or 42 days post-immunization. In Figure 2.2.4c, the bottom panels demonstrate that the model functioned as expected. Namely, that roughly 40% of the total B cell pool in the V_H1-2/LCL mice were specific for the CD4bs, and that this number was not altered by LCMV infection. Given that the

selection of the human V gene takes place early in B cell development, when B cells are still in the bone marrow, and that LCMV non-specifically activates B cells during infection, no difference between LCMV-infected and uninfected mice was expected, either at day 14 or day 42. The data presented in the middle panels suggests that eOD-GT8 priming was effective in these mice. At day 14, the sole mouse not immunized featured far fewer IgG1+ CD4bs-specific B cells than the immunized mice. There was also a nearly-significant difference between the LCMV infected and uninfected mice at that timepoint as well. While not relevant to the underlying hypothesis, it is interesting, and can be attributed to the specific gating; as GL7+ B cells were not excluded from the IgG1+ B cell pool for this figure, a portion of the IgG1+ B cells likely consists of recent GC emigrants or unswitched memory B cells that were induced to undergo class-switch recombination (CSR) by LCMV infection.[43] In the top panels, which compare the proportion of the total B cell pool that is specific for the KO tetramer, the LCMV-infected mice have more KO-specific B cells than the non-infected mice. Note that none of the mice had been previously exposed to this immunogen at any point. The asymmetric controls reinforce this observation as well, particularly at day 42.

The lack of distinction between the BCRs of the LCMV-infected and uninfected mice was, by this point, unsurprising. The majority of BCRs were predominantly unmutated, despite being class-switched, suggesting that they may have been early GC emigrants, or even extrafollicular in origin, and did not display any significant differences across LCMV-infected and uninfected mice in the degree to which they were somatically hypermutated, or by the length of their CDRH3s. Some likely underwent CSR long before either infection or immunization; these mice produce class-switched B cells with

CD4bs-specificity even at baseline, prior to any experimental interventions. Given the absence of demonstrable improvement in total neutralization capacity in sera, single-cell BCR sequencing represented a means by which it might be possible to detect early signs of progress towards greater neutralization breadth. None was found. In summary, the data obtained here do not support the hypothesis that impaired tolerance permits the production of HIV-specific autoreactive bnAbs. Significant limitations in the interpretation on this work are imposed by the short duration between immunization and sacrifice, and the use of single-immunization regimens, as opposed to prime/boost regimens. These elements of experimental design were expressly addressed in the design and execution of the work presented in chapter 3.

2.4 MATERIALS AND METHODS

2.4.1 Key Resources Table

Antibodies	**Source**	**Identifier**
Anti-mouse IgM, gk1.5	Bio-X Cell	Cat# BE0003-1
Anti-mouse Fc Block/CD16/CD32	BD Biosciences	Cat# 553142
Anti-mouse CD4-APC	BD Biosciences	Cat# 553051
Anti-mouse CD8-BV510	BD Biosciences	Cat# 563068
Anti-mouse CD19-FITC	BD Biosciences	Cat# 553785
Anti-mouse CD44-PE-Cy5	BD Biosciences	Cat# 561861
Anti-mouse PD-1-PE	Biolegend	Cat# 135205
Anti-mouse IgG-A488	Biolegend	Cat# 405319
Anti-mouse IgG-A647	Biolegend	Cat# 405322
Anti-mouse CD4-BV605	BD Biosciences	Cat# 563151
Anti-mouse CD8a-BV605	BD Biosciences	Cat# 563152
Anti-mouse IgM-PE-Cy7	BD Biosciences	Cat# 552867
Anti-mouse IgD-BV711	BD Biosciences	Cat# 564275
Anti-mouse CD19-PerCP-Cy5.5	BD Biosciences	Cat# 551001
Anti-mouse CD38-BV421	BD Biosciences	Cat# 562768
Anti-mouse GL7-PE	Biolegend	Cat# 144609
Anti-mouse IgG1-BV50	BD Biosciences	Cat# 742476

Chemicals, Peptides, and Recombinant Proteins	**Source**	**Identifier**
Pen/Strep	ThermoFisher Scientific	Cat# 15140122
199 media	ThermoFisher Scientific	Cat# 31100-035
sodium bicarbonate	Sigma-Aldritch	Cat# S5761
SeaKem agarose	Lonza	Cat# 50010
neutral red	Sigma-Aldritch	Cat# N4638
RPMI	ATCC	30-2001
Ambion SUPERase-In	ThermoFisher Scientific	Cat# AM2694
tRNA	Sigma-Aldritch	Cat# 10109541001
DTT	Invitrogen	Cat# 707265
RNAse inhibitor	Promega	Cat# N2511
oligo-dT	Invitrogen	Cat# AM5730G
taq and buffer	Qiagen	Cat# 201203
SYBRsafe dye	Invitrogen	Cat# S33102
EMEM	ATCC	Cat# 30-2003
FBS	ATCC	Cat# 30-2021
Agencourt AMPure beads	Beckman Coulter	Cat# A63881
SYBR safe DNA gel stain	ThermoFisher Scientific	Cat# S33102
Agarose	Fisher Scientific	Cat# BP160-500
EDTA-COATED TUBES FOR BLEEDS	BD Biosciences	Cat# 365974
Lonza BioWhittacker ACK Lysis buffer	ThermoFisher Scientific	Cat# BW10548E
Brilliant Stain Buffer	BD Biosciences	Cat# 563794
Lysogeny Broth, powder	Fisher Scientific	Cat# BP1427-500
Maxiprep kit	Qiagen	Cat# 12163
EZ Link NHS biotin	ThermoFisher Scientific	Cat# 20217
Streptavidin-A647	Biolegend	Cat# 405237
Streptavidin-A594	Biolegend	Cat# 405240
Streptavidin-A488	Biolegend	Cat# 405235
Kanamycin Sulfate	ThermoFisher Scientific	Cat# 11815024
Alhydrogel	Invivogen	Cat# vac-alu-250
LIVE/DEAD Blue viability dye	ThermoFisher Scientific	Cat# L23105
Critical Commercial Assays	**Source**	**Identifier**
Kapa Express Extract kit	Kapa Biosystems	Cat# KK7103
HiFi HotStart ReadyMix PCR kit	Kapa Biosystems	Cat# KK2602
PureLink viral RNA/DNA mini kit	ThermoFisher Scientific	Cat# 12280050
NEBNext rRNA depletion kit	New England Biolabs	Cat# E6310S
NEBNext Ultra RNA library prep kit	New England Biolabs	Cat# E7530S
NEBNext primers for Illumina	New England Biolabs	Cat# E7335b
High sensitivity D500 reagents	Agilent Technologies	Cat# 5067-5593
High sensitivity D500 ScreenTape	Agilent Technologies	Cat# 5067-5592
Mouse IgG Ready-SET-Go	eBioscience	Cat# 88-50400

5X Taq Master Mix	New England Biolabs	Cat# M0285L
Qubit dsDNA HS Assay	ThermoFisher Scientific	Cat# Q32854
HEp-2 ANA assay	Zeus Scientific	Cat# FA2400EB
BirA reaction kit	Avidity	Cat# BirA500
Pierce protein concentrators	ThermoFisher Scientific	Cat# 88521
MinElute Gel Extraction kit	Qiagen	Cat# 28606
Recombinant DNA	**Source**	
VRC4805	Vaccine Research Center	N/A
VRC4803	Vaccine Research Center	N/A
VRC4027	Vaccine Research Center	N/A
Bacteria and Virus Strains	**Source**	**Identifier**
One-Shot Mach1	ThermoFisher Scientific	Cat# C8620-03
LCMV Clone 13	this work	N/A
LCMV Armstrong	this work	N/A
Experimental Models/Organisms/Strains	**Source**	**Identifier**
BHK-21 cell line	ATCC	CCL-10
VERO cells	ATCC	CCL-81
V_H1-2/LCL mice	this work	N/A

2.4.2 The V_H1-2/LCL mouse model

All mice were housed at specific-pathogen-free facilities managed by the Massachusetts General Hospital Center for Comparative Medicine, and were handled according to animal protocol 2005N000360, approved by the Internal Review Board and the Institutional Animal Care and Use Committee.

Tail clips were collected from mice and treated with Kapa Express Extract kit according to the manufacturer's protocol. Resulting DNA was amplified by PCR using the Kapa HotStart ReadyMix PCR kit and the following conditions: 94ºC for 30 seconds, 30 cycles of 65ºC for 1 minute and 72ºC for 1 minute, followed by 72ºC for 5 minutes. The resulting DNA were assessed using a 1% agarose gel with SYBR safe intercalating dye, and imaged on a BioRad ChemiDoc Imaging System.

2.4.3 LCMV propagation and sequencing

Stocks of LCMV Clone 13 and Armstrong were kindly provided by Dr. Sharpe. BHK cells were plated at 20k cells/cm^2 24 hours prior to inoculation and grown in EMEM/10%FBS in 5% $C0^2$ at 37ºC. Plates were washed, with virus was added at an MOI of 0.05 in a volume of 40ul/cm^2 non-supplemented media, rocking occasionally, for 90 minutes. EMEM/FBS was added up to a final volume of 33ul/cm^2 and incubated for 48 hours. Supernatant was collected, centrifuged for 10 minutes at 350rcf at 4ºC, aliquoted, and frozen at -80ºC.

Viral RNA was isolated from fresh virus using the PureLink extraction kit, according to manufacturer's protocols, followed by ribosomal RNA depletion, using a modified version of the manufacturer's protocol in which a 2.2x SPRI bead cleaning was modified to 0.6X, given the relative size of the viral RNAs being isolated. cDNA synthesis was performed using the NEBNext kit, with a fragmentation time modified to 10 minutes and a 2^{nd} stage temperature modified to 30 minutes. During end prep and adaptor ligation, the adaptor was diluted 5x and 100x, respectively. Resulting DNA was enriched by PCR according to the manufacturer's protocol, assessed by TapeStation, quantified using Qubit, assayed on a Qubit 3.0 fluorometer, and sequenced using a MiSeq Nano V2 kit on a standard Illumina MiSeq.

2.4.4 LCMV infection, viral loads, and immunization

LCMV was validated in vivo by infection of 6-week-old C57BL/6 mice purchased from Jackson Labs. Mice were injected with either 4M PFU of Clone 13 via the

retroorbital sinus, or 200k PFU of Armstrong via the intraperitoneal cavity, and were reinfected the same way nine weeks later. CD4 depletion was achieved via two injections of 200ug anti-CD4 antibody 24 hours prior to and 24 hours after infection. Mice were bled via facial vein into EDTA-coated tubes, which were centrifuged at 1700rcf for 10 minutes at 4ºC. Plasma was aspirated, frozen on dry ice, and stored at -80ºC until being thawed for plaque assay assessment.

VLs were determined by plaque assay, performed as described in Kao et al.[157] Briefly, Vero cells were grown in EMEM/10%FBS/1% penicillin/streptomycin and plated in 6-well plates at 150k/well in 4ml of EMEM overnight. EMEM was removed and replaced with 400ul of diluted virus, prepared by diluting viral stocks, infected sera, or infected plasma with RPMI 1640. Plates were returned to the incubator for 60min, with gentle rocking every 10min. 199 media was prepared from powder at 2x concentration, buffered with sodium bicarbonate, and mixed 4:1 with FBS. This was combined 1:1 with a 1% agarose solution and cooled to 45ºC. 4ml of this was laid over the cells, which were returned to the incubator for 5 days. On day 6, another 2ml/well of agarose overlay was applied, this time 47.5% 2x 199 media, 47.5% 1% agarose, and 5% neutral red stain. Plates were returned to incubator overnight and plaques were blinded and counted 14h later.

eOD-GT8 immunizations consisted of 20ug of eO-GT8 per mouse, diluted to 100ul in PBS, combined with 100ul of Alhydrogel, and mixed by rotation at room temperature for 20 minutes. Immunizations were delivered via intraperitoneal injection.

2.4.5 T cell exhaustion

Blood obtained as described above, after plasma had been isolated, was resuspended in ACK lysis buffer for 2 minutes, diluted with PBS, centrifuged at 500rcf for 5 minutes at 4ºC, resuspended and washed in ice cold PBS, and stored in FBS/10% DMSO at -150ºC.

For FACS analysis, cells were thawed, washed once in ice cold PBS, and incubated with Blue Viability Dye for 30 minutes on ice. After being washed once with cold PBS, cells were incubated with Fc block/anti-CD16/anti-CD32 for 30 minutes on ice, washed with cold PBS/1% BSA, resuspended in PBS/Brilliant Stain Buffer, and stained for 30 minutes on ice with a cocktail of antibodies specific the following markers: CD4, CD8, CD19, CD44, and PD-1. Following this, the cells were washed with cold PBS/BSA and assayed on a five-laser LSR Fortessa flow cytometer.

2.4.6 Plasma IgG ELISA

Plasma antibody concentrations were established using the Ready-Set-Go kits manufactured by eBiosciences, according to their protocols. The finished plates were read on a Tecan Infinite M100 pro plate reader.

2.4.7 HEp-2 assay

To determine the presence or absence of cell-reactive antibodies, a human SLE clinical diagnostic assay was repurposed. The Zeus ANA Hep-2 test system was employed, substituting the kit's labeled antibody with goat-anti-mouse IgG antibodies. Other reagents were used as directed, with serum and plasma dilutions ranging from

1:40 to 1:1280. Serum from MRL mice was used as a control, and each well was imaged with identical microscopy settings on a Zeiss Axio Imager.Z2 with a Mamamatsu C11440 camera and a Tissue Gnostics slide scanner.

2.4.8 Protein production and labeling

Plasmids (VRC4805, VRC4803, and VRC4027), kindly provided by Dr. John Mascola at the National Institute of Allergy and Infectious Diseases, were transfected into Mach1 bacteria, grown in lysogeny broth supplemented with kanamycin, and isolated using a Qiagen maxiprep kit according to manufacturers' protocols.

Gp140 was expressed in HEK293F (ThermoFisher) cells and purified as described previously.[158-160] Briefly, cells were transfected with 0.5μg/mL plasmid DNA (polyethyleneimine, PEI) and were allowed to express for 5 days. Supernatants were clarified via centrifugation, filtered through a 0.22μm polyethersulfone membrane (EMD Millipore), and buffer exchanged using tangential flow filtration (TFF). The supernatant was incubated overnight with Ni-NTA Sepharose resin (Cytiva), washed with 20mM imidazole and eluted in 500mM imidazole. The protein was further purified via size exclusion chromatography (SEC) using the ÄKTA-pure protein purification system (GE Healthcare) and a Superdex200 Increase 10/300 GL column in 1X PBS. A similar procedure was used to produce eOD-GT8 and ΔeOD-GT8 constructs above, with a few modifications: expi293F cells (ThermoFisher) were used instead of HEK293F cells, expifectamine (ThermoFisher) served as the transfection reagent, and 1μg/mL plasmid DNA was used in the transfections.

Labeling of the eOD-GT8-Avi and eOD-GT8-Avi monomers was achieved beginning with biotinylation using an Avidity kit, according to the manufacturer's protocol and incubated at 4ºC overnight, followed by purification by SEC using a Superdex200 Increase 10/300 GL column in 1X PBS. Biotinylated proteins were then conjugated to fluorescently-labeled streptavidin. One quarter of the required moles of streptavidin were added to each biotinylated protein, then incubated, rotating, at room temperature, for 20 minutes, four times. Resulting flow probes were diluted in PBS and frozen at -80ºC.

2.4.9 Flow cytometry

Murine splenocytes were thawed, washed twice in ice cold PBS, resuspended in LIVE/DEAD Blue viability dye, and incubated for 30 minutes on ice. The cells were washed in PBS/1% BSA, then resuspended in a 1:40 dilution of FC block:PBS and incubated on ice for 30 minutes. Staining tetramers were added to a final concentration of 50nM and were incubated for 30 minutes on ice. 50ul of Brilliant Stain buffer were added, followed by staining antibodies, and incubated for an additional 30 minutes on ice. Cells were washed as above, resuspended in PBS, and assessed using a five-laser LSR Fortessa.

2.4.10 Single-cell sorting and BCR sequencing

Sorting was performed on an Aria II (SORP) using a 100um nozzle, and cells were sorted dry into 96-well plates, then flash frozen on dry ice. Cells were lysed in a tris buffer containing RNAse inhibitor, tRNA, and NP-40, under the following conditions:

95ºC 3min, 10ºC hold. RT buffer was added (2ul 5x first-strand buffer, 0.5ul 0.1M DTT, 0.5ul 10mM dNTPs, 10U of SuperScript III, 5pmol of oligo-dT), and cDNA synthesis was performed at 50ºC for 60min. PCR 1 consisted of 3ul cDNA, 1ul 10x PCR buffer, 1ul 2mM dNTPs, 10pmol primer 1+3, 10pmol primer 2, 0.5ul Taq, and 3.7ul water, and was performed as follows: 94ºC for 30s, 65ºC for 60s, 72ºC for 60s, repeating steps 1-3 34x, 72ºC 5min, 4ºC hold. PCR 2 consisted of: 1ul of template from PCR 1, together with: 0.2ul 10mM dNTPs, 10pmol primer 1+3, 10pmol primer 4, 0.1ul Taq, 1ul 10x PCR buffer, 5.6ul water, and was performed as follows: 94ºC 30S, 65ºC 60s, 72ºC 60s, repeat steps 1-3 25x, 72ºC for 5min, 4ºC hold.

PCR 2 reactions were run on a 1% agarose gel, visualized with SYBRSafe dye and brief UV illumination, excised, and gel-extracted using a Qiagen kit according to manufacturer's protocols. Amplicon concentrations were quantitated using a Nanodrop 2000 and Sanger sequenced by the Massachusetts General Hospital DNA Core Facility.

Collaborator contributions and acknowledgments
Dr. Alt contributed two V_H1-2/LC mice from which the V_H1-2/LCL mice were derived.
Dr. Seaman's laboratory contributed the neutralization assays reported in section 2.2.3.
Dr. Lingwood and Julia Bals contributed the gp140 immunogen used in section 2.2.3, as well as the proteins used to construct the flow probes used in 2.1.2 and 2.1.4
Dr. Murali contributed interpretations of the modified HEp-2 assay.
Mike Waring, Nathalie Bonheur, and Eric Koscher contributed FACS expertise.
Manuscript preparation: MK, SP, GK, JB.

CHAPTER 3: Impaired tolerance in the context of vaccine responses

"The Grim Squeaker"

Illustration by Paul Kirby, reproduced with permission from the artist

SUMMARY

Chapter 3 presents research performed concurrently with and consecutively to the work presented in chapter 2 and focuses initially on a large-scale vaccine study. The design of this study was intended to generate data responsive to three aims: to characterize novel HIV-vaccine immunogens, to investigate the effects of impaired immune tolerance upon a full time-course of longitudinal immunogens, and to assess the possibility of directing affinity maturation against a specific glycosylation site on HIV Env. However, shortly after the first immunization, a number of mice began to fall ill. Soon after, mice began dying, and by four weeks, had done so in numbers that suggested the deaths observed in this experiment represented a reproducible phenomenon of meaningful biological significance. While the experimental design was modified in order to preserve the original aims, we simultaneously investigated several possible causes of this unexpected mortality.

3.1 INTRODUCTION

3.1.1 Experimental design

In order to build on the data obtained from the experiments performed in chapter 2 and to increase the likelihood of acquiring data that were responsive to the original hypothesis—that the development of autoreactive bnAbs may be constrained by self-tolerance—we turned our attention to more longitudinal experimental designs featuring greater numbers of immunizations and follow-up timepoints. Then-unpublished data from the VRC (Vaccine Research Center, Bethesda, MD) suggested that broad neutralization had been achieved using a stepwise immunization strategy in the V_H1-2/LC mouse model. The study in question utilized eight to nine boosts,[161] leading our

collaborators to design novel immunogens for a similar stepwise immunization experiment, specifically aiming to explore the possibility of reducing the number of immunizations required (Fig. 3.1.1).

112 mice were immunized with the same prime immunogen, followed later with a different boosting immunogen. Following the first boost, the mice were to be divided into six groups. Five immunization regimens were to be tested, while in a sixth group, we would collect data responsive to the hypothesis tested in chapter 2: that impaired B cell tolerance, arising from persistent HIV infection, facilitates the development of autoreactive bnAbs. While chapter 2 used MRL/lpr mice and LCMV infection as contexts in which impaired self-tolerance would permit the production of autoreactive antibodies, this experiment was meant to use a chemical tolerance perturbation, pristane (used by Schroeder et al. as depicted in Figure 2.3 and discussed in section 3.1.5.). Of the six groups of mice intended for this experiment, two (Groups C and D) would receive identical immunization regimens, while one (Group D) would be injected intraperitoneally (IP) with pristane, and the neutralization breadth of C and D would be compared.

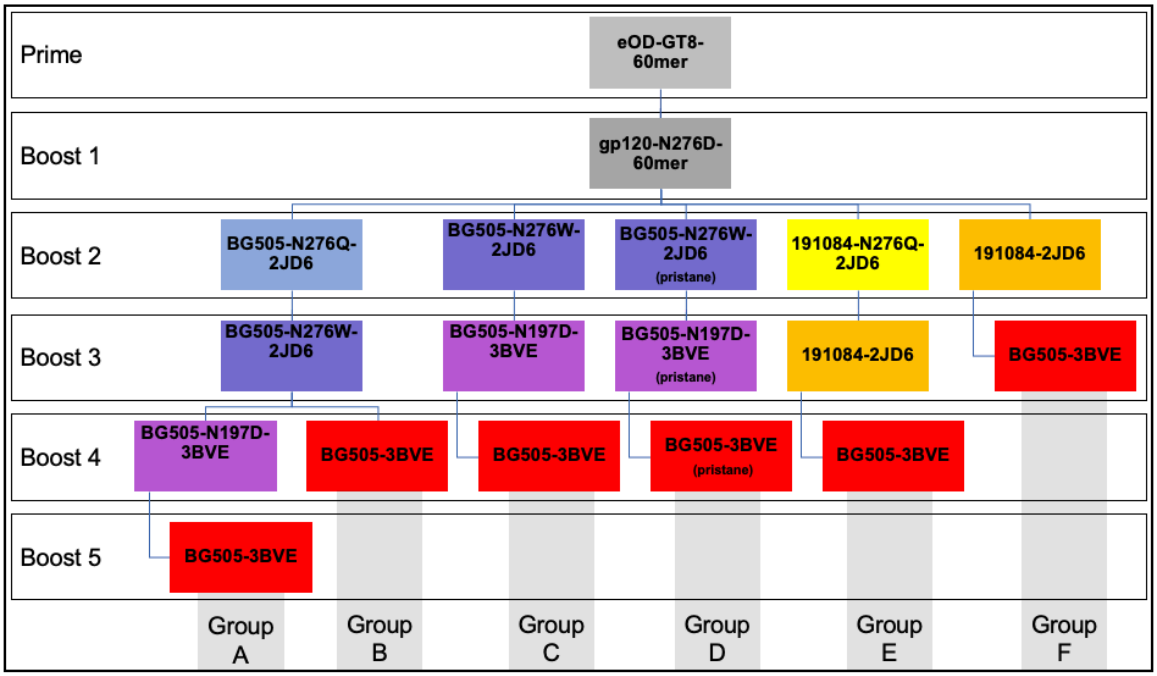

Figure 3.1.1. Immunization schema and experimental design. n = 112 V_H1-2/LCL mice with additional unimmunized controls. Immunizations took place six weeks apart, with four mice per group euthanized concurrently with immunizations. Blood draws were performed two weeks after each immunization. Spleens and lymph nodes were collected at euthanasia, processed, and cryopreserved for FACS and possible monoclonal antibody production. Immunogens in gray have been previously reported. Naming convention for immunogens intended for boosts two through five: BG505/191084 (HIV strains used as backbones on which to present the CD4bs), X###X (amino acid substitutions at or near the CD4bs), and 2JD6/3BVE (different ferritin scaffolds used to assemble the HIV backbones).

Each immunization took place six weeks apart, with blood draws taking place two weeks post-immunization. Four mice per group were sacrificed at each immunization timepoint, from which spleens and lymph nodes were processed and cryopreserved for future FACS analysis and possible monoclonal antibody expression. As the V_H1-2/LCL mice are not fully inbred, the litters which made up the mice used in this experiment—derived from eight breeding pairs—were divided across experimental groups by age, sex, and lineage.

3.1.2 Design elements of novel immunogens

The prime and boost immunogens used in this study were not novel and have been previously reported: eOD-GT8-d41-m3-60mer and gp120core-e-2CC-C1 N276D d41m3-60mer. eOD-GT8 is discussed in more depth in section 1.1.6, but the eOD-GT8 60mer consists of the 172 amino acid eOD-GT8, a 15 amino acid G/S linker, and a 154 amino acid tail. The d41-m3 variety features seven deliberate mutations (four in the tail region and three in the active site), introduced to improve melting temperatures and expression levels. The boost, gp120core-e-2CC-C1 N276D d41m3-60mer, is roughly similar in the tail region. The original core was modified from HIV gp120 in a number of ways, however. The coreceptor binding site was stabilized,[162,163] and the protein was locked into the receptor-bound state by filling hydrophobic pockets in the core and interdomain "stitching" by disulfide bonds.[164] Four pairs of disulfide bonds were tested, and the "2CC" designation refers to those immunogens which bear two of the four, spanning positions 96-275 and positions 109-428.

Following boost one, the nature of the immunogens differed dramatically. These subsequent immunizations consisted of 24mers in which the CD4bs is expressed on an HIV backbone and attached to a subunit of ferritin. It was modifications to these three elements—HIV backbone, ferritin scaffold, and CD4bs—that made up the differences between the five different stepwise immunization regimens designed for this study.

First, the HIV Env backbones used in this study came from either BG505, a subtype A T/F (transmitted/founder) virus whose sequence has seen the most use as stably-modified SOSIP trimers; or 191084, an older clade A strain, utilized here because viruses based on these sequences are generally neutralized more easily by VRC01-like

antibodies than viruses based on BG505-derived sequences. Other BG505 and 191084 sequences used in this study contain 11 alterations designed to improve yield, stability, and the antigenic profile of the CD4bs, collectively referenced as MD39. Likewise, all of the BG505 sequences contain additional glycosylations to the Env backbone which mask off-target epitopes, collectively referenced as G41. The relative ease with which 191084 is neutralized by VRC01 is the main reason it was utilized in these designs (unpublished communications with Dr. Schief). Several experimental groups in this study begin with 191084-based 24mers before transitioning to BG505-based 24mers as a way of lowering the bar for affinity maturation at the difficult transition from the proven boost one immunogen to the novel (but unproven) immunogens.

Second, the ferritin sequences used in this study differ from one another both by experimental group and by boost order. Ferritin has been studied for more than 30 years, and each monomer is a small protein consisting of five helices. The monomers self-assemble to form exceedingly stable nanospheres which display three- and four-fold axes of symmetry, permitting ferritin to be used for a number of different antigen-presentation purposes. The ferritin sequences used in this study are derived from either *Pyrococcus furiosus,* Protein Databank (PDB) ID: 2JD6 or *Helicobacter pylori* (PDB: 3BVE), and are referred to by their PDB tags in Figure 3.1.1. As these ferritin scaffolds are intended to be repeatedly administered in the context of an adjuvant, it is possible that an anti-scaffold immune response might arise. As the HIV epitopes in question are already difficult to target, these scaffold-specific immune responses might interfere with immunizations by altering immunodominance hierarchies and swamping the CD4bs-

specific response, or by setting the stage for a strong antibody response to the next immunization.

Lastly, the specific amino acids of the binding site region were modified in several groups of this experiment. In some cases, an experimental group progresses from the first boost, the deglycosylated gp120core-e-2CC-C1 N276D d41m3-60mer, straight to a glycosylated 24mer. In most groups, however, intermediate immunogens were designed with an eye towards guiding the affinity-maturing B cells. Several groups use an intermediate N276Q, as well as N276W, and/or modulate a nearby N-glycosylation site at N197, to minimize steric hinderance during BCR binding. All groups, however, eventually end with the same immunogen, BG505-MD39-G41-3BVE.

3.1.3 Modified experimental design

Roughly two weeks after the first immunization, several mice began to exhibit behavioral changes. They showed reduced animation in response to normal stimuli like cage movement and gentle handling. Some developed hunched posture and ruffled fur. Of those, several began shivering, trembling, or convulsing, though these terms are used strictly to describe the observed behavior, not to suggest any particular etiology. Several mice developed large skin lesions and were euthanized. When autopsied, most displayed pronounced ascites. It was observed during handling that the body temperature of the sickest mice was noticeably lower than that of their healthy cage-mates. When measured by hand-held infrared detector, the mice that appeared most sick were often around 25ºC, while their healthy cage-mates were closer to 30ºC. These measurements were merely a superficial snapshot of the temperature of their rear

dorsal fur, not a careful assessment of their internal body temperature, but it was dramatic enough that after having observed several instances of unassisted mortality following a precipitous drop in body temperature, it served as an additional metric by which to determine which mice were closest to dying. This permitted the acquisition of tissue samples from sick mice; tissues collected from dead mice were too disrupted for meaningful analysis.

Unassisted deaths began occurring roughly two to three weeks post-immunization, and before long had occurred in sufficient quantities to permit statistical analyses, which prompted alterations of the experimental design. A possible cause, discussed in section 3.3, was identified, and the experiment was altered according to two needs: first, to reduce the suffering of the mice, and second, to fulfill the original aims of the experiment. For the latter, all of the mice were pooled into what had been referred to as Group E (Fig. 3.1.1); all of the mice would receive the same immunizations, and be bled and sacrificed on the same timeline, in the hopes that sufficient samples could still be collected by the conclusion of the experiment. For the former, the majority of mice would receive their immunizations with an alum-based adjuvant, while only a small handful of mice would continue to receive the original adjuvant, Sigma Adjuvant System.

3.1.4 Sigma Adjuvant System

Sigma Adjuvant System (Sigma-Aldrich, product No. S6322) is an adjuvant that consists of only four ingredients: squalene, Tween-80, synthetic trehalose dicorynomycolate (TDM), and monophosphoryl lipid A (MPL). The latter two are

variations on bacterial glycolipids. Tween-80 is a non-ionic surfactant, and squalene is a short hydrocarbon oil that is used to create the oil-in-water emulsion that is eventually injected.

This product is known as SAS and is sometimes also referred to as RIBI. A former product (Sigma-Aldrich product No. M6536), which was discontinued by Sigma's supplier in 2007, also went by the name RIBI, was also a TDM/MPL adjuvant, and was used to induce experimental autoimmune encephalomyelitis (EAE) in mice. Sigma began manufacturing SAS under its own name, but the formulation has remained unchanged, according to MilliporeSigma Research Content and Reagents representatives.

3.1.5 Pristane and squalene

Pristane (2,6,10,14-tetramethylpentadecane) is an oil that has been used in research for decades. When administered by IP injection to mice, it causes inflammation,[165,166] autoantibody production,[167] and renal damage.[168] It induces lupus-like humoral autoimmunity even in non-autoimmune-prone mice. It was used as the self-tolerance perturbation in Schroeder et al., discussed in sections 2.1.3 and 2.3, and we intended to use it in Group D of this experiment to the same effect.

Other short hydrocarbons besides pristane have been shown to have similar immunomodulatory effects as well. Squalene is a naturally-occurring short hydrocarbon that is used as a synthetic intermediate in steroid synthesis[169] and is secreted by sebaceous glands in the skin.[170] An interesting study assessed the effects of IP injection of pristane, squalene, Incomplete Freund's Adjuvant (IFA), and several non-adjuvanted

medicinal mineral oils, and showed that both pristane and squalene induced autoreactive antibodies and inflammatory cytokine production.[171]

Squalene is a component of the Sigma Adjuvant System which was employed in the experiments detailed here.

3.2 RESULTS

3.2.1 Antibody responses to prime and boost one

Two weeks after priming all mice with eOD-GT8-60mer, sera were collected and tested by ELISA for binding against two targets: eOD-GT8 itself, and a modified eOD-GT8 in which only the CD4bs has been mutated (GT8-KO). All mice demonstrated the capacity to produce antibodies against the GT8 priming construct (Fig. 3.2.1).

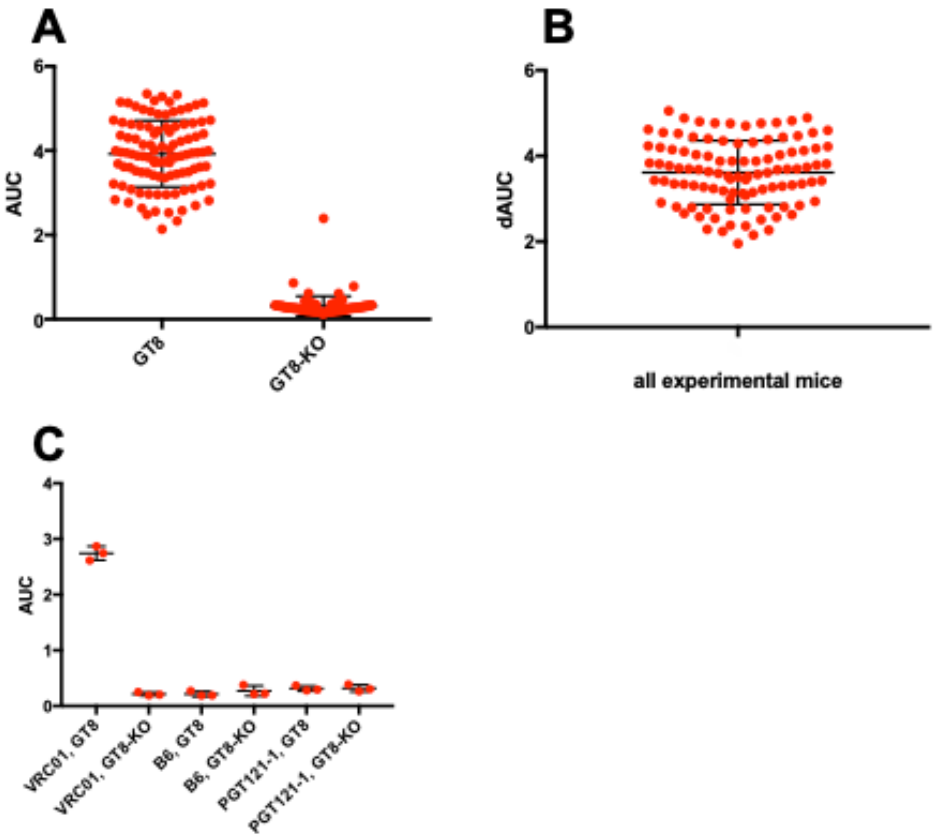

Figure 3.2.1a. Sera demonstrated low off-target antibody responses 14 days post-GT8-prime. (A) Sera were assessed by ELISA for binding to GT8 and GT8-KO immunogens. Sera were diluted 20-fold six times, and the AUC (area under curve) was calculated for binding to the GT8 as well as the GT8-KO. (B) Change in AUC between the binding to both constructs for each mouse, indicative of antibody responses which are specific for the CD4bs of GT8, n = 110. (C) AUC of bnAb controls for the same constructs. Error bars represent mean and standard deviation.

Likewise, almost all mice did not make appreciable antibodies against the construct with an altered CD4bs, implying that the antibodies being generated in these mice are specific not just for the immunogen, but for the CD4bs of the immunogen.

3.2.2 Antibody responses to boost two and boost three

Two weeks post boost two (191084-N276Q-2JD6, here referred to as boost N276Q) and two weeks post boost three (191084-2JD6, here referred to as boost N276), a portion of the mice were bled and their antibody responses were assessed.

After boost N276Q, all mice demonstrated antibodies against this immunogen, and these antibodies remained in circulation until after boost N276 (Fig 3.2.2). After boost N276Q, mice did not appear to be producing antibodies against any portion of the immunogen other than the CD4bs, as demonstrated by their lack of reactivity to the KO antigen. However, that changed after immunization with boost N276; at this timepoint, most mice appeared to be making antibodies against not only the N276Q and N276 immunogens, but also against the KO versions of those immunogens as well, implying that antibodies had been generated against portions of the immunogen other than the CD4bs. The AUC (area under the curve) against the 191084-N276-KO construct was considerably smaller than the AUC against the boosting immunogen, which implies that there were considerable antibody titers being created against the CD4bs of the N276 boosting immunogen. Binding to BG505 versions of these immunogens, however, was greatly diminished, suggesting that while the 276 blockade may have been overcome in the context of particles utilizing the 191084 HIV backbone, the same is not true in the context of particles utilizing the BG505 backbone. Most curious, however, is that the mice appeared to have antibodies against 191084-N276 not only after boosting with that immunogen, but also before having been exposed to it.

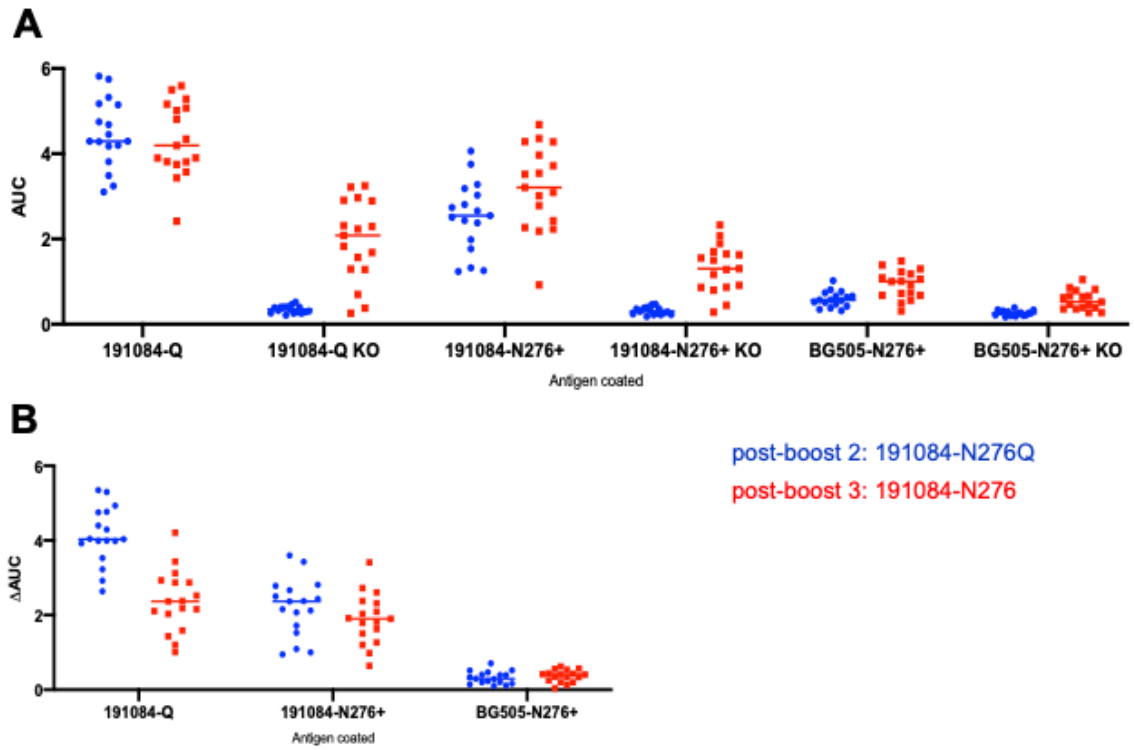

Figure 3.2.2. Sera demonstrated unusual patterns of affinity that do not suggest an N276 blockade. Sera from two timepoints, 14- and 20-weeks post prime (two weeks after boost two and two weeks after boost three) were assessed for binding to a panel of constructs. (A) AUC of binding against the boost two immunogen, boost three immunogen, and BG505 featuring a glycosylation at position 276, as well as their respective CD4bs mutants (KO). (B) Delta-AUC representations of Panel A. n = 17, those mice that survived to 20 weeks and from which sera was available at all previous timepoints. Figure adapted from Dr. Alessia Liguori, Scripps Research Institute.

3.2.3 Initial mortality

Shortly after the first immunization, several mice began expiring unexpectedly. The early experimental interventions took place as initially planned, and samples were banked: prime at week 0, blood draw at week two, boost and euthanasia at week six, and blood draw at week eight. Concurrently, data was collected on the distribution of mortality across a number of factors such as sex, lineage, and age, and compiled in the form of Kaplan-Meier plots (Fig. 3.2.3). These data represent mice that were found dead or had to be euthanized due to apparent suffering, while mice that were euthanized as

part of the originally scheduled timepoints were excluded from these analyses except where explicitly stated.

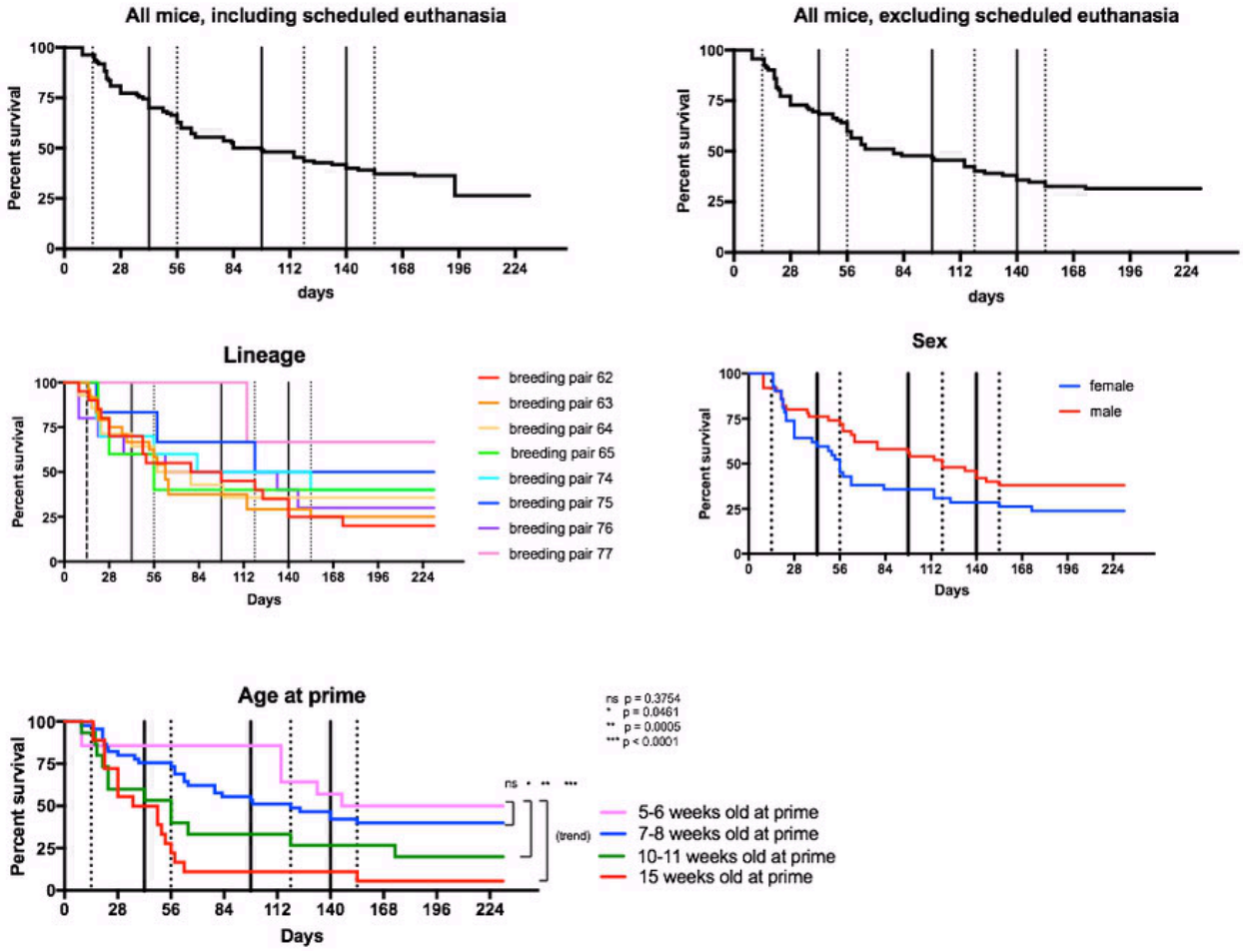

Figure 3.2.3. Unexpected mortality in VH1-2/LCL mice associated with age. Kaplan-Meier survival curves encompassing deaths that occurred during immunization. All panels except for top left are calculated excluding those mice that were euthanized on schedule for sample collection as part of the original experimental design. Other panels represent survival curves of the same mice but displayed according to the different criteria, including which breeding pair each mouse was derived from, the sex of each mouse, and the age of each mouse at prime. Solid vertical black lines represent immunizations and dotted vertical lines represent blood draws. n = 112 on day 0. p-values calculated using Mantel-Cox log-rank test. No statistical difference was observed by lineage or sex.

As the mice were derived from eight breeding pairs of partially-inbred mice, we first assessed the mortality by lineage—that is to say, from which breeding pair each

mouse had originated. No statistical significance was found. Likewise, the sex of the deceased mice was not statistically significant. However, there was a strong statistical association between mortality and the age of the mice at the onset of the experiment. Mice that were older when the experiment began were far more likely to die than mice that were younger. The pattern of mortality observed in this experiment has been observed in multiple experiments utilizing the V_H1-2/LCL mice immunized with eOD-GT8 and SAS (reported in chapter 4), and has occurred using multiple different batches of immunogen produced months and years apart.

3.2.3 Renal pathology

The symptoms observed in the ill mice were too general to indicate any one particular mechanism that might explain this unexpected mortality. Nevertheless, it was suspected that squalene might be playing a role, and this was the first possibility that was investigated. Given that a systemic SLE-like syndrome with glomerulonephritis is commonly observed when pristane is used to breach humoral self-tolerance, and that pristane and squalene had been shown to have similar effects in mice, kidneys were collected from seemingly healthy V_H1-2/LCL mice, as well as from mice that had been immunized as part of the stepwise immunization experiment, and that were euthanized between the first and second boost because they were perceived to be in pain or distress. H&E staining clearly demonstrated that each of the mice euthanized for apparent suffering had experienced profound kidney damage, while the unimmunized controls had not (Fig. 3.2.3a).

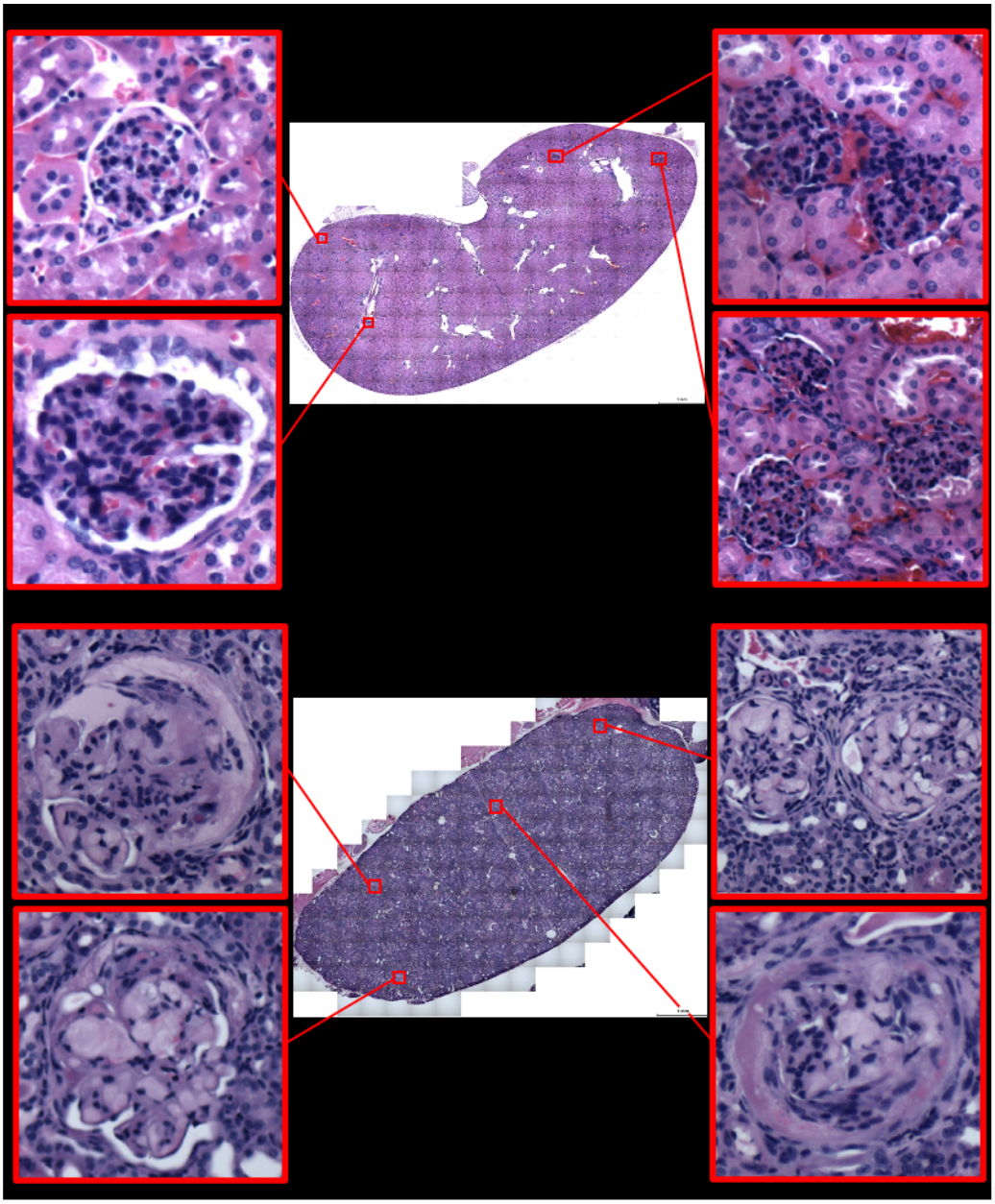

Figure 3.2.3a. Profound renal disruption was present in those mice euthanized for apparent illness, and only in those mice. Hematoxylin and eosin staining of kidneys collected from unimmunized, apparently-healthy V_H1-2/LCL (top) and immunized, apparently-ill mice (bottom) euthanized due to apparent suffering during the above stepwise immunization experiment. Panels are representative fields of view and are representative of five mice per group. Original magnification 400x, n = five per group.

The kidneys of the apparently-healthy mice that had not been immunized appeared fairly normal. Glomerular loops were thin, tubules normal, and Bowman's

spaces were unobstructed. In the apparently-sick mice, however, glomerular loops were quite thick, and Bowman's spaces were obstructed by fibrino-cellular crescents, typically a sign of rapidly progressive glomerulonephritis. In some fields of view, what appeared to be inflammatory cells were present in high frequency. Additionally, kidney sections were stained for murine IgM (Fig. 3.2.3b). IgM staining in apparently-healthy mice was minimal across the kidney as a whole, though some small pockets of signal were detected, almost exclusively within glomeruli. The glomeruli themselves were sometimes faintly outlined, while the pockets were very strongly stained. They did not appear to correspond to a particular cell type, though their brightness made such discrimination difficult. The variation in size suggested the possibility that they may have represented a combination of several different histological features. In the mice which had been immunized, appeared to suffer, and were euthanized, IgM staining in the kidney was profound and global. Every glomerulus was brightly stained.

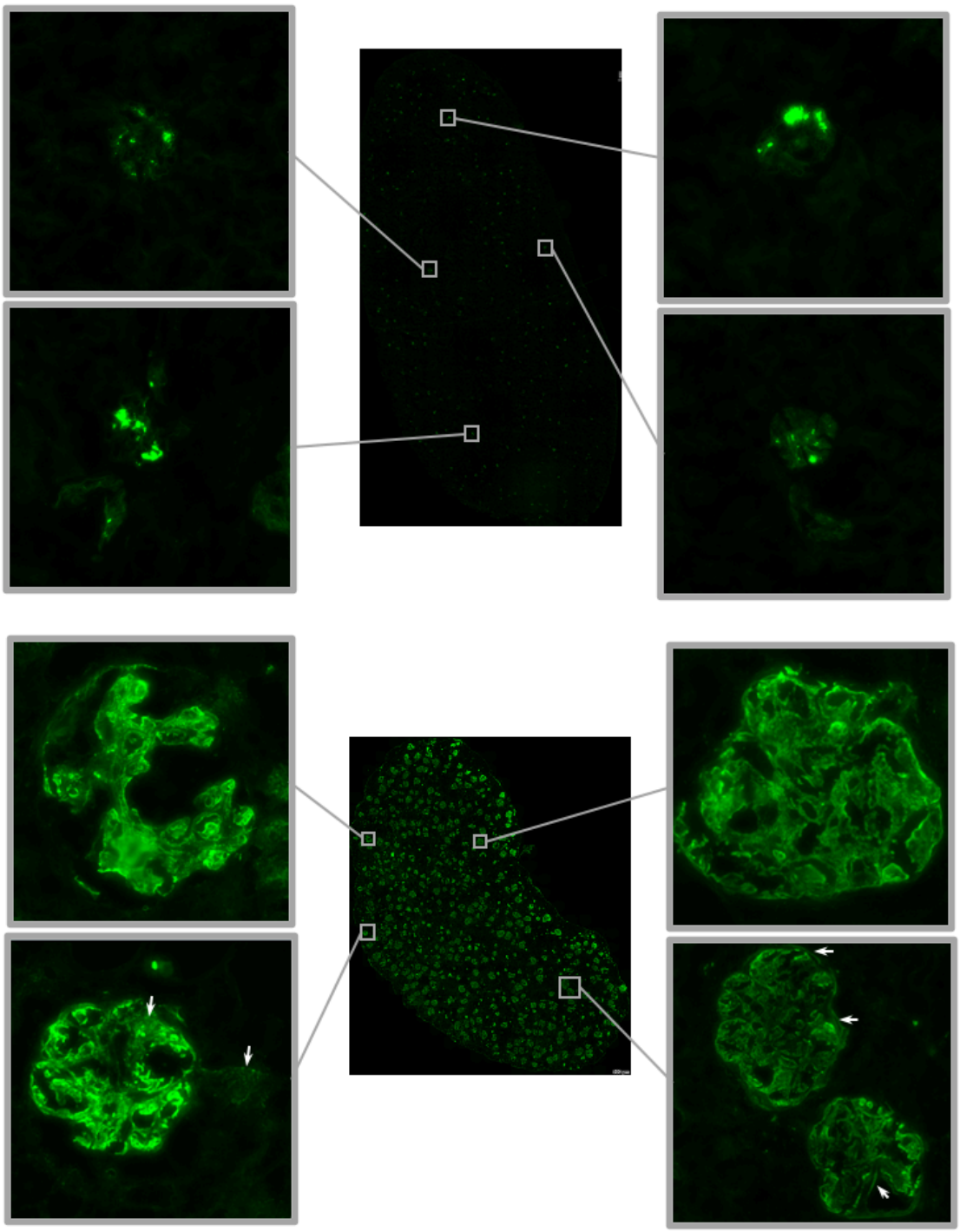

Figure 3.2.3b. IgM staining suggested that renal pathology was antibody-mediated. Immunofluorescent IgM staining of kidneys collected from unimmunized, apparently-healthy V_H1-2/LCL (top) and immunized, apparently-ill mice (bottom) euthanized due to apparent suffering during the above stepwise immunization experiment. Original magnification 400x. IgM depicted in green. Images acquired using identical microscope settings. White arrows denote examples of granular staining patterns (left), or linear staining patterns (right).

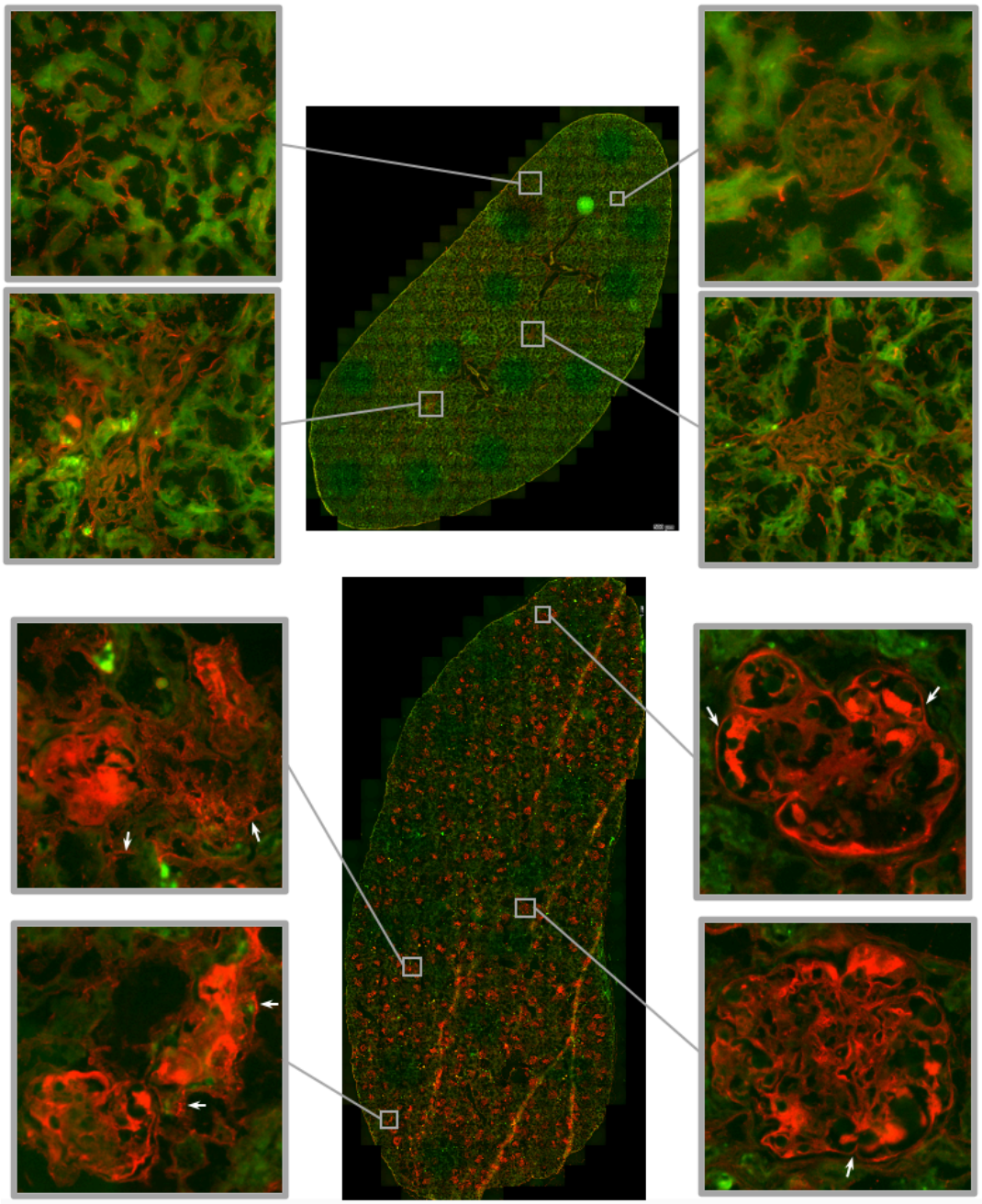

Figure 3.2.3c. IgG staining did not distinguish between direct antibody binding or immune complex deposition. Immunofluorescent IgG staining of kidneys collected from unimmunized, apparently-healthy V_H1-2/LCL (top) and immunized, apparently-ill mice (bottom) euthanized due to apparent suffering during the above stepwise immunization experiment. DAPI depicted in green. IgG depicted in red. Images acquired using identical microscope settings in the IgG channel. White arrows denote examples of granular staining patterns (left), or linear staining patterns (right). Original magnification 400x, n = five per group.

As in the IgM staining, in the mice that had been apparently-healthy when euthanized, IgG staining (Fig. 3.2.3c) in the kidney was dim and diffuse. However, in these mice, IgM and IgG appeared to stain different microscopic features. While the IgM staining consisted almost entirely of small bright dots, IgG staining, for the most part, did not. While a number of smaller IgG+ foci were present, IgG staining in these mice tended to outline glomerular basement membranes (GBM). In the mice that were euthanized as a result of their presumed suffering after immunization, IgG staining throughout the kidneys, like IgM, was extensive and global, with particular intensity within the glomeruli. The patterns observed could not rule out either direct antibody binding or immune complex deposition, as the characteristic linear and granular staining patterns often observed in those cases were both present in different fields of view. Both IgG and IgM appeared in places to be staining the mesangial spaces as well, though further immunohistochemistry would be required to validate these observations.

3.2.4 Observed mortality was due to the combination of SAS and the V_H1-2/LCL model

In order to elucidate which elements of the mouse-adjuvant-immunogen triad were either necessary or sufficient to generate the observed phenotype, a small study was conducted in which C57BL/6 and V_H1-2/LCL mice were immunized with various combinations of eOD-GT8 and SAS (Fig. 3.2.4).

A

Group	A	B	C	D	E
Strain	C57BL/6	C57BL/6	V_H1-2/LCL	V_H1-2/LCL	V_H1-2/LCL
SAS		✓	✓	✓	
eOD-GT8		✓	✓		✓

B

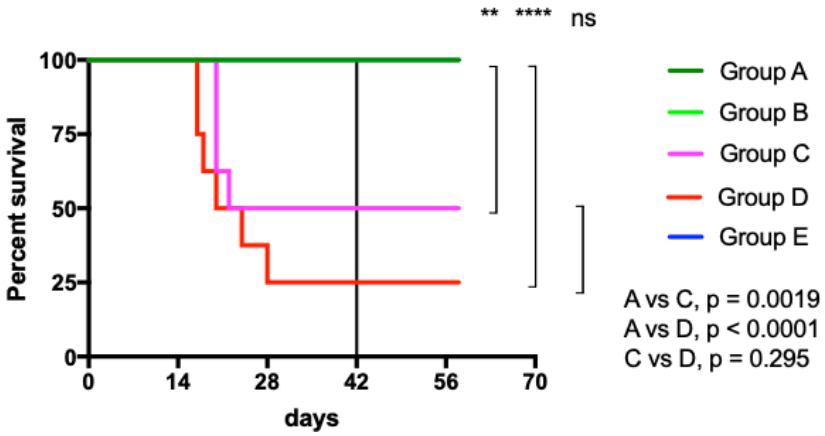

Figure 3.2.4. Lethal immune response requires both VH1-2/LCL mice and SAS. Groups of C57BL/6 or V_H1-2/LCL mice were immunized with SAS and/or eOD-GT8, with the same dose, volume, concentration, route, and timing as in the previous stepwise immunization experiment. (A) Immunization scheme and experimental design. (B) Kaplan-Meier survival curve. n = 8 mice per group, with the exception of Group A, where n = 16. p-values were calculated by Mantel-Cox log-rank test. Vertical black line represents boost.

Group A consisted of 16 C57BL/6 mice immunized only with PBS, and served as a baseline control for lethality that might be associated with the immunization process itself in the form of organ damage or sepsis. Group B also consisted of C57BL/6 mice, but was immunized both with GT8 and SAS, as was Group C. Both Groups B and C were immunized with the same preparation of adjuvant and immunogen. Groups C and D were likewise comprised on V_H1-2/LCL mice, and received either SAS alone or GT8 alone. Of the deaths which occurred as a result of this experiment, none were by euthanasia, and all took place within the timeframe suggested by the stepwise immunization experiment. Each death took place within Groups B or C: V_H1-2/LCL mice that had been injected with SAS, with and without GT8. No deaths occurred in any other

groups. There was no statistically significant difference between the survival curves of groups B and C.

3.3 DISCUSSION

3.3.1 Antibody responses following stepwise immunization

Two weeks post-prime, every mouse exhibited antibodies against the priming immunogen, eOD-GT8. This was expected, and their lack of affinity for the eOD-GT8-KO construct at the same timepoint suggests that antibody binding took place only at the CD4bs, without off-target binding elsewhere on the immunogen. This assay alone, however, does not distinguish between anti-GT8 antibodies that may have arisen from priming or those that may have been present in these mice prior to priming, the latter being a reasonable expectation given the high frequency of VRC01 precursor-like B cells present in these mice.

Six weeks post-prime, the mice were immunized with boost one (gp120-N276D), and six weeks after that, with the N276Q boost. Two weeks after the N276Q boost, all mice developed anti-N276Q antibodies. As after the GT8 prime, no off-target antibodies were detected with affinity for the N276Q-KO construct, implying that the antibodies after the N276Q boost were specific for the CD4bs. However, as before, this assay cannot distinguish between the presence of these antibodies that existed prior to immunization vs their elicitation by the N276Q boost.

Six weeks after the N276Q boost, the mice were immunized with the N276 (191084-N276-2JD6) boost, the most significant hurdle in this longitudinal time course, as it reintroduced the N-glycan at position 276. Antibody titers after the N276 boost

were higher than before, which can be cautiously interpreted to imply that the N276 boost was successful. However, off-target antibody responses arose concurrently at this timepoint. For the first time, most mice developed significant antibody responses to a knock-out version of the boosting immunogen, the N276-KO construct, suggesting that antibodies had been produced against non-CD4bs epitopes. This conclusion is supported by the simultaneous affinity, at the same timepoint, for other KO constructs. However, for most mice the AUC for antibodies against the 191084-N276-KO construct was considerably smaller than the AUC for antibodies against 191084-N276, which implies that significant amounts of 191084-N276-CD4bs-specific antibodies were successfully elicited by immunization.

However, these antibodies do not appear to cross-react with the equivalent CD4bs when presented on a BG505-based particle. Were this experiment to have continued as originally planned, it is reasonable to expect that the transition from the 191084-based particles to the BG505 particles would have stymied B cell affinity maturation. On the bright side, this does suggest that the incorporation of transitional immunogens based on the 191084 strain may have achieved its aim and might be a valid strategy going forwards.

Lastly, there remains the conundrum of why the mice produced copious amounts of antibodies specific for the CD4bs of 191084-N276 before having been immunized with it. That specific transition at the CD4bs, from deglycosylated N276Q to re-glycosylated N276, is exactly what this experiment was aimed at overcoming, presumably with great difficulty. The simplest interpretation of these data is that the first boost, gp120-core-E, was sufficient to generate antibodies capable of binding even the

glycosylated CD4bs, but only when presented on a 191084-based backbone; the same sera from the same timepoint assayed against the BG505-N276 particle shows almost no binding. This reinforces the interpretation that the use of the 191084 backbone in this study achieved its aim of lowering the bar for affinity maturation against CD4bs epitopes, and suggests that design elements like those intended for Groups A and B of this study (altering nearby positions like N197, as well as other less proximate residues), might warrant greater attention. However, these data also support the alternative view put forth recently that the N276 glycan can be a useful epitope during affinity maturation; that rather than merely generating steric hinderance that occludes antibody binding, it might provide favorable intermolecular interactions to drive affinity maturation.[172]

In the original experimental design, Groups C and D were meant to receive identical immunization regimens, while D was meant to also be injected with pristane in order to impair B cell tolerance and permit the production of autoreactive antibodies. The intent was to compare the sera of groups C and D and assess if impaired humoral self-tolerance was associated with a change in neutralization breadth. The unexpected lethality of the immunizations precluded this comparison, but may have been related to the theme of the experiment. It is possible that instead of impairing B cell tolerance in one group of mice, this experiment may have impaired it in all six groups.

3.3.2 Unexpected mortality

While the data collected up to this point do not permit a detailed mechanistic description of the lethal phenotype observed, they do provide a partial explanation. The

mortality observed in the stepwise immunization experiment was entirely unexpected, given that both the immunogen and adjuvant in question had been used so extensively in the literature. The V_H1-2/LCL mice were unremarkable, given that the chimeric mice that they are related to had been used in HIV-immunogen studies prior to this. One element distinguished them besides their being germline knock-ins and not blastocyst-derived chimeras. The V_H1-2/LC mouse model utilizes the human V gene roughly 40% of the time (Fig. 2.1.4), but does so in conjunction with two light chain options: the VRC01-like knock-in on one chromosome and the normal murine complement of light chain possibilities on the other. The V_H1-2/LCL model, in contrast, has two copies of the VRC01-like light chain, potentially doubling the number of VRC01-precursor-like naïve B cells. This also precludes the possibility of light chain receptor editing.

However, the simplest causes of death are usually the most likely: in this case, endotoxin in the immunogens, complications from retro-orbital blood draws, or cytokine storms induced by perforated bowels or intestines during IP injection.

Bowel perforation leading to sepsis and cytokine storm seems unlikely given the timing of the deaths. Such accidental deaths typically follow the precipitating event quite quickly, usually in a few days or less. In this experiment, however, the overwhelming majority of deaths took place more than 14 days after prime. Endotoxin contamination is also unlikely, given that each batch of protein had been tested for endotoxin levels prior to shipping. Contamination of the proteins during immunization is likewise unlikely, given that this effect has been observed in multiple experiments utilizing several different batches of protein, each made months or years apart. Complications from the retro-orbital bleeding could be said to match the general timeline of the deaths, given

that two to three weeks post-immunization refers to the same temporal window as zero to one week post-blood-draw, but these blood draws were performed by not one but two individuals, neither of whom have experienced any similar issues in other settings of retro-orbital bleeding.

As the mice were not formally inbred, we assessed the possibility that the mice might be dying as a result of some genetic factor inherited by only a portion of the pool of experimental mice. The Kaplan-Meier survival data, when sorted by lineage (breeding pair), suggest that this is unlikely to contribute to why some mice died and others did not. And while the lineage of the mice had no correlation with mortality, age did. Not only were older groups of mice more likely to die than younger groups, but the *trend* across the age groups was decisive ($p = <0.0001$).

As this experiment had been designed to explore whether broadly neutralizing antibody development and impaired B cell tolerance were related, impaired B cell tolerance was one possible explanation for the mortality that had been observed. An investigation was undertaken into factors that might have predisposed the mice towards developing a pathological autoimmune response. That SAS might have impaired humoral self-tolerance is supported by the historical use of the product in experimental autoimmune encephalomyelitis models, as well as the published similarities between the effects of injected squalene and pristane in mice. Furthermore, this notion better fits the patterns mentioned above: age and timing. If the cause of death were dependent on an overwhelming adaptive immune response, a five-week-old mouse might be less likely to produce such a response than a 15-week-old mouse. The timing is also better explained by induced autoimmunity than by other causes of death, as the overwhelming

majority of mice that died after the first prime did so between 14-21 days post-immunization. This would be a bit early by the standards of a typical primary immune response, but is far more probable than a two-week-delayed case of sepsis, and is not outside the realm of possibility if the immune response in question is taking place simultaneously in up to 40% of the transitional and naïve B cell population. And the timing is similar for the mice that died after the second immunization, albeit somewhat faster, which would also be expected of a secondary adaptive immune response. The gradual decrease in deaths after SAS was replaced by an aluminum hydroxide-based adjuvant supports this hypothesis, but it could also be claimed that those mice that were most likely to fall ill had already done so.

With our attention firmly on SAS and suspecting that the squalene may have played a role in these deaths, we began by looking for a finding often observed in pristane-induced autoimmunity, glomerulonephritis. The ascites discovered during necropsies was suggestive of kidney damage, and the histology demonstrated conclusively that severe renal damage had occurred. The H&E staining suggested the extent of the damage, while the immunofluorescent (IF) staining demonstrated that antibodies were present in a manner which suggests a profound abnormality but does not at this time distinguish between direct antibody binding to a renal antigen or the deposition of immune complexes in the kidney. The IF staining did clearly outline the GBM, suggesting that the mice might have autoantibodies directed against the basement membrane, as in Goodpasture's Syndrome. However, immune complex deposition near the glomerular basement membrane is a nonspecific marker in several conditions, so the seeming-specificity for the GBM should be interpreted cautiously.

Several HEp-2 assays were performed using the sera of the sick mice, but no meaningful signal was detected. This ruled out the presence of antibodies to double stranded DNA. These data could be further interpreted as suggesting that the antigens bound directly by these antibodies (in the tissue or as circulating immune complexes) were mouse-specific or kidney-specific, and therefore would not be detectable in human HEp-2 cells. Several anti-C3 IF stains were performed and did not detect meaningful signal within the kidneys, but technical issues have not yet been sufficiently ruled out to say with certainty that complement is not present in the kidneys. As a result, at this time there remains some uncertainty as to whether the mice generated autoantibodies against a specific renal autoantigen, or suffered immune complex deposition near the GBM as part of an immune complex disease.

Only after establishing solid histological evidence that our hypothesis was grounded in reasonable fact were we prepared to perform what amounted to a final lethal challenge study. We posit that this experiment (Fig. 3.2.4) demonstrates that the mortality observed is due to the combination of the modified BCR and the exposure to SAS. The absence of any mortality in the 16 C57BL/6 mice injected with PBS suggests that injection error is not to blame, and the absence of any mortality in the C57BL/6 mice immunized with SAS and GT8 suggests that it is not the combination of the adjuvant and immunogen either. This is supported by the deaths of the V_H1-2/LCL mice that were immunized only with SAS.

3.3.3. Conclusions

After nearly half of the mice had died partway through what would have been a nine-month longitudinal experiment, the decision was made to provide all of the mice with the same immunization series. This abandoned the possibility of comparing the different regimens. The requirement that all non-essential mouse experiments be ended during the early months of the SARS-CoV-2 pandemic precluded the possibility of collecting samples or data from the final timepoint as well. As such, no conclusions can be drawn as to the relative efficacy of the different regimens, or as to the likelihood that the final immunization might have elicited antibodies capable of binding with high affinity to the CD4bs of the BG505 construct. The data from the initial immunizations, however, are still of some use. They do not discount the future use of 191084 as a context on which to present rationally-designed epitopes, as was done here. The pronounced difference in sera binding, at multiple timepoints, to the 191084-N276 construct vs the BG505-N276 construct suggests that future immunogen design should pay close attention not only to the immediate epitope being targeted or bound, but also to the local structures in which they are being displayed.

The data obtained from studying the unexpected mortality strongly suggest that an antibody-mediated immune response results in profound kidney damage, but additional experiments would be required to elucidate an exact mechanism.

3.4 MATERIALS AND METHODS

3.4.1 Immunogen production

eOD proteins were produced by collaborators in Hek293F cells grown in FreeStyle media. 293Fectin was used for transfections of a pHLSec plasmid coding for the immunogen of interest with a C-terminal His_{6x} tag. After 96 hours, proteins were purified from supernatant using a GE HIS-TRAP column followed by Superdex 75 size exclusion chromatography using an AKTA express system. Endotoxin was assessed using the PyroGene Recombinant Factor C Endotoxin Detection System (Lonza). If endotoxin levels exceeded 2EU/50ug at a protein concentration of 1mg/ml, protein preparations were further purified with the ProtoSPin Endotoxin Removal Kit (Norgen).

3.4.2 ELISAs

Microlon 96-well plates were coated overnight with 2ug/ml of eOD-GT8 (or other immunogen as needed) in 25ul. Wells were washed and blocked with PBS + 1% FBS + 5% skim milk + 0.2% Tween20 for 60 minutes. Serum was serially diluted in PBS+ 1% FBS + 0.2% Tween20, added to each well, and incubated for 120 minutes. Plates were washed and alkaline-phosphatase-labeled goat-anti-mouse IgG, diluted 1:200 in PBS + 1% FBS + 0.2% Tween20, was added for 60 minutes. Plates were washed and absorbance was measured at 450nm.

3.4.3 Immunizations, bleeds, and sacrifices

Each vial of SAS was warmed to 42ºC, combined with 2ml of sterile PBS and immunogen, and vortexed for five minutes. Mice were injected IP with 200ul, for a final

dose of 20ug immunogen per mouse. At later timepoints, immunogens were diluted in PBS, combined 1:1 with aluminum hydroxide, mixed, and injected IP as described in section 2.4.4.

Blood was obtained by retro-orbital bleeding via capillary tubes following isoflurane sedation, allowed to coagulate for 30 minutes at room temperature, and centrifuged at 10krcf for 10 minutes. Sera were aspirated and frozen at -80ºC.

Mice were euthanized on the basis of several criteria, as follows. Mice with poor body condition and ruffled fur were put under special observation. Mice that were unresponsive to gentle cage handling had their temperatures taken with an IR thermometer. Those which were dramatically cooler than similarly-housed mice were euthanized if they also displayed poor body condition or ruffled fur. No normally-responsive mice exhibited such cooling. Mice that developed significant dermal lesions were euthanized

3.4.4 Renal processing and microscopy

During necropsy, both kidneys were removed from each mouse; one was frozen and the other way fixed. Frozen kidneys were embedded in Tissue-Tek OCT medium, frozen at -80ºC, and sectioned by cryotome. Frozen slides were air dried, washed in acetone for 10 minutes, and air dried again. Antibodies were diluted with PBS/BSA and incubated for 60 minutes: IgG 1:100, IgM 1:50, and C3 1:20. Stained slides were rinsed in PBS and coverslipped with Vectashield mounting media, with and without DAPI. Formaldehyde-fixed kidneys were progressed through increasing ethanol gradients, into

xylene, then embedded in Surgipath embedding media. Sections were prepared by microtome.

Collaborator contributions and acknowledgments

Dr. Alt contributed two V_H1-2/LC mice from which the V_H1-2/LCL mice were derived. Immunogens were produced in the laboratory of Dr. William Schief, Scripps Research Institute, as were the ELISAs presented in Figures 3.2.1 and 3.2.2. Figure 3.2.2 was created by Dr. Alessia Liguori, Scripps Research Institute.
Dr. Ivy Rosales and Dr. Andrew Lichtman contributed expertise during the interpretation of the histology.
Histological staining was performed at the MGH Histopathology Research Core by Tricia Dellapella and Nicole Brousaides.
Manuscript preparation: MK, SP, GK.

CHAPTER 4: Multiomic analysis of human and murine memory B cells

SUMMARY

The developmental origins of switched memory B cells are unclear and there is limited knowledge as to how these cells differ at the proteome level from naïve B cells and germinal center B cells. Detailed mass spectrometry-based proteomic studies were undertaken of human tonsillar naïve B cells, switched memory B cells, and germinal center B cells, and the same sorted samples were also transcriptomically analyzed using RNAseq. RNAseq was also undertaken on human plasma cells and murine B cell populations. While germinal center B cells differ considerably from other B cell populations, as expected, human switched memory B cells closely resembled naïve B cells proteomically, differing primarily in proteins that relate to DNA replication and cell cycle.

4.1 INTRODUCTION

Memory B cells are long-lived B cells that can mediate anamnestic antibody responses to antigens after infection or immunization. One goal of vaccinations is to produce long-lived plasma cells that secrete high-affinity antibodies for extended periods of time and also to generate memory B cells that can initiate more rapid responses upon re-exposure to a pathogen.

Although IgM memory B cells represent a significant proportion of memory B cells,[173] class-switched memory B cells predominate. The development of memory B cells has only been examined in rodents and it is generally considered that most switched memory B cells emerge relatively early from germinal centers.[109,110] Other studies have revealed that switched memory B cells can also be generated in the absence of germinal centers.[115,174,175] To date no human studies have established

whether switched memory B cells develop in a germinal center-dependent or GC-independent manner.

Although switched memory B cell development requires signals from the BCR and CD40, these cells may develop in the context of less robust T cell help, poorer induction of mTORC1, and the induction of high levels of BACH2.[125,176] Apart from BACH2, transcriptional regulators that induce memory B cell differentiation include HHEX and TLE3.[121] More robust T cell help and consequently higher mTORC induction induces c-MYC and MIZ-1 and these transcriptional regulators promote plasma cell differentiation while repressing the development of memory B cells.[120,177,178] However, less is known about the factors that mediate the maintenance of switched memory B cells.

Identification of human memory B cells has long relied on CD27, a member of the TNF receptor superfamily, and this marker has been used to differentiate antigen-experienced, post-GC B cells such as memory B cells, plasma cells, and plasmablasts from non-antigen-experienced B cells such as immature, transitional, and naïve B cells. However, marginal zone B cells, which secrete low-affinity IgM and self-renew in the periphery, express CD27, as do a subset of B cells in human cord blood. Well-defined markers, similar to CD27 in humans, are lacking for murine memory B cells. Several groups have made strides in identifying and classifying memory B cells in mice,[106,179] but a single phenotypic definition of murine memory cells has yet to be widely agreed upon. That being said, informative studies can and have been performed using definitions based on a combination of flow cytometry phenotypes and functional criteria,

such as antigen-specificity and the length of time between initial and secondary exposure to that antigen.

The biology and origins of switched memory B cells still remain poorly understood. Although most immune cells are generally studied in great detail in transcriptomic terms, functional differences in cells would obviously best be revealed by unbiased proteomic approaches. Indeed, studies comparing unbiased proteomics and transcriptomics on pancreatic cancers, performed in parallel, have revealed a very different profile of protein and gene expression.[180]

There have been many transcriptomic studies on human and murine memory B cells, but far fewer proteomic studies to date. One such study was a broad survey on all human blood cells and the depth of information accrued on memory B cells was limited.[181] We performed both transcriptional and proteomic studies on purified naïve, switched memory, and germinal center B cells from human tonsils to better understand the biology of memory B cells and to also gain additional knowledge about germinal center B cells.

Steady state transcriptomic data captures alterations in gene expression that reflect transcription, RNA processing, and RNA stability. Steady state proteomic data reflect transcriptomic states amended by layers of protein translation, regulation of translation by miRNAs, post-translational changes, and eventual protein stability. We note here that in cells that are vastly different, such as germinal center B cells on one hand and naïve or memory B cells on the other, there is significant overlap between transcriptomic and proteomic data, whereas in more similar cells, such as memory B cells and naïve B cells, there is very little overlap between transcriptomic and protein

data and it is proteomic data that provides a clear picture of the pathways that define and distinguish memory B cells from their naïve counterparts. To ask whether switched memory B cells can develop in the absence of germinal centers, we studied memory B cells in thoracic lymph nodes of severe COVID-19 patients who lack discernible germinal centers. These data indicate that, as has been established in rodents, switched memory B cells in humans can also be generated in the absence of germinal centers.

4.2 RESULTS

4.2.1 Memory and naïve B cells have largely overlapping transcriptomes

Principal component analysis of the RNAseq libraries generated from human B cells shows clustering of naïve and memory B cells, as well as of GC and antibody secreting cells (ASCs) (Fig. 4.2.1a). These data are consistent with the known metabolic profiles of these populations, with naïve and memory B cells exhibiting far less need for ongoing anabolic processes involved in either the rapid cell division of GC B cells or the high-volume protein synthesis and secretion seen in ASCs.

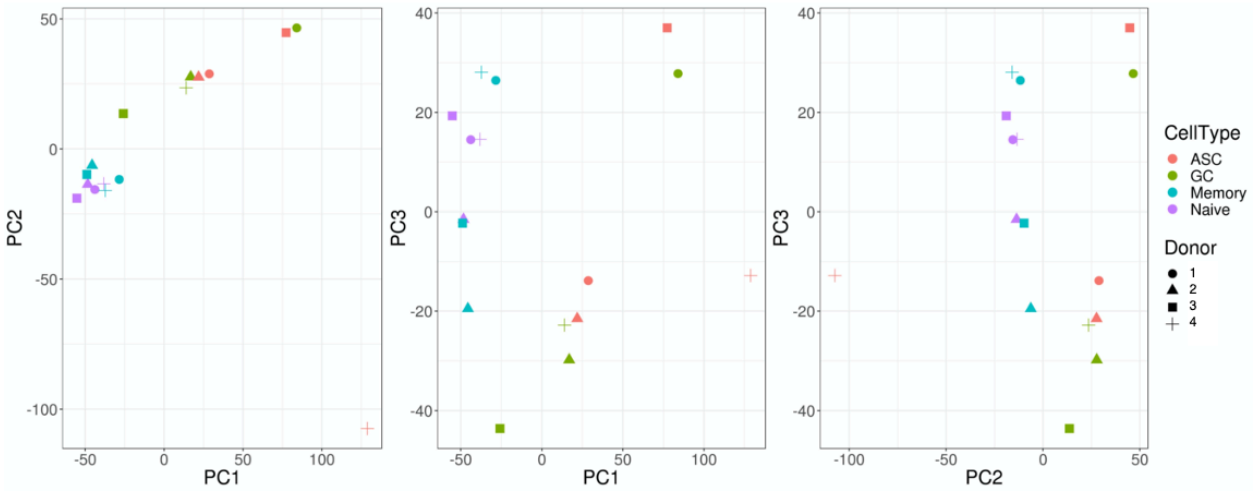

Figure 4.2.1a. Profiles of transcriptomic similarities between human naïve, GC, memory, and ASCs. Principal component analysis of bulk RNAseq data obtained from four cell types sorted from four human tonsil tissue donors.

Breaking down the top 100 hits between human memory and naïve B cells, as well as GC vs memory B cells, permitted greater resolution. As might be expected, *CD27,* as well as class-switched immunoglobulin constant region transcripts were upregulated in memory B cells, *IGHD* transcripts were found in greater frequency in naïve B cells, and *AICDA* was observed at the highest frequency in GC B cells (Fig. 4.2.1b).

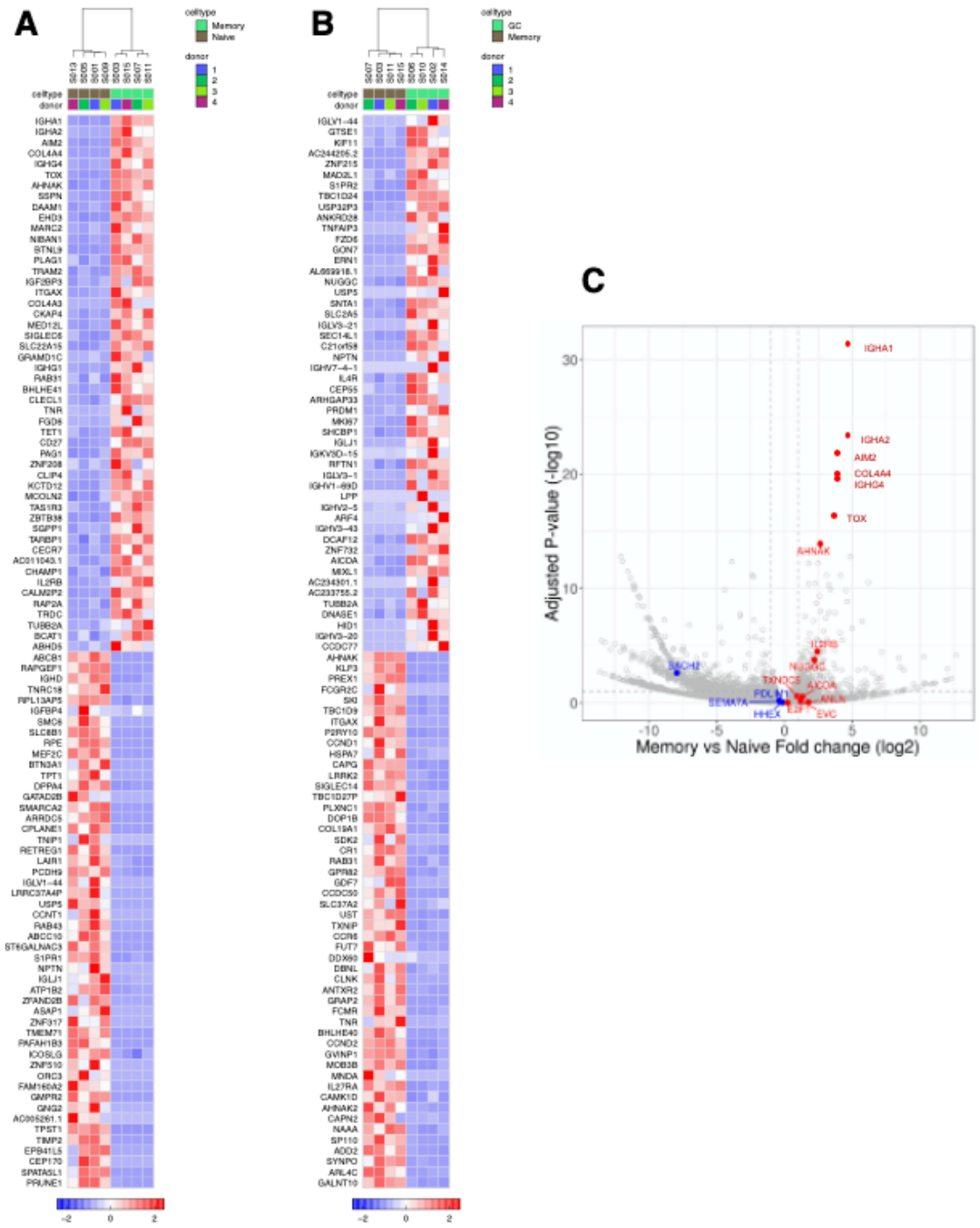

Figure 4.2.1b. Identification of specific DE transcripts between memory, germinal center, and naïve human B cells. Relative RNA expression profiles of human memory vs naïve B cells (A) and GC vs memory (B). (C) Volcano plot consisting of -log10(p-value) by log2(fold change), comparing memory vs naïve human B cells. Transcript names in red represent genes upregulated in memory B cells compared to naïve B cells, and annotations include intuitive and counterintuitive hits, later discussed in further depth. Dotted lines signify 2-fold increase in log2 space (vertical), and FDR (false discovery rate) <10% in log10 space (horizontal).

HHEX, recently identified as promoting the differentiation of GC B cells into memory, appeared in our data in greater frequency in GC B cells than in either memory or naïve B cells ($p= 0.006$, $6.5e^{-8}$), while the adjusted p-values of *TLE3* were not significantly different across cell types. Interestingly, *IL2RB*, the transcript encoding the b chain of the IL-2 and the IL-15 receptors (CD122) was significantly upregulated in both murine and human memory B cells ($p=3.0e^{-4}$, $3.2e^{-5}$) compared to naïve B cells. This receptor might function in memory B cells to downregulate *BACH2* in order to facilitate differentiation into plasma cells.[182]

Intriguingly, several of the more statistically-significant enriched transcripts observed in murine memory B cells were not enriched in human memory B cells, but were instead found at higher levels in human naïve and GC B cells. These included Anln, an actin-binding protein which regulates cytokinesis,[183] Txndc5, a disulfide isomerase which assists protein-folding in the ER and may perform anti-apoptotic functions,[184] and E2F1, a well-known transcription factor that plays a crucial role in regulating cell cycle, proliferation, and apoptosis.[185]

Gene set enrichment analysis of the human B cell RNAseq data revealed that pathways upregulated in memory B cells vs naïve B cells pertained to B cell activation (humoral immunity, B cell receptor signaling, complement activation, etc.), and when networked, largely formed a single cluster based on these broad functions (Fig. 4.2.1c).

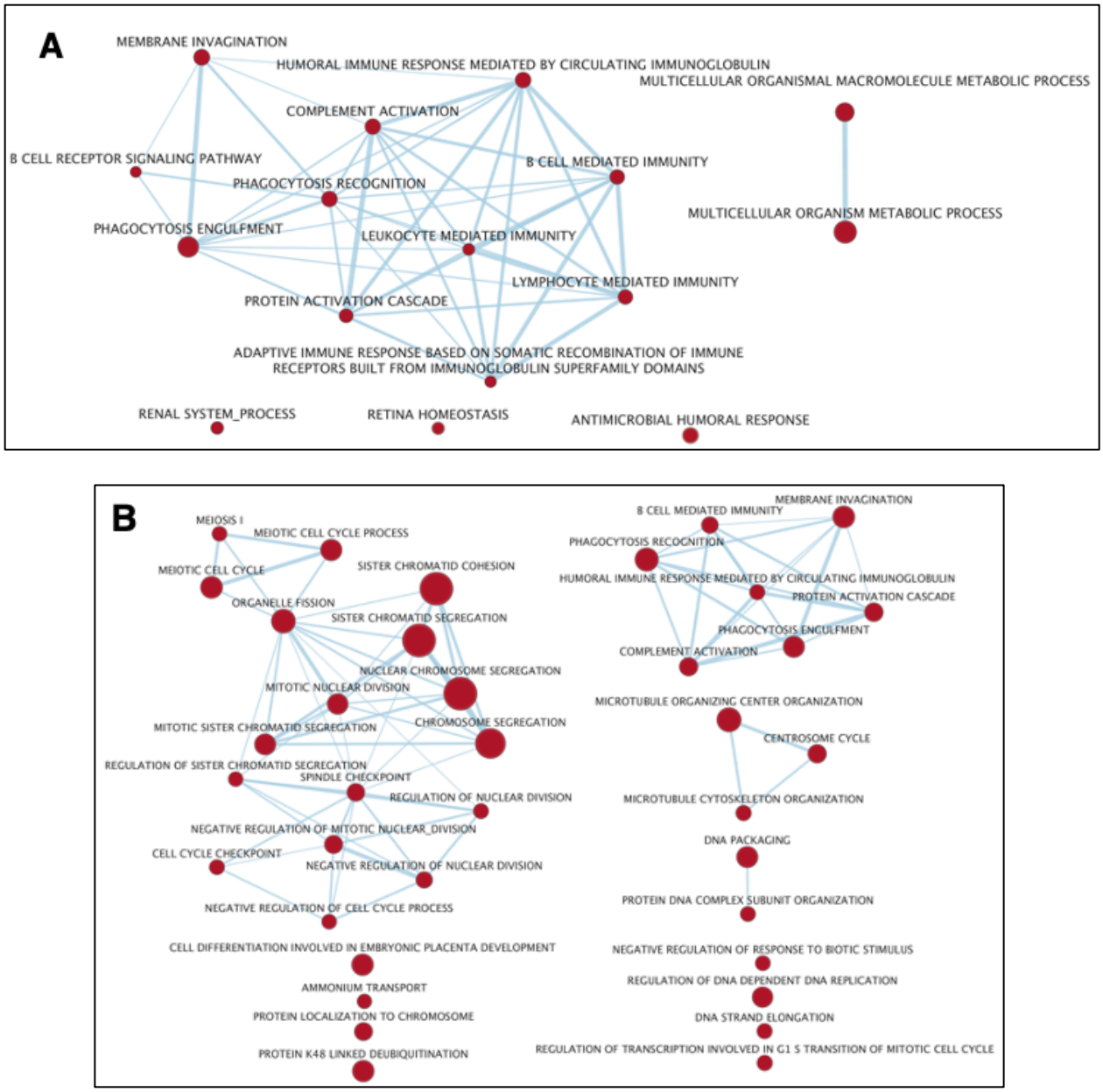

Figure 4.2.1c. Network analysis of interactions between gene ontology terms derived from human DE transcripts. Comparisons between (A) memory vs naïve B cells, FDR<0.25, and (B) GC vs MBCs, FDR<0.1. Edge width connotates similarity between terms, while node size connotates significance (-log10 FDR q-value).

The gene ontology pathways of significance in GC B cells when compared to memory B cells, however, predominantly formed two clusters: the smaller related to B cell activation (humoral immunity, complement activation, etc.), while the larger

clustered around DNA repair, replication, and cell-cycle related pathways. Interestingly, gene ontology pathways that were upregulated in memory B cells compared to germinal center B cells were very limited and skewed strongly towards neural pathways and interferon gamma signaling compared to germinal center B cells.

4.2.2 Proteomic and transcriptomic analyses of human memory B cells reveal largely divergent patterns of cell-specific transcripts and proteins

An unbiased proteomic analysis of human switched memory B cells and naïve B cells revealed that these cells not only share similar transcriptomes, but also share somewhat similar proteomes as well. However, the comparison of memory and naïve B cells (Fig. 4.2.2a) is a fairly telling example of the considerable differences that can be revealed from proteomic data versus transcriptomic data. Pathway analyses using gene ontology terms revealed pathways that proteomically and transcriptomically distinguish memory B cell and naïve B cells. However, the most statistically significant transcriptomic pathways that distinguished memory B cells from naïve B cells did not overlap with the proteomic pathways that were specific to memory B cells. When looking at differentially-expressed genes versus differentially-expressed proteins, there was a small overlap of 11 genes that were enriched in memory B cells compared to naïve. However, some of the overlapping genes such as *AHNAK* and *PBK*, discussed below, among others, are key to the pathways that help define memory B cells as revealed by proteomic analyses.

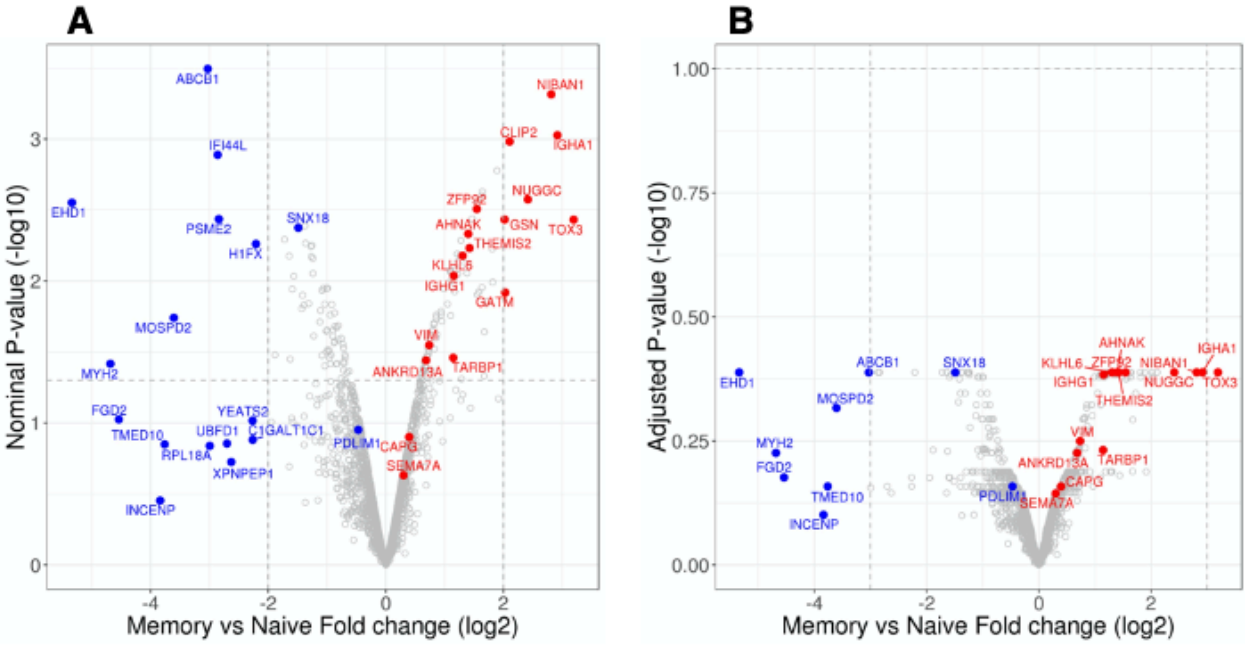

Figure 4.2.2a. Proteomic comparison of human memory and naïve B cells. Volcano plot of human memory vs naïve B cell proteomic data, consisting of log2(fold change) vs –log10(nominal p-value), with a horizontal dotted line at p<0.05 (A), and –log10(adjusted p-value), with a dotted horizontal line at FDR<0.1 in log10 space (B).

Comparing the overlaps between the transcriptomic and proteomic gene set enrichment analyses, or the lack thereof, was likewise informative. Of the gene ontology pathways that were significantly different between memory and naïve B cells, none is shared across the transcriptomic and proteomic datasets (Fig. 4.2.2b).

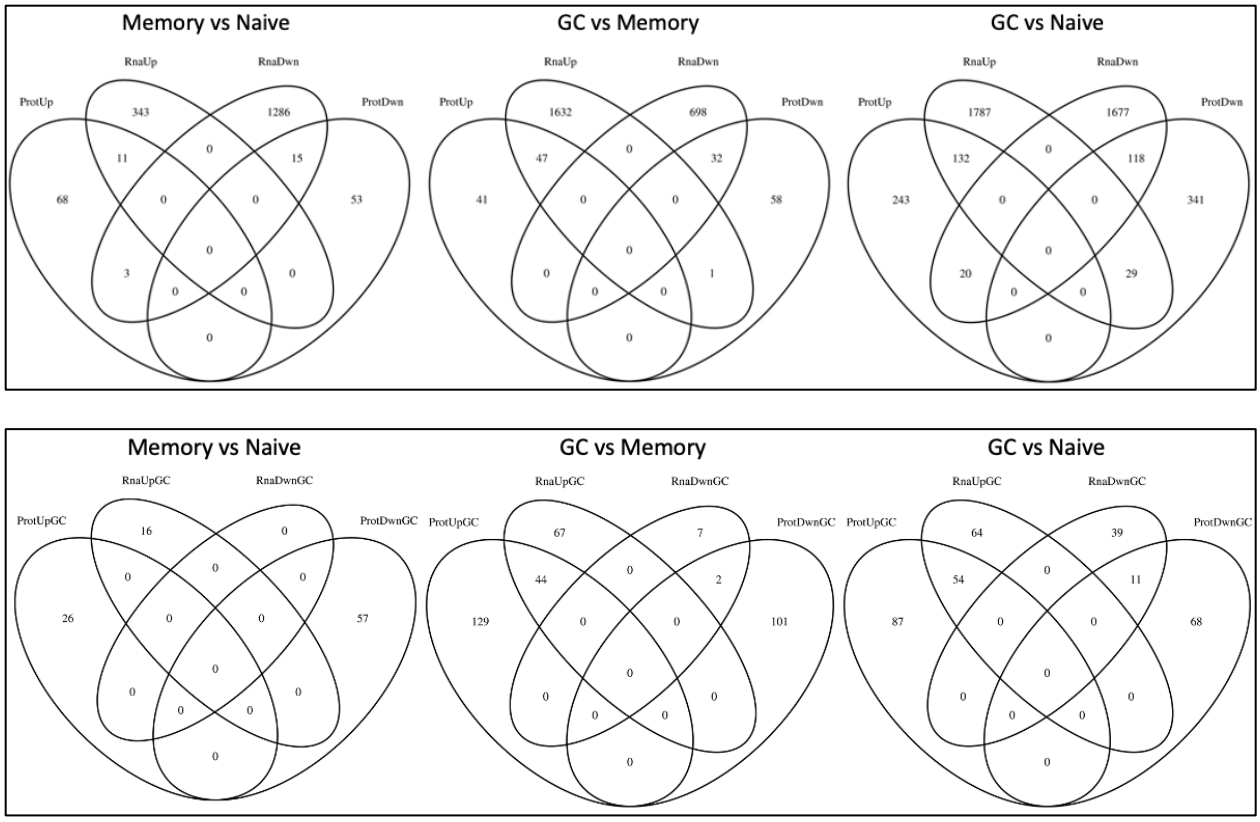

Figure 4.2.2b. Summary of proteomic and transcriptomic overlap in human datasets. Venn diagram breakdowns of individual hits (top), and gene ontology terms (bottom). Memory vs naïve RNA (FDR<0.1), protein (p<0.05); GC vs memory, both RNA and protein (FDR<0.1); GC vs naïve, both memory and protein (FDR<0.1).

There are 11 gene ontology pathways that are downregulated in GC B cells in both proteins and transcripts, as well as 54 that are up in GC B cells in both as well. There are 44 gene ontology pathways that are up in GC B cells compared to memory B cells in both datasets, and, interestingly, only two that are elevated in memory B cells compared to GC B cells. Those two are “interferon gamma mediated signaling pathway” and “response to interferon gamma.”

Lastly, while not explored in depth here, the murine RNAseq dataset allows for cross-referencing across species on the transcriptomics side. While some hits in the murine RNAseq don’t appear in the human dataset, like *Anln*, *Txndc5*, or *E2f1*, most do.

For example*, Il2rb*, upregulated in human GC B cells ($p = 3.2e^{-5}$), is likewise upregulated in murine GC B cells ($p = 0.037$). *NUGGC*, upregulated in human GC B cells ($p = 3.33e^{-10}$) is likewise upregulated in murine GC B cells ($p = 7.73e^{-7}$).

4.2.3 The memory B cell proteome reflects the reversal of quiescence and ongoing proliferation

Our previous transcriptomic, metabolic, and cellular signaling studies on naïve follicular B cells[186] have revealed that naïve B cells have acquired a state of metabolic quiescence, concomitant with the shut off of mTOR signaling by the induction of AMPK activity.

Our proteomic studies of memory B cells reveal that the major difference from naïve B cells lies in pathways related to cell cycle progression and cytoskeletal changes and signaling that reflects a level of ongoing mitosis and an increase in baseline metabolism.

Many gene ontology terms, some overlapping, including DNA replication, mitotic DNA integrity checkpoint, mitosis, microtubule cytoskeletal organization, cytoskeletal organization establishment of cell polarity, mitotic spindle organization, and organelle fission, etc., capture the ongoing mitotic activity in memory B cells compared to naïve B cells. A separate set of pathways captures the enhanced metabolic state of memory B cells compared to naïve B cells. These include cellular amino acid biosynthetic process, alpha amino acid biosynthetic process, alpha amino acid metabolic process, and dicarboxylic acid metabolic process, which speaks to the reversal of quiescence in memory B cells.

When comparing memory B cells with GC B cells, 698 transcripts and 58 proteins were significantly enriched in memory B cells. An additional 32 hits were enriched in memory B cells in both the transcriptomic and proteomic datasets (Figure 5). Examples include CHAF1a, the core of the CAF1 histone loading complex, which may play a role in heterochromatin maintenance in proliferating cells and has recently been shown to regulate EBV latency,[187] and BACH2, discussed earlier. Similarly, 11 transcript-protein pairs were upregulated in memory B cells vs naïve B cells.

Of these, a number are of considerable interest. Semaphorin 7a (CD108), was enriched in memory B cells as compared to germinal center and naïve B cells across both transcriptomics and proteomics. It is a membrane-bound protein found on activated lymphocytes that plays roles in modulating inflammation,[188] integrin signaling,[189] and axon outgrowth,[190] continuing the trend of associations with neuronal processes. *NUGGC* (also mentioned above), which codes for a nuclear GTPase previously reported in GC B cells with a possible role in suppressing somatic hypermutation and preventing apoptosis,[191] was increased in memory B cells (as well as in GC B cells) when compared to naïve B cells both at the level of RNA and protein. *AHNAK*, or Desmoyokin, mentioned above, is a scaffold protein with actin-binding properties that may play a role in neuronal development as well.[192] *KLHL6*, shown to regulate GC B cell maturation and BCR signaling,[193,194] and that was upregulated in GC B cells across both datasets, was also found to be upregulated in memory B cells by RNAseq. *NIBAN1*, a tumor marker for several types of cancer,[195,196] had a similar profile across both datasets, and regulates apoptosis.[197]

4.3 DISCUSSION

The human proteomic and transcriptomic datasets presented here from naïve, germinal center, and memory B cells were obtained from paired aliquots of the same cells sorted from the same tissue donors, yet most of the transcriptomic hits were unreported in the proteomics. This is likely due in some small part to the vastly smaller number of hits obtained by mass spectrometry compared to RNAseq. This highlights the importance of validating transcriptomic studies, even when observational, with proteomic comparisons (when feasible).

Our previous transcriptomic, metabolic, and cellular signaling studies on naïve follicular B cells[186] have revealed that naïve B cells have acquired a state of metabolic quiescence, concomitant with the shut off of mTOR signaling by the induction of AMPK activity. The similarity suggest by the proteomic data between the metabolic profiles of naïve and MBCs within pathways related to cell cycle progression, cytoskeletal changes, and signaling may reflect the stem-like property of MBCs. The increased metabolism likely reflects the more ready response to antigen of memory B cells compared to naïve B cells, while a separate set of pathways captures the enhanced metabolic state of MBCs compared to naïve B cells. These include the cellular amino acid biosynthetic process, alpha amino acid biosynthetic process, alpha amino acid metabolic process, and dicarboxylic acid metabolic process, and speak to the reversal of quiescence in memory B cells. In those hits that were specifically annotated here by virtue of appearing in multiple datasets, a curious number of them related to neuronal pathways and gene ontology terms. It is possible that superficial similarities in the roles of neurons and memory B cells (extended periods of relative metabolic inactivity

concurrent with a high degree of responsiveness) might be reflected in biological mechanisms that overlap in specific proteins and transcripts.

Germinal center B cells divide extremely rapidly, are very active metabolically, and need specialized DNA repair machinery to facilitate somatic hypermutation, which is reflected in both our proteomic and transcriptomic analyses of germinal center B cells vs naïve and memory cells. An enormous number of proteins and transcripts are differentially expressed in germinal center B cells, and given this large number of relevant genes and their products, there is an easily distinguished overlap between the transcriptome and the proteome in these cells. Proteomic analyses combined with pathway analyses reveal very high levels of proteins reflecting enhanced B cell signaling, enhanced metabolism, enhanced translational initiation, the induction of a wide range of biosynthetic processes, cell cycle progression, DNA replication, mitotic progression, DNA repair, sister chromatid exchange, protein ubiquitination, and processing of noncoding RNAs and nonsense-mediated RNA decay, among other pathways.

Intriguingly, pathway analyses also revealed there was striking enhancement of Ig heavy and light chain protein levels far in excess of what is seen in memory B cells. In addition, there was high level expression of proteins that are linked to the biogenesis of the endoplasmic reticulum and that are responsible for high level protein secretion from this compartment—features of plasma cells. These proteins included the ribosome binding protein RRBP1, which helps ribosome docking on the endoplasmic reticulum, as well as the MOSPD2 protein, which is an ER-resident protein involved in inter-membrane contact formation and which may contribute to the ER expansion that is

needed for plasma cell biogenesis. Pathway analyses implicate an increase in the establishment of protein localization to the ER, as well as increased translational initiation and RNA processing, all of which may be preserved in plasma cells. While germinal center B cells revealed the activation of high levels of DNA replication, cellular proliferation, and mitosis, some changes in these cells may reflect their partial differentiation towards a plasma cell fate. Clearly the vast majority of these highly purified cells do not express the surface characteristics of plasma cells, but they do show striking changes in terms of the high levels of antibodies and in the machinery involved in translocating proteins into the ER through the Sec 61 channel. At the transcriptomic level, GC B cells and plasma cells share many characteristics, in keeping with their widely-accepted origin from the germinal center.

4.4 MATERIALS AND METHODS

4.4.1 Key Resources Table

Antibodies	**Source**	**Identifier**
Anti-human CD3-A700	BD Biosciences	Cat# 557943
Anti-human CD19-APC-Cy7	BD Biosciences	Cat# 557791
Anti-human IgD-BV650	BD Biosciences	Cat# 740594
Anti-human CD38-PE	BD Biosciences	Cat# 555460
Anti-human CD10-BV711	BD Biosciences	Cat# 740770
Anti-human CD27-BUV395	BD Biosciences	Cat# 563815
Anti-human CD138-APC	BD Biosciences	Cat# 347193
Anti-mouse CD4-A700	BD Biosciences	Cat# 561025
Anti-mouse CD8-A700	BD Biosciences	Cat# 557959
Anti-mouse CD19-BUV395	BD Biosciences	Cat# 563557
Anti-mouse IgM-BV650	BD Biosciences	Cat# 564027
Anti-mouse IgD-BV786	BD Biosciences	Cat# 563618
Anti-mouse IgG1-BV421	BD Biosciences	Cat# 562580
Anti-mouse IgG2a-BV421	Biolegend	Cat# 407117
Anti-mouse IgG2b-BV421	BD Biosciences	Cat# 743174
Anti-mouse IgG3-BV421	BD Biosciences	Cat# 565808
Anti-mouse GL7-PE	BD Biosciences	Cat# 561530
Anti-mouse CD38-BV510	BD Biosciences	Cat# 740129
Anti-mouse CD138-BUV737	BD Biosciences	Cat# 564430
Anti-mouse CD16/CD32	BD Biosciences	Cat# 553142

Chemicals, Peptides, and Recombinant Proteins	**Source**	**Identifier**
SYTOX™ AADvanced™ Dead Cell Stain Kit	ThermoFisher Scientific	Cat# S10349
LIVE/DEAD™ Fixable Blue Dead Cell Stain Kit	ThermoFisher Scientific	Cat# L34961
OneComp eBeads	ThermoFisher Scientific	Cat# 01-1111-41
Lysogeny Broth, powder	Fisher Scientific	Cat# BP1427-500
100um Cell Strainers	Corning	Cat# 352360
FBS	ATCC	Cat# 30-2021
DMSO	Sigma Aldritch	Cat# D8418
Lonza BioWhittacker ACK Lysis buffer	ThermoFisher Scientific	Cat# BW10548E
EZ Link NHS biotin	ThermoFisher Scientific	Cat# 20217
Streptavidin-A647	Biolegend	Cat# 405237
Streptavidin-A488	Biolegend	Cat# 405235
Bovine serum albumin	Sigma Aldritch	Cat# A9418
DMEM	Sigma Aldritch	Cat# D1145
LIVE/DEAD viability dye	ThermoFisher Scientific	Cat# L23105
Brilliant Stain Buffer	BD Biosciences	Cat# 563794
Bovine Serum Albumin	Fisher Scientific	Cat# 9048-46-8
RLT buffer	Qiagen	Cat# 79216
BME	Sigma Aldritch	Cat# 63689
PhosSTOP	Sigma Aldritch	Cat# 4906845001
cOmplete protease inhibitor cocktail	Sigma Aldritch	Cat# 11697498001
eOD-GT8 60-mer	Dr. William Schief and Julia Bals	N/A
eOD-GT8-Avi-His	Dr. William Schief and Julia Bals	N/A
delta-eOD-GT8-Avi-His	Dr. William Schief and Julia Bals	N/A
SYBR safe DNA gel stain	ThermoFisher Scientific	Cat# S33102
Agarose	Fisher Scientific	Cat# BP160-500
Agencourt AMPure beads	Beckman Coulter	Cat# A63881
Sigma Adjuvant System	Sigma Aldritch	Cat# S6322
Critical Commercial Assays	**Source**	**Identifier**
Maxiprep	Qiagen	Cat# 12163
BirA reaction kit	Avidity	Cat# BirA500
Pierce protein concentrators	ThermoFisher Scientific	Cat# 88521
RNeasy Plus Micro kit	Qiagen	Cat# 74034
NEBNext Poly(A) mRNA magnetic isolation module	NEB	Cat# E7490S
NEBNext Ultra RNA library prep kit for Illumina	NEB	Cat# E7530S
NEBNext Multiplex Oligoes for Illumina	NEB	Cat# E7335S
Nextseq 500/550 High Output V2.5 150 cycles	Illumina	Cat# 20024907
Kapa Express Extract kit	Kapa Biosystems	Cat# KK7103
HiFi HotStart ReadyMix PCR kit	Kapa Biosystems	Cat# KK2602
Qubit dsDNA HS Assay	ThermoFisher Scientific	Cat# Q32854
Recombinant DNA	**Source**	**Identifier**
VRC4805	Vaccine Research Center	N/A
VRC4803	Vaccine Research Center	N/A
VRC4027	Vaccine Research Center	N/A
Biological Samples	Source	Identifier
human tonsil tissue	N/A	protocol 2010-000632
murine splenocytes	N/A	protocol 2005N000360
Bacteria and Virus Strains	**Source**	**Identifier**
One-Shot Mach1	ThermoFisher Scientific	Cat# C8620-03

Experimental Models/Organisms/Strains	Source	Identifier
Vh1-2/LCL	this paper	N/A
Oligonucleotides	**Source**	**Identifier**
ATGGAAACCCCAGTGCAGCT	Ming Tian, private communication	VRC01LC_F1
CGCGAATTCATACTGCTGACAGTAATACACTGC	Ming Tian, private communication	VRC01LC_R1
TGGACCTGGAGGATCCTCTT	Ming Tian, private communication	Vh1-2_F1
CGCACGCGTCCAGGTGTACAGGTTAGTT	Ming Tian, private communication	Vh1-2_R1
TTCCCAACTTCTCTCAGCCG	Ming Tian, private communication	JhB_del_F1
ACAGGCTCGAGAACTTTAGC	Ming Tian, private communication	JhB_del_R1
TTCGGGCTCAGCTTGGTTTT	this paper	Vh5-2_F2
CAGCTGCACCTCACACTGTA	this paper	Vh5-2_R2
AGCAAAGCTGGGAATAGGCT	this paper	Jk_F1
TGGTGTCCCTTCACTCAACC	this paper	Jk_R1

4.4.2 Experimental model and subject details

Human study participants

Samples were obtained in the form of excess tissue resected from tonsillectomies of anonymous donors under Massachusetts General Hospital protocol 2010-000632, by the Massachusetts General Hospital Pathology Tissue Bank.

Murine study subjects

The mice used in this study were bred under specific pathogen-free conditions in a Massachusetts General Hospital Center for Comparative Medicine animal research facility. All mouse work was performed according to protocol 2005N000360, approved by the Internal Review Board and Institutional Animal Care and Use Committee of Massachusetts General. Two mice were obtained from Dr. Alt, each with features from the V_H1-2/LC mouse model, previously described. [154] One featured the human IGHV1-2*02 human V gene knocked-in in place of murine V_H81X and an inactivated intergenic control region. The other featured a heavy chain J_H deletion and a light chain integration that consisted of the rearranged human VRC01 Igk variable region exon. These two

mice were crossed into C57BL/6 mice purchased from Jackson Laboratories, pups (V_H1-2/LCL) were genotyped by PCR, and the light chain modifications were bred to homozygosity.

4.4.3 Method Details

Genotyping

Tail clips were collected from mice and treated with Kapa Express Extract kit according to the manufacturer's protocol. Resulting DNA was amplified by PCR using Taq 5X Master Mix from NEB and the following conditions: 94ºC for 30 seconds, 30 cycles of 65ºC for 1 minute and 72ºC for 1 minute, followed by 72ºC for 5 minutes. The resulting DNA were assessed using a 1% agarose gel with SYBR safe intercalating dye, and imaged on a BioRad ChemiDoc Imaging System.

Immunizations

Mice were immunized with 20ug of eOD-GT8, adjuvanted with Sigma Adjuvant System, prepared according to manufacturer's protocols. Intraperitoneal injections were administered at week 0 and week 13, and mice were sacrificed at week 19.

Tissue processing and cryopreservation

Human tonsil tissues were dissected in ice cold sterile PBS, filtered at 100um, centrifuged at 500xg for five minutes, resuspended in ACK lysis buffer for 45 seconds, topped off with cold PBS, washed once in cold PBS, resuspended in a mixture of

FBS+10% DMSO, frozen at -80ºC, and transferred to -150ºC. Murine spleens were similarly processed.

Protein Production

Plasmids (VRC4805, VRC4803, and VRC4027), kindly provided by Dr. Mascola, were transfected into Mach1 bacteria, grown in LB, and isolated using a Qiagen maxiprep kit according to manufacturer's protocols. Proteins were expressed in expi293F (ThermoFisher) cells and purified as described in section 2.4.8. Briefly, cells were transfected with 1µg/mL plasmid DNA (expifectamine, Thermofisher) and were allowed to express for 5 days. Supernatants were clarified via centrifugation, filtered through a 0.22µm polyethersulfone membrane (EMD Millipore), and buffer exchanged using tangential flow filtration (TFF). For purification of eOD-GT8 and ∆eOD-GT8, the supernatants were incubated overnight with Ni-NTA Sepharose resin (Cytiva), washed with 20mM imidazole and eluted in 500mM imidazole. For purification on the eOD-GT8 60mer, the supernatant was incubated overnight with galanthus nivalus (GNA) immobilized lectin (EY Laboratories), washed with 1X PBS, and eluted with 0.2M mannose. All proteins were further purified via size exclusion chromatography (SEC) using the ÄKTA-pure protein purification system (GE Healthcare). A Superose6 10/300 GL column (GE Healthcare) was used for the eOD-GT8 60mer, and a Superdex200 Increase 10/300 GL column (GE Healthcare) was used for both eOD-GT8 and ∆eOD-GT8.

FACS probes

Resulting proteins were biotinylated using an Avidity kit, according to the manufacturer's protocol, incubated at 4ºC overnight, and re-purified by SEC using a Superdex200 Increase 10/300 GL column in 1X PBS. Biotinylated proteins were then conjugated to fluorescently-labeled streptavidin. One quarter of the required moles of streptavidin were added to each biotinylated protein, then incubated, rotating, at room temperature, for 20 minutes, four times. Resulting flow probes were diluted in PBS and frozen at -80ºC.

FACS sorting

Human samples

Human tonsil cells were thawed, washed twice (supplemented with DMEM+1% BSA, then centrifuged at 500rcf for five minutes), and resuspended in Brilliant Stain Buffer. Antibodies were added and incubated on ice for 30 minutes. Cells were washed, resuspended in DMEM, and incubated with LIVE/DEAD viability dye on ice for 30 minutes. Cells were washed and resuspended in PBS. Shortly before sorting, cells were stained with SYTOX. Cells were sorted using an Aria II SORP and a 100um nozzle. After excluding doublets, non-viable cells, and cells positive for CD4 or CD8, four populations were sorted: CD19+, IgD+, CD27-, CD38-, CD10- (naïve); CD19+, CD27+, CD38+, CD10+ (GC); CD19+, CD27+, non-GC, CD38-, CD138- (memory); and CD19+, CD27+, non-GC, CD38+, CD138+/- (ASC). Cells used for RNAseq were sorted, centrifuged at 500rcf for five minutes, resuspended in RLT+1% BME, frozen on dry ice, and stored at -80ºC. Cells used for proteomics were sorted and processed in 1-hour

increments by centrifugation at 500rcf for five minutes, resuspension in either PBS or cOmplete protease inhibitor cocktail and PhosSTOP, and storage at -80ºC.

Murine Samples

Murine splenocytes were thawed, washed twice as above, resuspended in a 1:40 dilution of FC block:PBS, and incubated on ice for 30 minutes. Staining tetramers were added to a final concentration of 50nM, and were incubated for 30 minutes on ice. 50ul of Brilliant Stain buffer were added, followed by staining antibodies, and incubated for an additional 30 minutes on ice. Cells were washed as above and resuspended in PBS. Shortly before sorting, the cells were stained with SYTOX. Cells were sorted using an Aria II SORP and a 100um nozzle. After excluding doublets, non-viable cells, and cells positive for CD4 or CD8, four populations were collected: CD19+, IgD+, IgG-, GL7-, IgM+/- (naïve); CD19+, IgD+, IgG-, GL7+, IgM+/- together with CD19+, IgG+, GL7+, CD138- (GC); CD19+, IgG+, GL7-, CD138- (memory); and CD19+, IgG+, GL7-, CD138+ (ASC). Cells were sorted, centrifuged at 500rcf for five minutes, resuspended in RLT+1% BME, frozen on dry ice, and stored at -80ºC.

RNAseq library preparation

Cell lysates were homogenized by pipetting, RNA was purified using a Qiagen RNeasy Plus Micro kit, and mRNA was isolated using an NEB mRNA enrichment kit. RNAseq libraries were generated using an NEB Ultra kit and primers, quantitated using

Qubit, assayed on a Qubit 3.0 fluorometer, and sequenced using a Nextseq 500/550 High Output kit on an Illumina NextSeq 500.

4.4.5 Quantification and Statistical Analyses

Protein Quantification and Statistical Analysis

Cell pellets were lysed, reduced, and alkylated and underwent tryptic digest as previously described.[198] 50µg of the resulting peptides were subsequently labeled using TMT-10plex reagents (Thermo Scientific) according to manufacturer's instructions. Labeled samples got combined and fractionated using a basic reversed phase HPLC.[198] The resulting fractions were analyzed in a 3-hour reversed phase LC-MS2/MS3 run on an Orbitrap fusionLumos. MS3 isolation for quantification used Simultaneous Precursor Selection (SPS) as previously described.[199-201] Proteins were identified based on MS2 spectra using the sequest algorithm searching against a human data base (uniprot 2020)[202] using an in-house built platform.[203] Search strategy included a target-decoy database-based search in order to filter against a false-discovery rate (FDR) of protein identifications of less than 1%.[204] The protein intensity data was normalized using a median normalization method. Briefly, the average intensity across all samples is calculated for each protein (row) and each protein row's mean is adjusted to the median of all row averages. Following the protein normalization, the median of each sample (column) is scaled to be equal to the median across all of the sample medians. Data from technical replicates were averaged to generate data across two biological replicates.

Differential Expression Analysis

The normalized protein intensity values were converted into log2 space to reduce effects of outliers prior to differential expression analysis. Differential expression of proteins was tested in a pairwise manner between GC, memory, and naïve cells harvested. We fit a linear model controlling for the donor using the LIMMA R package to determine differential expression between conditions.[205] Fitted model moderated t-statistic p-values were adjusted for multiple hypothesis testing using the Benjamini-Hochberg method. Significant differentially expressed proteins were defined with an adjusted p-value (FDR) < 0.1. Three different comparisons were performed, GC vs naïve, memory vs naïve, and GC vs memory. All analyses and plots were generated in R (v3.4) (R core team 2017). The functional enrichment of the differentially-expressed proteins from each comparison was determined using the pre-ranked GSEA (geneset enrichment analysis) tool from the Eli and Edythe L. Broad Institute of MIT and Harvard.[206] The differentially expressed proteins were ranked based on weights calculated as follows: (sign of log2 fold change) * -log10(nominal p-value). We focused on the GO biological process geneset collection provided by MSigDB (v6.2).[207] Enrichments were calculated using 10,000 permutations for genesets with a minimum of 15 members. An FDR (q-value) < 0.25 defined the statistically significant genesets.

Human mRNA-seq Differential Expression Analysis

RNA-seq raw read counts from single samples of naïve, GC, and memory cells across four donors were tabulated from the Salmon output. Three comparisons, GC vs naïve, GC vs memory, and memory vs naïve were done. For each comparison, low

expression genes were removed and genes with at least a sum of 10 reads across samples were kept for differential expression analysis. Differential expression analysis was performed using DESeq2 using the protocol found in the DESeq2 package RNA-seq analysis vignette and controlled for donor effects.[208] Significant differential genes were defined using an Benjamini-Hochberg corrected p-value < 0.1. Pre-ranked gene lists were generated and GSEA for each comparison was run as described previously for the protein data. A network analysis tool was used to visualize the significant functional terms found in the memory vs naïve (FDR<0.25) and GC vs memory (FDR<0.1) comparisons using the Enrichment Map App v3.3[209] from Cytoscape v3.8.2.[210] All analyses and plots except as previously mentioned were generated in R (v3.4).

Additional References:

R Core Team (2017). R: A language and environment for statistical computing. R Foundation for Statistical Computing, Vienna, Austria. URL https://www.R-project.org/.

Collaborator contributions and acknowledgments

Marshall Karpel, Robert Morris, Johannes Kreuzer, Rui Guo, Julia Bals, Gray Karpel, Wilhelm Haas, and Shiv Pillai all contributed to this work.
MK and SP designed experiments.
JB expressed and purified proteins.
MK created tetramers for FACS.
MK performed mouse experiments and processed, stained, and sorted murine and human tissues.
JK performed mass spectrometry.
RM, MK, RG, and SP performed data analysis.
RM, MK, and RG made figures.
MK, SP, RM, GK, and JB prepared the manuscript.
MK, SP, and GK edited the manuscript.
This work was supported by NIH U19 AI110495 to SP.

CHAPTER 5: DISCUSSION

5.1 Limitations of experimental frameworks: chapter 2

In retrospect, the breeding program established for this project was not ideal. Two mice were obtained from Dr. Alt, each with features from the V_H1-2/LC mouse model, as previously described. [154] One featured the human IGHV1-2*02 human V gene knocked-in in place of the murine V_H81X gene, and also featured an inactivated intergenic control region. The other featured a heavy chain J_H deletion and a light chain integration, which consisted of the rearranged human VRC01 Igk variable region exon (see Fig. 2.1.4). Our first step was to breed them both with B6 mice to ensure the traits would continue in our colony even in the unlikely event of an accidental death. However, that introduced variables into the subsequent breeding program, as none of the subsequently crossed litters could be said to be truly homozygous at any specific allele. If future work were to be pursued, continued backcrossing into the B6 line could always be performed. However, this lack of complete homozygosity was unlikely to have caused any particular difficulty in any specific experiment, but remained, for the duration of the project, a variable that had to be accounted for. Each experiment reported here featured litters of mice that were distributed across experimental groups explicitly for this purpose. In section 3.2.3 the possibility that lineage might be playing a role in vaccine responses was tested statistically; no association was noted between vaccine responses in mice and which breeding pair the mice came from.

Another drawback to this study is the treatment of impaired B cell tolerance as a blank check. Given the complexity of self-tolerance, it is unlikely that all autoreactive antibodies or BCRs are treated equally by the immune system. The underlying assumption inherent in this experimental framework is that if the development and

secretion of some types of autoreactive antibodies are permitted by impaired self-tolerance, then the development and secretion of autoreactive bnAbs will likewise be permitted by the same breaches in tolerance. The mechanisms by which self-tolerance constrains the development of autoreactive BCRs in central and peripheral tolerance are well known, but the mechanisms that constrain autoreactive affinities that develop as a result of SHM are less well understood. Several mechanisms have been demonstrated to date: GC B cells that have acquired autoreactivity by SHM can reduce it with further SHM[211] and can be deleted when presented with self-antigens by FDCs.[212] Polyreactive MBCs, for their part, appear to be selected against over time,[213] while, simultaneously, autoreactive GC B cells can also drive the activation of other autoreactive B cells in a cascade that can become self-perpetuating.[214] How these different mechanisms function together to constrain SHM-derived autoreactivity is complex and unlikely to treat all autoreactive antibodies equally. The presence of autoantibodies in genetically autoimmune-prone mice, or in other mice after the injection of pristane or LCMV, does not guarantee that autoreactive bnAbs will likewise be permitted to develop.

For the time being, future work on this project is unlikely. It accomplished its aim. This experimental framework is not ideal for generating a bnAb (which was never its goal), but once a murine model exists in which bnAbs are reproducibly and reliably elicited by immunization, the framework might be suitable for use once more to determine if tolerance has in fact been constraining this process. That reproducible, reliable positive control would be crucial, however.

5.2 Towards establishing mechanism: chapter 3

As was discussed in section 3.3.3, the first limitation of this work was the lack of samples, either sera or splenocytes, from the intended endpoint of any of the five immunization regimens. Given the decline in deaths that took place after the substitution of SAS with an aluminum adjuvant, enough mice would almost certainly have survived to the final endpoint because all of the remaining mice had been lumped together into Group C. The timing of the SARS-CoV-2 pandemic dictated that all non-essential mouse experiments be terminated, and these mice were included in that culling. As such, it remains unclear whether the fourth and final boost, BG505-3BVE, would have been sufficient to confer BG505-specificity in these mice under these conditions. Because no final endpoint data was collected, the cryopreserved cells remain unsorted, unsequenced, and unexpressed. For the same reason, neutralization breadth assays were not performed. Samples of sera remain, so this possibility is still feasible, but after the original experimental design was discarded it became impossible to test the impaired tolerance hypothesis, as there were no longer two identical groups varying only by the introduction of pristane.

That said, B cell tolerance may have been impaired in every group through the use of the SAS, and the published literature on the effects of squalene (as well as its presence in the SAS), was sufficient to direct attention to the kidneys. However, while squalene has been linked to SLE-like glomerulonephritis, and while SAS is clearly involved in the lethal phenotypes observed here, chapter 3 contains no direct evidence that the lethality is due to the squalene in the SAS and not another component. In fact, were squalene to be responsible, this would be an extraordinarily fast example of

hydrocarbon-induced glomerulonephritis; pristane, for example, often takes much longer.[215] There was also very little squalene injected into each of these mice. Sigma-Aldrich product materials refer to SAS as a 2% oil-in-water solution, and each vial is diluted by the user up to a 2mL final volume that is subsequently used to inject 10 mice, implying that each mouse receives somewhere around 4ul of squalene per injection; nothing like the hundreds of microliters of squalene or pristane that are often used to impair B cell tolerance in murine models of SLE. Supporting the alternative interpretation that squalene may not have been the determining factor in the SAS are the Hep-2 assays conducted using the sera from the sick mice. In a typical pristane- or squalene-treated mouse, one might expect cell-reactive antibodies to be present, but none were observed. There are histological effects whereby the HEp-2 assay can report false negatives when the concentration of autoantibodies is too high, but this is an unconvincing explanation for the absence of such a reasonably-anticipated datapoint.

Furthermore, the work performed here does not explore the other components of SAS: Tween-80, trehalose dicorynomycolate, and monophosphoryl lipid A (MPL). MPL first featured in research more than 50 years ago when Dr. Edgar Ribi (whose name is still associated with the SAS product) manufactured it from bacterial LPS.[216] It is now used in a handful of GlaxoSmithKline products such as Cervarix and Fendrix.[217] MPL is a TLR4 ligand, and can induce activation in dendritic cells and T cells *in vitro*.[218] Beyond its function as a TLR ligand, it is difficult to imagine that MPL might be somehow directly responsible for the accumulation of antibodies in the kidneys of the sick mice. That said, a tenuous connection between MPL and the BCRs of the mice at least warrants a mention here. MPL signals through TLR4, but so does HIV gp120.[219] If gp120 and MPL

can both bind to TLR4, it is vaguely possible, though profoundly unlikely, that both gp120 and MPL can bind to the VRC01-precursor-like BCRs that are present in such high numbers in the V_H1-2/LCL mice. In the context of the immunostimulatory effects of the SAS, direct and widespread BCR engagement of such a large population of B cells could have profound effects.

Trehalose dicorynomycolate, or TDM, is an analogue of trehalose dimycolate, from the cord factor of *Mycobacterium tuberculosis.* It is recognized by Mincle, a C-type lectin receptor found on macrophages[220,221] TDM can be used to induce EAE, if WT mice are immunized with myelin oligodendrocyte glycoprotein,[222] suggesting that the TDM in SAS, rather than the squalene, may be responsible for the use of SAS in EAE models. However, this is purely speculation; further investigation would be required to identify which elements of SAS, alone or in combination, induced the lethal phenotype.

The first step would be to distinguish the source of the antibody observed in the kidneys: immune complex deposition in the kidneys and/or direct antibody binding to specific renal antigens, likely in the GBM. This could be accomplished using further complement staining in renal tissue, while ELISAs performed on serum C3 and C4 could help; if the antibodies observed in the kidneys are binding directly to renal antigens rather than forming immune complexes, C3 and C4 levels in sera might be expected to be normal. If massive compliment and immune complex deposition is taking place inside the kidneys, C3 and C4 levels might be expected to be lower. *In vivo* depletion of B cells prior to injection with SAS might also be informative; none of the data in hand at this time rules out *any* cause of death. An entirely T cell-mediated phenomenon in an entirely different organ is still a hypothetical possibility. Periodic acid-

Schiff staining can help to examine glomerular capillary pathology, and trichrome staining can provide insight as to whether the fibrino-cellular deposits observed by H&E staining were fibrin or collagen. It might be informative to inject V_H1-2/LCL mice with the individual components of the SAS alone, or to cross them with B6 and test the offspring, in order to observe if the homozygosity of the light chain is the critical factor after all. Lastly, collecting other organs besides kidneys from seemingly-sick and seemingly-healthy mice might help. The lungs, for example, might show evidence of Goodpasture's syndrome.

The goal of the original experiment was to study the relationship between the development of autoreactive bnAbs and impaired B cell tolerance. While the intention was to do so in a single group of mice in a larger experiment, it appears that it may have occurred simultaneously in each group. What resulted may well prove to be an effective model in which to continue to study this phenomenon. It is particularly interesting that it took place in a mouse model featuring a VRC01-like bnAb precursor population. A number of bnAbs have been knocked into mouse models, and, in many cases, the resulting B cells have been subject to strict immunological tolerance. This is true of 2F5,[223-225] a 2F5 germline variant,[226] 4E10,[224,227] and 3BNC6U.[228] However, two types of VRC01-like bnAbs, a germline VRC01 with an affinity-matured CDRH3[229] and a non-rearranged VRC01 germline,[84] were not tolerized. Some VRC01-class bnAbs have demonstrated some degree of autoreactivity, but not all.[17] The VRC01-like precursor B cells in this model certainly were not expected to be autoreactive (nor have they yet been proved to be). However, these data suggest the possibility that tolerance may in fact be acting on some VRC01-like precursors in ways which have not been previously

appreciated, and may represent an opportunity to study further whether B cell tolerance might be constraining bnAb development. Whether or not the profound renal damage was the exact cause of death, and whether or not the antibodies observed in the kidneys were there by virtue of their directly binding to renal antigens or by immune complex deposition, the lethal phenotype required both the SAS and the VRC01-like BCR modifications present in these mice, suggesting that the phenomenon might not be unrelated to our initial hypothesis.

5.3 Searching for the same needle in three haystacks: chapter 4

The greatest limitation of this study is that it can only be said to compare human memory B cells and murine memory-like B cells. Without a single, wildly-accepted flow cytometry phenotype to sort from, this study took advantage of a functional definition instead: those B cells which were class-switched, not GC B cells, not plasma cells or plasmablasts, and antigen-specific, present in the mice months after immunization. Rather than try to define (or further subdivide) MBCs as a population, this study was predicated on the notion that the exact surface marker expression phenotype of the MBCs was less important than the biological relevance of the data that were captured. Genes and proteins that are genuinely meaningful, and that exert a strong influence over the pathways responsible for the differentiation and maintenance of MBCs, should be identifiable even in the absence of a widely-agreed upon FACS profile.

During the initial analysis of the proteomics data, the decision was made to discard one of the MBC samples due to low data quality, which resulted in a wildly different proteomic profile than any other cell type, including other MBC samples, and even from other aliquots of MBCs from that donor. Unfortunately, this impacted the

statistical significance of the results. This is, to a large extent, why the proteomics data concerning human MBCs is so often not statistically significant. For example, 695 proteins are expressed at statistically significantly different amounts between the human GC and naïve B cells (FDR < 10% and adjusted p-value < 0.05). Between the memory and naïve, there are none. They're there, they just aren't statistically significant. For example, the penultimate hit, as defined by adjusted p-value, is NIBA1, or NIBAN, a regulator of p53-mediated apoptosis. Its expression was seven times greater in MBCs than it was in naïve B cells, its p-value was 0.00048, and its adjusted p-value was a mere 0.409. Another top hit was expressed 40 times more often in naïve than in MBCs, its p-value was 0.00279, and its adjusted p-value was likewise 0.409. The proteomics data for the MBCs are useful for their ability to promote to our attention proteins which are of biological relevance and interest. However, they limit the strength of the analyses that can be conducted between proteomics and transcriptomics, for example. Fortunately, more samples were obtained, sorted, and cryopreserved than have yet been assayed by mass spectrometry, and at least one more sample has been assayed by mass spectrometry than has been included in these analyses. The immediate next steps in this project are the inclusion of all of the remaining samples and data, and the comparison of the top hits reported here with the top hits as reported in that more-complete dataset. Depending on the degree of change present within those sets, alternative hits not yet apparent within this dataset may be pursued.

5.4 Conclusions and implications

When studying an aspect of biology that has a direct impact on public health, particularly when that impact is associated with a significant unmet medical need, the

search for objective truth is rarely the sole aim. This is particularly true for topics like HIV vaccine design; an unstated goal is sometimes permissible. Objectivity is required in the practice of the science itself, as always, but whatever the scientifically-reasonably-stated *aim* of the experiment was, there may have always been a less objective *goal*.

That is certainly true of this dissertation. The goal was to learn if B cell tolerance constrains the development of autoreactive bnAbs in humans. What was tested experimentally was slightly different: whether impaired B cell tolerance permits the development of autoreactive bnAbs. The difference between the two is the same as the difference between "X doesn't work because of Y" and "X will work if Y is removed." Chapter 2 accomplished its aim when it generated negative data responsive to the hypothesis, but the disconnect between the aim and the goal is the broadest limitation of this dissertation. Namely, it is entirely possible that the negative data collected here, for all the validation that was done in chapter 2, is accurate, and yet in humans, B cell tolerance might still be constraining the development of autoreactive bnAbs. Our experimental framework benefitted from consisting entirely of well-studied elements (known mice, immunogens, and tolerance perturbations), but could never perfectly recapitulate the phenomenon that would serve as the best positive control: an optimal mouse/immunogen system that, only in the context of impaired self-tolerance, could lead to the production of autoreactive bnAbs.

The data obtained in chapter 3, however, have direct implications for HIV vaccine design. The glycosylation at position 276 did not appear to present much difficulty for the mice; all of the 17 mice tested had acquired affinity for the N276 position before

even having been immunized with it. The more significant blockade appeared to be the transition from the N276 epitope presented on 191084 to the same epitope presented on BG505. Greater attention should be paid not only to key glycosylation sites, but also to the local structures in which they are presented.

APPENDIX

Table S1, Murine RNAseq, Memory vs Naïve

Top 100 by adjusted p-value

Gene name	log2 Fold Change	Adjusted p value
Anln	6.902884468	6.87E-61
Slc12a5	8.387527644	1.07E-20
Gm32312	-23.38004332	4.08E-18
Pogk	-1.944401005	4.47E-09
Fscn1	5.519280676	5.41E-09
Gm30948	-24.01149365	3.82E-05
Iglv2	5.189387767	3.82E-05
Txndc5	23.61047014	5.76E-05
Fas	2.430422695	0.000260631
Gm5373	21.69586068	0.000342162
Gm15429	21.78082712	0.000342162
Clcn1	21.55902263	0.000342162
Rad54b	20.70353725	0.000342162
Vmn1r91	21.69588284	0.000342162
Treml4	21.69588284	0.000342162
Ckap2	21.64237094	0.000342162
Gm10720	21.64237111	0.000342162
Il2rb	21.66671344	0.000342162
Kit	21.40343318	0.00042248
Gen1	6.709127923	0.000562582
Rgs10	20.72546557	0.000870163
Ptgr1	20.63351359	0.000924936
Zfp982	3.588410797	0.001174057
Xntrpc	20.31341675	0.001239605
mt-Tw	2.547963041	0.002405398
Chst1	2.150898277	0.002443922
mt-Tc	3.005490728	0.003248007
Gm43663	6.71335721	0.003410655
Ryr2	6.357284545	0.005106279
Ptdss2	6.302667393	0.006151738
Src	6.150657	0.006151738
Plbd1	2.392127447	0.006370048
Tmem159	6.168072414	0.007150606
Hoxa5	6.155894944	0.007437194
Lap3	6.16315926	0.007437194
Gm10660	1.004974306	0.008879846
Sox4	5.987079506	0.009453054
Igkv18-36	6.120424776	0.011126126
Gm48774	6.01947178	0.014811089
mt-Ty	6.402415087	0.021560943
Inpp1	8.804111026	0.021560943
Cd55	6.355639563	0.021560943
Evc	1.838757263	0.023215667
Olfr600	3.456775941	0.024531063
Apobr	5.123058218	0.034166276
E2f1	7.600906289	0.037041426
Sema7a	9.075515938	0.037081768
Ccl5	1.544061474	0.040458384
Chchd6	5.86027072	0.040458384
Dchs1	5.364523199	0.040851549
Inhba	3.642957451	0.051226773
Rasgef1b	1.423229568	0.05401885
Cd300c2	1.803282684	0.05401885
Derl3	4.723610993	0.054809977
Klrc1	7.819176785	0.055533919
Ccl22	4.309665194	0.072870765
Prkcg	2.716776232	0.076371992
C920009B18Rik	5.344357129	0.078570743
Usp7	4.53537257	0.085939487
Slc5a12	2.745250701	0.091817573
Pdlim1	0.962096743	0.097218211
Nckap5l	1.913677759	0.097872382
Vill	6.400665484	0.103340513
Vmn2r69	8.752661304	0.128129418
S100a6	8.912048364	0.149387368
Duxf3	5.997926798	0.170901177
Rab39b	6.686091582	0.171603588
Smarce1-ps1	2.628928114	0.182479638
Ighv1-76	-6.815631038	0.19466004
Olfr767	5.126839488	0.216240653
Cpt1c	2.640835641	0.221418883
Tlr13	7.124214142	0.223139263
Tagln2	2.955104299	0.230301749
Gm2026	3.959294191	0.230636798
Tmem106a	4.834978615	0.233509179
Ttll12	3.831145513	0.262269772
Nxnl2	-6.244482366	0.262538941
Tlr4	-6.495203485	0.266382541
Adarb2	3.442652988	0.27712028
Trbc1	-4.932929946	0.281844957
Vmn2r26	3.685579863	0.281844957
Gm48348	5.131402129	0.301987992
Gm47587	2.160991059	0.301987992
Gm36816	7.432282691	0.301987992
Rnf219	0.925800344	0.301987992
Abhd14b	4.792177893	0.301987992
Pakap	4.322687673	0.301987992
Gm40841	1.649757572	0.301987992
Vwa3b	4.626171863	0.301987992
Gm44578	-4.67721578	0.301987992
Mcm3ap	1.392516836	0.301987992
Tcf25	5.183102536	0.310545738
Apoe	-5.492934478	0.317981688
Plpp1	-2.789392185	0.32388674
Nup93	-0.982907121	0.32388674
Zfp600	5.298804897	0.32388674
Vmn1r168	5.010871191	0.36485661
Gm2912	4.148497736	0.382325787
F2r	2.014221466	0.395642763
Crip3	1.039833154	0.395642763

Table S2, Murine RNAseq, Germinal Center vs Naïve

Top 100 by adjusted p-value

Gene name	log2 Fold Change	Adjusted p-value
Ighg1	5.913427249	7.41E-09
Gcsam	8.908823572	3.39E-07
Kntc1	6.91496134	7.73E-07
Nuggc	10.37681157	7.73E-07
Rrm2	4.847075694	3.11E-06
Osbpl3	4.392889184	5.55E-06
Mef2b	5.763057836	1.91E-05
H1f10	8.76824949	2.63E-05
Rgs13	5.876990193	2.63E-05
Ighg3	2.28193721	2.63E-05
Pclaf	5.105924517	3.50E-05
Tox	5.246157556	3.50E-05
Gm28439	23.04932399	6.31E-05
Aicda	5.242239763	6.88E-05
Uhrf1	3.604058262	0.000253138
Basp1	3.862871307	0.000266538
Anxa2	2.344620617	0.000282326
Lipc	2.741268966	0.000411547
Esco2	5.107827565	0.000440828
Cenps	3.781961101	0.000864211
Nuf2	4.255188089	0.001168684
Hist1h2ap	3.277396026	0.001861931
Mybl2	4.576439678	0.00202436
Psip1	1.541279278	0.00202436
Cdk1	4.748884996	0.002208067
Hmgn2	1.355550855	0.002293416
Cenpf	4.50998384	0.002293416
Neil1	2.692339058	0.002293416
Kif14	6.917943331	0.002293416
Klhl6	1.449892388	0.00384955
Nek2	4.552676992	0.004762058
Sorcs3	18.55676388	0.005758858
Tcf19	3.44146299	0.007295263
Ncapg	3.822712557	0.008614097
Kif18b	5.97782246	0.010055261
Mybl1	4.997135571	0.012110883
Mki67	4.548232518	0.01422272
Tpx2	5.440991051	0.014373919
Pbk	4.868740885	0.015378383
Lig1	3.04204076	0.015378383
Nusap1	3.579711546	0.015409748
Cdca3	5.954720477	0.016575596
Mxd3	6.21273321	0.017575288
Sgo1	5.760394016	0.018887673
Impdh2-ps	16.44647565	0.019010638
2500002B13Rik	7.415085648	0.019010638
Cped1	-17.2285421	0.020593757
Tox2	8.599765307	0.020593757
Mcm10	5.518258003	0.022428626
Dtl	3.411579771	0.025048014
Mcm5	2.586426194	0.030751719
Ccna2	4.789927382	0.030751719
Brip1	3.167279213	0.030751719
Anp32b	1.212599265	0.033378241
Ube2c	5.33741688	0.035149031
Pabpc2	16.29816951	0.035149031
Kifc1	5.27667963	0.036693211
Nova1	7.286898469	0.03790848
Cdc20	4.230438933	0.041465132
Pif1	6.750623042	0.041465132
Txn1	1.626899008	0.041891756
Cdc6	4.314028089	0.042458297
Nid1	-1.815883753	0.04358635
Plxnb2	2.393559407	0.04358635
Mcm6	2.163428004	0.048150953
Kif23	4.035143322	0.048150953
Cenpm	5.234071963	0.048150953
Gm13698	15.78554094	0.048150953
Gm10715	5.442230285	0.048150953
Zfp91	8.087721928	0.048150953
Ctss	-0.651862163	0.049794557
Ccnb1	5.244385598	0.05068879
Gm15899	-7.820474818	0.05194754
Gh	3.418306046	0.05716381
Gpsm2	5.687525436	0.057645186
Top2a	3.621590364	0.057840475
Lrr1	6.062082821	0.058207076
Kif20a	3.622415551	0.064450554
Ranbp1	1.323406743	0.064450554
E2f1	2.345584396	0.064450554
Cdca8	4.74877766	0.064450554
Mad2l1	1.909554141	0.066756216
Eaf2	4.193819551	0.073715057
Lars2	1.568004368	0.073715057
Hmgb2	2.447730333	0.073715057
Gm7146	14.19056675	0.073715057
Stmn1	3.668377272	0.076614402
Arhgap8	5.105615451	0.085747197
Prr11	2.643892221	0.091454419
Cdkn3	5.751417007	0.095324301
Ighe	4.662499362	0.095924855
Asf1b	3.133843491	0.098030219
Ptma	0.73791856	0.098030219
Gm41787	13.71515985	0.098030219
Rassf6	3.623400438	0.101336933
Gm10721	4.753383561	0.101336933
Cachd1	14.70524153	0.106746161
Gm10719	4.836771461	0.109483977
Rgcc	4.237945557	0.111171047
Tuba1b	1.279173616	0.11620105

Table S3, Murine RNAseq, ASC vs Naïve

Top 100 by adjusted p-value

Gene name	log2 Fold Change	Adjusted p-value
Ighg3	6.499310713	9.64E-54
Ighg1	8.819829985	3.25E-23
Ighg2b	6.93373171	3.07E-15
Jchain	3.662305756	6.93E-12
Ighv8-11	7.069644613	3.40E-11
Morf4l1-ps1	-20.4628044	8.98E-11
Iglv1	3.259165083	2.03E-08
Selp	-16.47368842	2.63E-07
Slpi	5.298218298	1.22E-06
Iglc1	2.804354271	1.22E-06
Gm26377	-19.02364473	1.29E-06
Tent5c	3.296004842	2.43E-06
Rexo2	2.386058271	1.24E-05
Gm41787	21.87905229	1.24E-05
Gm7146	21.85153638	1.47E-05
Gm10715	8.335432396	1.47E-05
Gm10721	7.797288415	1.95E-05
Gm9755	22.76962183	5.17E-05
Gm10800	7.66552628	5.17E-05
Gm10801	7.679119536	5.17E-05
Gm13698	22.82056211	5.17E-05
Gm10719	7.683581173	5.17E-05
Gm10717	7.597243779	5.20E-05
Gm28439	22.6524554	5.20E-05
4930470O06Rik	22.60511657	5.20E-05
Gm19276	22.6051169	5.20E-05
Gm50033	22.60511696	5.20E-05
Olfr1300-ps1	22.53368386	5.50E-05
Dbhos	5.708218697	5.96E-05
Gm10718	7.418187502	5.96E-05
Gm17535	7.643556375	6.01E-05
Tcf25	2.793935633	7.62E-05
Evi5	4.078006753	0.000101706
Gm11168	7.314988375	0.000101706
Cachd1	21.82224815	0.000106474
Gm21738	7.450896288	0.000106474
Gm30948	6.385700653	0.000127885
Gm5373	9.102427885	0.000143867
Gm10722	7.618538729	0.000186157
A930017K11Rik	21.18552903	0.000210312
4930470H14Rik	7.759516834	0.000251036
Olfr767	4.215617617	0.000314313
Derl3	3.068736144	0.000322934
Cldn34c1	5.094605014	0.000322934
Igkc	1.93490141	0.000404664
Ube2g2	2.572899615	0.000413413
Pycr1	4.908718108	0.000496645
Impdh2-ps	19.52343229	0.000496645
Rps12l1	-20.1695903	0.000555183
Zfp91	10.33092366	0.000699618
Olfr545	10.21855419	0.000721361
Pon3	5.204382749	0.00094695
Vmn2r113	6.018334987	0.001018842
Gm10720	7.102625593	0.001020274
Mmp28	8.992450596	0.001141776
Gm48309	5.570974544	0.001290064
Vmn2r59	4.515848937	0.001294118
Stard13	9.026249652	0.00134657
Eri3	3.637942334	0.001405729
Olfr107	4.621865511	0.00145416
Rnf8	-4.219601207	0.00151788
Gm45179	4.402110933	0.001859055
Cd247	4.077427822	0.003559389
8430429K09Rik	5.826289784	0.003559389
Cacng4	3.816984688	0.004002554
Sel1l	2.839520438	0.004002554
Gm48774	6.979324982	0.004632777
Hdac4	2.541521529	0.005745893
Gm44873	3.146953466	0.006011143
Gm48104	10.10787732	0.006011143
Zmym1	-6.809727451	0.006287301
Bhlha15	3.457432296	0.006287301
Pgam1-ps2	9.690139525	0.006287301
Tmem154	2.779973722	0.007094132
Trip10	3.857704439	0.007156415
Creld2	1.940162892	0.007156415
Nol10	-4.994265901	0.007156415
Itm2c	2.087241936	0.007189192
Zfp36	-1.014533115	0.007282822
Lrrc42	3.530407088	0.007506642
Slx1b	2.347418522	0.007514509
Tyms	3.874073348	0.007640371
Plec	-2.067529464	0.007830315
Ccdc34	3.821745026	0.008581991
Hsp90b1	1.18753308	0.008582697
4930534H03Rik	5.474193216	0.008582697
Itgb6	9.157976361	0.008776979
Trp53rka	-5.243081554	0.008776979
Fscn1	5.917582843	0.008850256
Txndc5	1.093571444	0.008856726
Cplane1	-6.917305044	0.009227065
Gm42863	5.211508545	0.009227065
Gm43794	8.06136594	0.009227065
Gm42785	4.385705363	0.009227065
Gm47355	5.445999207	0.009227065
Gm49534	3.805958717	0.009227065
Gm21833	5.131186824	0.009578215
Gm37324	3.810069794	0.009705782
Cenpc1	2.677878382	0.009904484
Vmn1r168	6.667350027	0.009904484

Table S4, Human RNAseq Genes, Memory vs Naïve

FDR < 0.1, top 100 by adjusted p-value

Gene Symbol	log2 Fold Change	Adjusted p-value
IGHA1	4.726015635	4.18E-32
IGHA2	4.699898759	3.88E-24
AIM2	3.95065163	1.80E-22
COL4A4	3.941615747	1.14E-20
IGHG4	3.977785932	2.57E-20
TOX	3.686741285	5.05E-17
AHNAK	2.640506861	1.26E-14
ABCB1	-12.07062051	1.72E-13
SSPN	4.856417463	1.75E-13
RAPGEF1	-11.9466995	4.07E-13
IGHD	-3.87654987	4.60E-13
DAAM1	2.473221109	6.59E-13
EHD3	1.769387513	6.59E-13
TNRC18	-11.56302833	3.51E-12
RPL13AP5	-2.394845452	6.93E-12
MARC2	4.141684025	7.28E-12
NIBAN1	3.087687074	7.28E-12
IGFBP4	-2.273965402	9.93E-12
SMC6	-11.34700505	1.23E-11
BTNL9	6.185096724	2.96E-11
PLAG1	2.247261925	3.74E-11
TRAM2	1.801004771	4.01E-11
RPE	-11.11193497	4.75E-11
SLC8B1	-11.12587325	4.75E-11
MEF2C	-11.0955704	4.95E-11
IGF2BP3	3.263577654	4.96E-11
TPT1	-11.06307967	8.27E-11
BTN3A1	-11.11129804	8.27E-11
ITGAX	3.381646401	1.25E-10
DPPA4	-4.424132861	1.25E-10
GATAD2B	-11.08213396	1.33E-10
COL4A3	4.544999695	1.58E-10
SMARCA2	-10.77453079	4.29E-10
CKAP4	2.583956414	4.44E-10
ARRDC5	-10.71400379	5.62E-10
CPLANE1	-10.6992018	6.46E-10
MED12L	4.62816691	1.41E-09
SIGLEC6	2.352010176	1.90E-09
TNIP1	-10.80827523	3.01E-09
RETREG1	-10.41406125	3.75E-09
SLC22A15	2.638913816	9.62E-09
GRAMD1C	3.272628826	1.26E-08
IGHG1	3.70517188	1.33E-08
LAIR1	-3.292297874	1.76E-08
PCDH9	-3.29051819	2.61E-08
RAB31	1.501127578	2.76E-08
IGLV1-44	-10.07202384	3.56E-08
LRRC37A4P	-9.999910334	3.68E-08
USP5	-10.00081517	3.72E-08
BHLHE41	3.052178567	3.91E-08
CCNT1	-10.21618106	3.91E-08
RAB43	-9.956054207	4.86E-08
ABCC10	-9.959942484	5.16E-08
ST6GALNAC3	-8.858953985	5.80E-08
S1PR1	-2.239447929	6.04E-08
NPTN	-9.883026687	6.51E-08
CLECL1	2.112962463	6.79E-08
TNR	5.723300248	7.69E-08
IGLJ1	-7.028762963	1.62E-07
ATP1B2	-4.756018597	2.61E-07
ZFAND2B	-9.839944533	2.68E-07
ASAP1	-9.777549321	2.75E-07
FGD6	4.967420523	3.05E-07
ZNF317	-9.685648717	3.18E-07
TMEM71	-9.668951491	3.21E-07
PAFAH1B3	-9.609835655	3.95E-07
ICOSLG	-1.60915919	4.02E-07
ZNF510	-9.544328062	4.62E-07
ORC3	-9.515378263	5.26E-07
TET1	2.887380626	5.27E-07
FAM160A2	-9.520071307	5.27E-07
GMPR2	-9.571436013	5.39E-07
CD27	4.086778063	7.59E-07
PAG1	1.845983372	9.22E-07
GNG2	-9.388464248	1.10E-06
AC005261.1	-9.604521598	1.13E-06
TPST1	-9.425738342	1.29E-06
TIMP2	-9.411523369	1.31E-06
EPB41L5	-9.59561624	1.31E-06
CEP170	-9.292291942	1.34E-06
SPATA5L1	-9.422998187	1.35E-06
PRUNE1	-8.810050071	1.55E-06
ANKRD28	-9.724818143	1.55E-06
TTC39B	-2.14302744	1.82E-06
IGHM	-2.676228164	1.91E-06
ZNF208	2.34888438	2.69E-06
CLIP4	3.131329596	2.75E-06
PIGG	-9.326647775	2.75E-06
PECAM1	-1.641925356	3.01E-06
KCTD12	1.73692087	3.08E-06
MCOLN2	2.442136538	3.19E-06
MIS12	-9.163844074	3.28E-06
TAS1R3	4.255446832	3.41E-06
HECTD4	-13.4831323	3.75E-06
ZNF772	-9.116663477	4.01E-06
ZBTB38	2.584762101	4.07E-06
RTTN	-9.132830414	4.84E-06
CELF2	-13.2282168	5.15E-06
APIP	-4.594876377	5.47E-06
FAM169A	-9.071022359	7.39E-06

Table S5, Human RNAseq Genes, Germinal Center vs Memory
FDR < 0.1, top 100 by adjusted p-value

Gene Symbol	log2 Fold Change	Adjusted p-value
AHNAK	-6.090598519	2.25E-32
IGLV1-44	16.25801484	1.04E-21
KLF3	-5.711458714	1.60E-16
PREX1	-4.445551729	3.47E-16
GTSE1	3.059238124	4.34E-16
KIF11	2.543749074	4.76E-16
FCGR2C	-5.680790897	1.26E-15
SKI	-2.994320275	1.43E-15
TBC1D9	-4.279332348	4.20E-14
ITGAX	-4.970125724	4.20E-14
P2RY10	-3.221666112	1.25E-13
CCND1	-5.374525097	1.39E-13
HSPA7	-3.723191501	3.75E-13
AC244205.2	9.114266892	3.89E-13
ZNF215	12.25459576	1.96E-12
TBC1D24	12.02326756	7.07E-12
MAD2L1	2.593425151	7.07E-12
S1PR2	2.415387893	7.07E-12
USP32P3	2.804785751	7.89E-12
CAPG	-4.531806004	4.46E-11
ANKRD28	11.76230003	4.74E-11
LRRK2	-3.036161196	4.74E-11
TNFAIP3	11.94827852	5.23E-11
SIGLEC14	-5.810667931	6.24E-11
FZD6	11.59915834	6.54E-11
TBC1D27P	-4.356046508	6.54E-11
PLXNC1	-3.083402785	9.09E-11
GON7	11.5441254	9.22E-11
ERN1	3.219195342	1.15E-10
AL669918.1	11.7775796	1.66E-10
USP5	11.63589808	3.33E-10
NUGGC	3.228478868	3.33E-10
DOP1B	-3.810989529	3.33E-10
COL19A1	-3.121211044	4.37E-10
SNTA1	2.654241827	4.54E-10
SLC2A5	2.482687768	5.04E-10
C21orf58	11.23012427	5.52E-10
IGLV3-21	5.613944445	5.52E-10
SEC14L1	3.378384148	5.52E-10
NPTN	11.04780158	1.34E-09
SDK2	-9.278598824	1.36E-09
IGHV7-4-1	5.853410708	1.56E-09
IL4R	2.232531394	2.78E-09
CR1	-3.159322535	2.85E-09
GPR82	-2.519683113	3.97E-09
RAB31	-3.228956576	3.97E-09
CEP55	2.506989787	4.06E-09
PRDM1	15.76785062	4.32E-09
ARHGAP33	9.862979008	4.32E-09
MKI67	3.891377203	4.99E-09
GDF7	-4.912153133	5.57E-09
CCDC50	-3.013646933	7.42E-09
SHCBP1	2.637657142	1.00E-08
IGLJ1	8.785798388	1.34E-08
IGKV3D-15	4.108847478	1.39E-08
SLC37A2	-2.644514136	1.39E-08
RFTN1	2.105223794	1.44E-08
TXNIP	-3.131422555	1.46E-08
UST	-5.387117853	1.46E-08
CCR6	-6.454402518	1.56E-08
IGLV3-1	5.110551934	1.74E-08
FUT7	-5.823097962	1.95E-08
DDX60	-4.247682721	2.09E-08
IGHV1-69D	5.224195606	2.35E-08
LPP	22.49045808	2.39E-08
IGHV2-5	5.193166012	2.79E-08
ARF4	10.87935384	2.87E-08
IGHV3-43	11.96065314	3.69E-08
DCAF12	3.729079271	4.55E-08
ZNF732	8.895499293	5.94E-08
AICDA	3.47606129	6.22E-08
MIXL1	3.949084989	6.67E-08
DBNL	-1.97615706	6.67E-08
CLNK	-7.863954655	6.96E-08
ANTXR2	-4.885280898	7.09E-08
AC234301.1	4.905018918	7.87E-08
GRAP2	-8.933571776	7.87E-08
AC233755.2	5.972429479	8.98E-08
TUBB2A	2.776489921	9.90E-08
DNASE1	2.000279965	1.16E-07
FCMR	-4.125296964	1.29E-07
TNR	-6.489752217	1.29E-07
BHLHE40	-5.497675203	1.35E-07
HID1	11.23861009	1.50E-07
CCND2	-4.691267636	1.50E-07
IGHV3-20	5.219515146	1.52E-07
GVINP1	-2.381257433	1.91E-07
CCDC77	10.04883946	1.92E-07
IGHV1-24	13.92406205	1.99E-07
MOB3B	-4.468794165	2.75E-07
MNDA	-5.136251295	3.01E-07
AC233755.1	3.982630526	3.17E-07
IL27RA	-2.669475622	3.27E-07
NCAPD2	1.736100914	3.31E-07
IGLV3-9	5.691333699	3.40E-07
CAMK1D	-2.378873445	3.40E-07
IGHV4-61	4.35241284	3.53E-07
NT5C2	13.93528754	3.62E-07
PKD1L1	3.125582233	3.68E-07
APOLD1	10.37671958	4.12E-07

Table S6, Human RNAseq Genes, Germinal Center vs Naïve
FDR < 0.1, top 100 by adjusted p-value

Gene Symbol	log2 Fold Change	Adjusted p-value
NUGGC	5.436969578	5.55E-71
LOXL2	5.091341323	3.93E-53
IGHA1	4.564155889	3.93E-53
TUBB2A	5.388970244	5.89E-43
MEF2B	4.252774243	9.85E-43
SAPCD2	4.525934667	1.78E-41
IGLV8-61	4.984020129	2.02E-38
DCAF12	5.064441482	1.41E-35
IGHG4	4.564766402	4.64E-34
NIBAN1	3.961411498	5.10E-34
E2F2	4.366327485	1.65E-32
P2RY10	-3.576577235	2.95E-31
EVC	5.194187922	3.14E-31
SHCBP1	3.849020194	1.04E-30
IGLV1-44	6.165828306	1.31E-30
AC244205.2	6.171454012	2.87E-29
UBE2J1	3.492445788	2.87E-29
MIXL1	5.072367145	2.18E-28
CKAP2L	4.2236488	2.18E-28
KLF3	-6.305322135	3.71E-28
CENPE	4.134901675	1.29E-27
COL19A1	-5.10508362	1.79E-26
PRKCA	4.126809598	2.20E-26
IGKV1-39	5.381202861	3.27E-26
HASPIN	3.907887123	8.14E-26
TXNDC5	4.507729529	1.35E-25
FRZB	9.990574917	1.57E-25
CCDC50	-2.403834118	2.14E-25
SPAG5	3.756733492	7.63E-25
ASF1B	3.662089003	1.02E-24
CKAP4	5.435506841	1.09E-24
IGHG1	4.694480922	1.09E-24
FGD6	7.030220708	1.28E-24
IGLV3-1	5.95076321	2.71E-24
TOX	4.23251488	1.71E-23
QPCT	3.913794751	2.49E-23
ARL4C	-4.461995792	4.31E-23
FANCA	4.097895589	4.71E-23
UGGT1	1.957840259	7.47E-23
S1PR2	3.45890032	1.73E-22
IGLV7-46	4.661425711	1.84E-22
MYBL1	5.644140696	2.37E-22
TREML2	-2.427392083	2.37E-22
PAPSS1	2.945868047	2.89E-22
IGHV5-10-1	4.607269959	3.89E-22
SEC14L1	3.779162452	7.44E-22
CD27	5.415640272	7.08E-21
CPEB4	2.703805872	1.02E-20
FNDC3B	13.05294767	2.24E-20
IGHV2-70D	6.447425146	3.40E-20
UST	-6.185954019	5.04E-20
EXT1	3.160706332	5.23E-20
SIDT1	-2.738889237	6.33E-20
RGCC	5.097350115	7.81E-20
PAG1	2.474730249	7.97E-20
PREX1	-3.456205263	2.52E-19
TOP2A	4.624474006	2.92E-19
IGHV4-31	6.274195114	3.27E-19
HJURP	4.423175345	5.81E-19
CDCA8	3.893618372	6.23E-19
AC233755.2	5.214625567	6.71E-19
KANK2	9.75895879	7.00E-19
AICDA	4.84696826	7.81E-19
FEN1	2.660875456	9.27E-19
AIM2	3.631788959	9.73E-19
GLCCI1	2.787448502	9.73E-19
TERF2	2.560320862	1.07E-18
RGS13	6.125455694	1.84E-18
IGHV2-5	5.464513326	2.59E-18
SCARB1	2.963753025	3.61E-18
HS2ST1	2.339856202	3.61E-18
IGLV3-21	6.148956089	3.86E-18
CELF2	-12.16093886	3.87E-18
B3GLCT	2.772121857	4.18E-18
RAP2A	2.85167034	5.12E-18
PHACTR1	-2.238115836	5.46E-18
PELI1	2.560282676	6.98E-18
GTSE1	4.377409418	7.17E-18
IGKV1D-13	5.730771241	9.03E-18
XBP1	6.106455106	1.39E-17
SDK2	-10.88863556	1.57E-17
KLHL6	2.726844412	2.42E-17
USP32P3	3.486049336	2.48E-17
CITED2	2.768145365	4.42E-17
SKI	-2.801034436	6.63E-17
BAIAP2L1	5.800962654	6.83E-17
CKS2	2.937686722	8.12E-17
HMGB1P6	2.303205962	8.46E-17
RPRD1B	2.822726253	9.72E-17
CDR2	2.840583243	1.02E-16
GBP4	-3.684102128	1.32E-16
IGKV1-6	6.533968528	1.48E-16
HMCES	2.871732976	1.48E-16
IGHA2	4.323044171	1.61E-16
NDC80	3.649475528	1.62E-16
IGKV3D-11	5.449407905	2.74E-16
IGKV1-17	5.192700458	3.16E-16
IGKV6D-21	4.497193921	3.45E-16
IGLV1-51	5.009542879	3.65E-16
IGHV3-20	5.591337445	3.96E-16

Table S7, Human RNAseq GSEA, Memory vs Naïve

Up in Memory

FDR < 0.25

Name	FDR q value
MULTICELLULAR ORGANISM METABOLIC PROCESS	0.06001629
PHAGOCYTOSIS ENGULFMENT	0.07360295
MULTICELLULAR ORGANISMAL MACROMOLECULE METABOLIC PROCESS	0.09368128
MEMBRANE INVAGINATION	0.1274628
ANTIMICROBIAL HUMORAL RESPONSE	0.13167854
PHAGOCYTOSIS RECOGNITION	0.13281861
HUMORAL IMMUNE RESPONSE MEDIATED BY CIRCULATING IMMUNOGLOBULIN	0.13441542
COMPLEMENT ACTIVATION	0.1357199
B CELL MEDIATED IMMUNITY	0.14926401
LYMPHOCYTE MEDIATED IMMUNITY	0.15188183
PROTEIN ACTIVATION CASCADE	0.16376208
RENAL SYSTEM PROCESS	0.19076346
RETINA HOMEOSTASIS	0.19739702
LEUKOCYTE MEDIATED IMMUNITY	0.20985462
ADAPTIVE IMMUNE RESPONSE BASED ON SOMATIC RECOMBINATION OF IMMUNE RECEPTORS BUILT FROM IMMUNOGLOBULIN SUPERFAMILY DOMAINS	0.21666574
B CELL RECEPTOR SIGNALING PATHWAY	0.23074354

Down in memory

FDR < 0.25 = none

Table S8, Human RNAseq, GSEA, Germinal Center vs Memory
Up in GC
FDR < 0.25, top 100

Name	FDR q value
NUCLEAR CHROMOSOME SEGREGATION	0.00607441
SISTER CHROMATID SEGREGATION	0.006164157
SISTER CHROMATID COHESION	0.006294231
CHROMOSOME SEGREGATION	0.009764046
MICROTUBULE ORGANIZING CENTER ORGANIZATION	0.02329388
ORGANELLE FISSION	0.02396471
PHAGOCYTOSIS RECOGNITION	0.026500266
MEIOTIC CELL CYCLE	0.032299496
MEMBRANE INVAGINATION	0.03252484
CELL DIFFERENTIATION INVOLVED IN EMBRYONIC PLACENTA DEVELOPMENT	0.033979293
PROTEIN K48 LINKED DEUBIQUITINATION	0.0343765
MEIOTIC CELL CYCLE PROCESS	0.035143916
PHAGOCYTOSIS ENGULFMENT	0.035974316
DNA PACKAGING	0.03602652
MITOTIC SISTER CHROMATID SEGREGATION	0.03658939
MITOTIC NUCLEAR DIVISION	0.038958564
REGULATION OF DNA DEPENDENT DNA REPLICATION	0.03961695
PROTEIN ACTIVATION CASCADE	0.05265464
CENTROSOME CYCLE	0.054640707
COMPLEMENT ACTIVATION	0.054989915
NEGATIVE REGULATION OF MITOTIC NUCLEAR DIVISION	0.055777565
PROTEIN LOCALIZATION TO CHROMOSOME	0.05783893
SPINDLE CHECKPOINT	0.059695274
B CELL MEDIATED IMMUNITY	0.07120197
NEGATIVE REGULATION OF NUCLEAR DIVISION	0.07296832
REGULATION OF TRANSCRIPTION INVOLVED IN G1 S TRANSITION OF MITOTIC CELL CYCLE	0.085975654
MICROTUBULE CYTOSKELETON ORGANIZATION	0.08624446
DNA STRAND ELONGATION	0.087636404
HUMORAL IMMUNE RESPONSE MEDIATED BY CIRCULATING IMMUNOGLOBULIN	0.087908916
REGULATION OF NUCLEAR DIVISION	0.08989317
CELL CYCLE CHECKPOINT	0.0900719
PROTEIN DNA COMPLEX SUBUNIT ORGANIZATION	0.0904972
NEGATIVE REGULATION OF RESPONSE TO BIOTIC STIMULUS	0.09129417
NEGATIVE REGULATION OF CELL CYCLE PROCESS	0.0935606
MEIOSIS I	0.09378967
REGULATION OF SISTER CHROMATID SEGREGATION	0.09589385
AMMONIUM TRANSPORT	0.09818077
REGULATION OF CHROMOSOME SEGREGATION	0.10083835
SIGNAL TRANSDUCTION IN RESPONSE TO DNA DAMAGE	0.103145555
NEGATIVE REGULATION OF CHROMOSOME SEGREGATION	0.10323392
DNA STRAND ELONGATION INVOLVED IN DNA REPLICATION	0.10339004
DNA CONFORMATION CHANGE	0.10442368
CENTROMERE COMPLEX ASSEMBLY	0.10518155
MITOTIC CELL CYCLE	0.10567901
MEIOTIC CHROMOSOME SEGREGATION	0.10657595
MITOTIC SPINDLE ORGANIZATION	0.107367225
NEGATIVE REGULATION OF CELL CYCLE G2 M PHASE TRANSITION	0.10770168
CHROMATIN ASSEMBLY OR DISASSEMBLY	0.107799254
CELL CYCLE PROCESS	0.10985064
MITOTIC CYTOKINESIS	0.11054417
ER NUCLEUS SIGNALING PATHWAY	0.11164798
NEGATIVE REGULATION OF INTRINSIC APOPTOTIC SIGNALING PATHWAY IN RESPONSE TO DNA DAMAGE	0.116749674
IRE1 MEDIATED UNFOLDED PROTEIN RESPONSE	0.11813941
REGULATION OF INTRINSIC APOPTOTIC SIGNALING PATHWAY IN RESPONSE TO DNA DAMAGE	0.118455455
G2 DNA DAMAGE CHECKPOINT	0.123271145
MITOTIC CELL CYCLE CHECKPOINT	0.12359716
DNA INTEGRITY CHECKPOINT	0.12460397

REGULATION OF MICROTUBULE POLYMERIZATION OR DEPOLYMERIZATION	0.12500317
CYTOSKELETON DEPENDENT CYTOKINESIS	0.12501514
REGULATION OF LIPOPOLYSACCHARIDE MEDIATED SIGNALING PATHWAY	0.1251991
NEGATIVE REGULATION OF CELL CYCLE PHASE TRANSITION	0.12630418
CHROMOSOME LOCALIZATION	0.12666877
CELL DIVISION	0.12845778
MICROTUBULE BASED PROCESS	0.131425
METAPHASE PLATE CONGRESSION	0.13329989
PROTEIN UBIQUITINATION INVOLVED IN UBIQUITIN DEPENDENT PROTEIN CATABOLIC PROCESS	0.13499564
NEGATIVE REGULATION OF CELL DIVISION	0.13693202
REGULATION OF ENDOTHELIAL CELL APOPTOTIC PROCESS	0.13760312
NEGATIVE REGULATION OF RESPONSE TO DNA DAMAGE STIMULUS	0.13862677
POSITIVE REGULATION OF MONOOXYGENASE ACTIVITY	0.1388939
POSITIVE REGULATION OF DNA REPAIR	0.1413507
DNA DEPENDENT DNA REPLICATION	0.14263757
B CELL RECEPTOR SIGNALING PATHWAY	0.1467538
ER ASSOCIATED UBIQUITIN DEPENDENT PROTEIN CATABOLIC PROCESS	0.15789588
MITOTIC G2 M TRANSITION CHECKPOINT	0.15826865
POSITIVE REGULATION OF NITRIC OXIDE SYNTHASE ACTIVITY	0.15934289
NEUTRAL AMINO ACID TRANSPORT	0.16504087
DNA RECOMBINATION	0.17712983
REGULATION OF MICROTUBULE BASED PROCESS	0.17823927
REGULATION OF CENTROSOME CYCLE	0.17836025
RETROGRADE VESICLE MEDIATED TRANSPORT GOLGI TO ER	0.17889902
ERAD PATHWAY	0.18364125
CELL CYCLE	0.18690252
CHROMOSOME CONDENSATION	0.18855956
SPINDLE ASSEMBLY	0.18963687
SOMATIC DIVERSIFICATION OF IMMUNOGLOBULINS	0.19127986
DNA REPLICATION INDEPENDENT NUCLEOSOME ORGANIZATION	0.19146714
LEUKOCYTE MEDIATED IMMUNITY	0.19190468
POSITIVE REGULATION OF EXOCYTOSIS	0.19726545
LYMPHOCYTE MEDIATED IMMUNITY	0.19784595
REGULATION OF CELL DIVISION	0.20823863
REGULATION OF DNA REPAIR	0.2125895
MITOTIC DNA INTEGRITY CHECKPOINT	0.21417753
PROTEIN EXIT FROM ENDOPLASMIC RETICULUM	0.21606901
RESPONSE TO TOPOLOGICALLY INCORRECT PROTEIN	0.21624483
POSITIVE REGULATION OF OXIDOREDUCTASE ACTIVITY	0.2165297
VISUAL BEHAVIOR	0.21675439
IMMUNOGLOBULIN PRODUCTION	0.21731317
PROTEIN K63 LINKED DEUBIQUITINATION	0.21822898
REGULATION OF RESPONSE TO DNA DAMAGE STIMULUS	0.21831495

Down in GC
FDR < 0.25

Name	FDR q-value
INTERFERON GAMMA MEDIATED SIGNALING PATHWAY	0.206013
LEUKOCYTE CHEMOTAXIS	0.22996613
SYNAPSE ORGANIZATION	0.23438194
REGULATION OF DENDRITIC SPINE MORPHOGENESIS	0.23487836
FOREBRAIN CELL MIGRATION	0.24026863
CHEMOKINE MEDIATED SIGNALING PATHWAY	0.24442133
BODY MORPHOGENESIS	0.24600795
RESPONSE TO INTERFERON GAMMA	0.24807915
NEGATIVE REGULATION OF GLIOGENESIS	0.2498118

Table S9, Human RNAseq, GSEA, Germinal Center vs Naïve
Up in GC
FDR < 0.25, top 100

Name	FDR q value
NUCLEAR CHROMOSOME SEGREGATION	5.59E-05
CHROMOSOME SEGREGATION	8.39E-05
SISTER CHROMATID SEGREGATION	8.42E-05
COMPLEMENT ACTIVATION	0.000169346
PROTEIN ACTIVATION CASCADE	0.00018638
SISTER CHROMATID COHESION	0.000211737
MITOTIC SISTER CHROMATID SEGREGATION	0.000567677
DNA PACKAGING	0.000665788
B CELL MEDIATED IMMUNITY	0.001098796
ORGANELLE FISSION	0.001217235
HUMORAL IMMUNE RESPONSE MEDIATED BY CIRCULATING IMMUNOGLOBULIN	0.001268409
MITOTIC NUCLEAR DIVISION	0.001282733
PHAGOCYTOSIS ENGULFMENT	0.001346377
MEMBRANE INVAGINATION	0.001352429
PHAGOCYTOSIS RECOGNITION	0.003066471
ADAPTIVE IMMUNE RESPONSE BASED ON SOMATIC RECOMBINATION OF IMMUNE RECEPTORS BUILT FROM IMMUNOGLOBULIN SUPERFAMILY DOMAINS	0.003091909
DNA CONFORMATION CHANGE	0.003646173
CHROMATIN ASSEMBLY OR DISASSEMBLY	0.004600627
LYMPHOCYTE MEDIATED IMMUNITY	0.004618425
PROTEIN DNA COMPLEX SUBUNIT ORGANIZATION	0.004793946
IRE1 MEDIATED UNFOLDED PROTEIN RESPONSE	0.005693434
LEUKOCYTE MEDIATED IMMUNITY	0.005787344
CENTROMERE COMPLEX ASSEMBLY	0.006178492
ENDOTHELIAL CELL PROLIFERATION	0.008303737
MEIOTIC CELL CYCLE PROCESS	0.010542356
METAPHASE PLATE CONGRESSION	0.010770621
REGULATION OF TRANSCRIPTION INVOLVED IN G1 S TRANSITION OF MITOTIC CELL CYCLE	0.01102248
DNA REPLICATION INDEPENDENT NUCLEOSOME ORGANIZATION	0.013089298
POSITIVE REGULATION OF B CELL ACTIVATION	0.013152253
FC GAMMA RECEPTOR SIGNALING PATHWAY	0.013801825
PHAGOCYTOSIS	0.018258294
RESPONSE TO COPPER ION	0.019001303
ER ASSOCIATED UBIQUITIN DEPENDENT PROTEIN CATABOLIC PROCESS	0.019205946
B CELL RECEPTOR SIGNALING PATHWAY	0.0269172
MITOTIC CELL CYCLE	0.032201767
ERAD PATHWAY	0.032556273
SPINDLE LOCALIZATION	0.03335151
CHROMOSOME LOCALIZATION	0.033483483
HUMORAL IMMUNE RESPONSE	0.036892112
CHROMOSOME CONDENSATION	0.03714998
REGULATION OF TRIGLYCERIDE METABOLIC PROCESS	0.037720937
ESTABLISHMENT OF SPINDLE ORIENTATION	0.038178086
REGULATION OF SISTER CHROMATID SEGREGATION	0.04684451
PROTEIN LOCALIZATION TO CHROMOSOME	0.04702194
REGULATION OF B CELL ACTIVATION	0.053963937
CELL CYCLE PROCESS	0.065860525
CENTROSOME CYCLE	0.06941582
REGULATION OF CHROMOSOME SEGREGATION	0.07421569
RESPONSE TO TOPOLOGICALLY INCORRECT PROTEIN	0.079768546
MICROTUBULE ORGANIZING CENTER ORGANIZATION	0.079885356
REGULATION OF ERAD PATHWAY	0.080136456
MEIOTIC CELL CYCLE	0.080246866
CELL CYCLE CHECKPOINT	0.08039117
MICROTUBULE BASED PROCESS	0.08058941
SOMATIC DIVERSIFICATION OF IMMUNE RECEPTORS	0.08106302
CELLULAR RESPONSE TO TOPOLOGICALLY INCORRECT PROTEIN	0.08345611
CELL DIVISION	0.08493251
POSITIVE REGULATION OF CELL CYCLE ARREST	0.08558009

HISTONE EXCHANGE	0.0869989
DEFENSE RESPONSE TO BACTERIUM	0.09063051
DNA INTEGRITY CHECKPOINT	0.09082548
MEIOSIS I	0.09293435
POSITIVE REGULATION OF PROTEIN OLIGOMERIZATION	0.09492329
PROTEIN DEGLYCOSYLATION	0.09598392
ATP DEPENDENT CHROMATIN REMODELING	0.09681081
ALPHA AMINO ACID BIOSYNTHETIC PROCESS	0.09724347
MICROTUBULE POLYMERIZATION OR DEPOLYMERIZATION	0.09803017
MICROTUBULE CYTOSKELETON ORGANIZATION	0.098115645
CELL CYCLE PHASE TRANSITION	0.09847491
IMMUNOGLOBULIN PRODUCTION	0.09853206
DNA STRAND ELONGATION INVOLVED IN DNA REPLICATION	0.10359302
DNA DEPENDENT DNA REPLICATION	0.10388573
REGULATION OF ENDOTHELIAL CELL APOPTOTIC PROCESS	0.1043416
SOMATIC DIVERSIFICATION OF IMMUNOGLOBULINS	0.10636967
REGULATION OF NUCLEAR DIVISION	0.10788146
ER NUCLEUS SIGNALING PATHWAY	0.10906362
MITOTIC SPINDLE ORGANIZATION	0.11799759
RETROGRADE VESICLE MEDIATED TRANSPORT GOLGI TO ER	0.1191756
PRODUCTION OF MOLECULAR MEDIATOR OF IMMUNE RESPONSE	0.12159807
CELL CYCLE	0.12689751
DNA REPLICATION	0.12819934
MITOTIC CELL CYCLE CHECKPOINT	0.12912461
REGULATION OF DNA DEPENDENT DNA REPLICATION	0.13054912
DNA GEOMETRIC CHANGE	0.13136981
REGULATION OF MICROTUBULE POLYMERIZATION OR DEPOLYMERIZATION	0.13160226
CHROMOSOME ORGANIZATION	0.1341385
NEGATIVE REGULATION OF CELL CYCLE PROCESS	0.13481165
NUCLEOSIDE BISPHOSPHATE BIOSYNTHETIC PROCESS	0.1352902
RECEPTOR MEDIATED ENDOCYTOSIS	0.13544236
CELL CYCLE G1 S PHASE TRANSITION	0.13611215
RESPONSE TO ENDOPLASMIC RETICULUM STRESS	0.13665497
MITOTIC DNA INTEGRITY CHECKPOINT	0.14242855
PROTEIN N LINKED GLYCOSYLATION	0.14335142
NEGATIVE REGULATION OF RESPONSE TO ENDOPLASMIC RETICULUM STRESS	0.14820907
PURINE RIBONUCLEOSIDE BISPHOSPHATE METABOLIC PROCESS	0.14951092
REGULATION OF CHROMATIN SILENCING	0.15618584
DNA LIGATION	0.15707347
CELLULAR AMINO ACID BIOSYNTHETIC PROCESS	0.17732792
NEGATIVE REGULATION OF CELL CYCLE PHASE TRANSITION	0.19536585
REGULATION OF DNA DAMAGE RESPONSE SIGNAL TRANSDUCTION BY P53 CLASS MEDIATOR	0.19731578

Down in GC
FDR < 0.25

Name	FDR q value
DEFENSE RESPONSE TO VIRUS	0.003562246
INTERFERON GAMMA MEDIATED SIGNALING PATHWAY	0.013880002
REGULATION OF CHEMOTAXIS	0.028220007
RESPONSE TO VIRUS	0.06033028
POSITIVE REGULATION OF CHEMOTAXIS	0.070175044
POSITIVE REGULATION OF LEUKOCYTE MIGRATION	0.07155539
CHEMOKINE MEDIATED SIGNALING PATHWAY	0.07526398
POSITIVE REGULATION OF T CELL PROLIFERATION	0.077823564
ANTIGEN PROCESSING AND PRESENTATION OF ENDOGENOUS ANTIGEN	0.07923104
LEUKOCYTE MIGRATION	0.08211768
REGULATION OF NEUTROPHIL MIGRATION	0.08240936
CELLULAR RESPONSE TO INTERFERON GAMMA	0.09072795
CELLULAR DEFENSE RESPONSE	0.09511582
LYMPHOCYTE COSTIMULATION	0.107501835
REGULATION OF CYTOKINE PRODUCTION INVOLVED IN IMMUNE RESPONSE	0.11348495
LEUKOCYTE CHEMOTAXIS	0.1160459
CRANIAL SKELETAL SYSTEM DEVELOPMENT	0.11672272
REGULATION OF ANTIGEN PROCESSING AND PRESENTATION	0.11739909
NEGATIVE REGULATION OF LYMPHOCYTE MEDIATED IMMUNITY	0.1267263

NEGATIVE REGULATION OF LEUKOCYTE MEDIATED IMMUNITY	0.12728642
CELL CELL RECOGNITION	0.12902658
LAMELLIPODIUM ORGANIZATION	0.13059244
NEGATIVE REGULATION OF IMMUNE RESPONSE	0.13237222
ACTOMYOSIN STRUCTURE ORGANIZATION	0.13270245
REGULATION OF SKELETAL MUSCLE TISSUE DEVELOPMENT	0.1344437
RESPONSE TO INTERFERON GAMMA	0.13500673
NEGATIVE REGULATION OF VIRAL PROCESS	0.13520876
SENSORY PERCEPTION OF MECHANICAL STIMULUS	0.13611539
NEGATIVE REGULATION OF VIRAL GENOME REPLICATION	0.13783523
SKELETAL MUSCLE ORGAN DEVELOPMENT	0.14680913
REGULATION OF VASCULAR ENDOTHELIAL GROWTH FACTOR RECEPTOR SIGNALING PATHWAY	0.161474
LYMPHOCYTE DIFFERENTIATION	0.18033254
SUPEROXIDE METABOLIC PROCESS	0.18268868
RESPONSE TO TYPE I INTERFERON	0.18537802
POSITIVE REGULATION OF TISSUE REMODELING	0.2046587
POSITIVE REGULATION OF CELL ADHESION	0.21120381
POSITIVE REGULATION OF CELL CELL ADHESION	0.21377867
CELL CHEMOTAXIS	0.21792439
REGULATION OF HISTONE DEACETYLATION	0.21821348
T CELL DIFFERENTIATION	0.22222096
REGULATION OF CELL SUBSTRATE ADHESION	0.22315535
EMBRYONIC CRANIAL SKELETON MORPHOGENESIS	0.22947961
CELL SURFACE RECEPTOR SIGNALING PATHWAY INVOLVED IN CELL CELL SIGNALING	0.23033716
SPERM EGG RECOGNITION	0.23375207
REGULATION OF MYOBLAST DIFFERENTIATION	0.23545477
REGULATION OF T CELL PROLIFERATION	0.23799117
POSITIVE REGULATION OF LEUKOCYTE CHEMOTAXIS	0.23802212
POSITIVE REGULATION OF LIPID KINASE ACTIVITY	0.24210592
REGULATION OF GRANULOCYTE CHEMOTAXIS	0.24267752
ANATOMICAL STRUCTURE MATURATION	0.2460095

Table S10, Human Proteomics Proteins, Memory vs Naïve
Up in memory
FDR < 0.1 = none

Table S11, Human Proteomics, Germinal Center vs Memory
Up in GC
FDR<0.1, top 100 by adjusted p-value

Protein	Gene Name	logFC	Adjusted p-value
AHNK	AHNAK	-4.6960946	0.00389413
A0A286YES1	IGHG3	4.70448705	0.00389413
IGHG1	IGHG1	4.19743434	0.00623841
VIME	VIM	-4.0002421	0.00821495
CAPG	CAPG	-4.0691965	0.0092352
H3BNQ7	ABAT	-3.4428084	0.0092352
RRBP1	RRBP1	3.56954831	0.0092352
HV270	IGHV2-70	5.52978655	0.0092352
MX2	MX2	-3.2691764	0.01166493
PDCD4	PDCD4	-3.0964668	0.013146
CD38	CD38	3.06367456	0.013146
PML	PML	-3.0911961	0.013146
LV321	IGLV3-21	3.64756178	0.0131837
MSPD2	MOSPD2	3.10860572	0.01325401
AURKB	AURKB	3.1406556	0.01367089
SCMC1	SLC25A24	-3.6977822	0.0165567
RAB7L	RAB29	-2.9787169	0.0165567
TMM43	TMEM43	-2.8558299	0.0165567
A0A087X1N8	SERPINB6	-3.186222	0.01683615
CDK1	CDK1	2.89418589	0.01735406
DTX3L	DTX3L	-2.6370493	0.01774998
MECP2	MECP2	-2.7202175	0.01907787
FLNA	FLNA	-2.6640357	0.01907787
HV343	IGHV3-43	3.29621765	0.01907787
A0A2R8YD85	DOCK10	-2.5230785	0.01907787
DDX60	DDX60	-2.5642033	0.01907787
TBCD4	TBC1D4	3.00941736	0.02137724
A0A087X279	IFIT2	-2.6957949	0.02147107
PP14A	PPP1R14A	-4.1363703	0.02147107
SERA	PHGDH	2.42570158	0.02147107
A0A087X211	CIP2A	2.39967484	0.02147107
HVCN1	HVCN1	-2.6634797	0.02147262
M3K5	MAP3K5	-2.3735857	0.02176643
KMO	KMO	-2.3322975	0.02378665
BACH	ACOT7	2.29805779	0.02476739
A0A5F9ZHB6	PRIM1	2.20704543	0.03075727
HV333	IGHV3-33	2.58961839	0.03075727
DPOD3	POLD3	2.30596519	0.03346283
SLIP	NUGGC	2.79308547	0.03346283
RIR1	RRM1	2.25619667	0.03609858
ANXA4	ANXA4	-2.7392455	0.03675476
VAV3	VAV3	2.07217994	0.03675476
PCNA	PCNA	2.2719396	0.03675476
NMI	NMI	-2.0826138	0.03675476
SNX18	SNX18	-2.1149032	0.03675476
CND1	NCAPD2	2.82784018	0.03675476
TM263	TMEM263	2.06639148	0.03675476
TOPK	PBK	4.19362302	0.03811406
NDC80	NDC80	2.40017057	0.03811406
RGS19	RGS19	-2.0444671	0.03811406
IGLC3	IGLC3	2.46150568	0.03811406
A0A0B4J231	IGLL5	3.06928697	0.03811406
KVD07	IGKV3D-7	2.04708936	0.03811406
ITPR1	ITPR1	-2.0152492	0.03811406
KVD39	IGKV1D-39	2.40452063	0.03811406
SEM4A	SEMA4A	2.93594722	0.03811406
KIF2C	KIF2C	3.06853624	0.04159787
SMC2	SMC2	2.31413734	0.04161786
SIAS	NANS	1.97524821	0.04161786
STMN1	STMN1	1.94944602	0.04161786
PTTG3	PTTG3P	4.39008827	0.04161786
DHE3	GLUD1	-1.924921	0.04161786
PTGR3	ZADH2	-2.0510487	0.0417394
TSPO	TSPO	-1.9852873	0.0417394
CKAP2	CKAP2	2.39547941	0.04197981
FBX5	FBXO5	2.84736888	0.04197981
MCM6	MCM6	2.00015892	0.04197981
SELH	SELENOH	-1.9807652	0.04197981
HMGB2	HMGB2	2.40640704	0.04306829
B7WPE2	EML3	-1.9728243	0.04306829
PCKGM	PCK2	-1.9275227	0.04306829
KPCB	PRKCB	-2.3252606	0.0437094
KI67	MKI67	2.72812603	0.0437094
PAR14	PARP14	-1.8792018	0.0437094
LV861	IGLV8-61	2.24495948	0.0437094
Q5VV89	MGST3	-2.6728175	0.0437094
CO3	C3	-1.8376734	0.0437094
CY24B	CYBB	-1.8471198	0.0437094
SMC4	SMC4	2.26285694	0.0437094
MCM7	MCM7	2.29691381	0.0437094
SQOR	SQOR	-1.9631907	0.0437094
VIGLN	HDLBP	1.83665266	0.04468315
B5MBZ0	EML4	-1.8127493	0.0447924
LMNA	LMNA	-1.810888	0.04540234
FND3A	FNDC3A	1.80608122	0.04540234
FOCAD	FOCAD	1.79716375	0.04540234
ENPL	HSP90B1	1.81176038	0.04540234
J3KSJ5	CYBC1	-1.8597689	0.04540234
MAP2	METAP2	2.01011009	0.04540234
CAF1A	CHAF1A	2.45348585	0.04540234
H0YBH7	SARAF	-1.8015113	0.04540234
CBPM	CPM	1.7659366	0.04577338
I2BPL	IRF2BPL	-1.8163003	0.04619546
HLAE	HLA-E	-2.1358841	0.04619546
IL16	IL16	-1.8074124	0.04697557
PTN1	PTPN1	-1.7845697	0.04712124
MORC3	MORC3	-1.7666023	0.04712124
KIF4B	KIF4B	2.61374533	0.04712124
B4DWJ3	EAF2	1.73359769	0.04714657
DDX58	DDX58	-1.8065149	0.04714657

Table S12, Human Proteomics, Germinal Center vs Naïve
Up in GC
FDR < 0.1, top 100 by adjusted p-value

Protein	Gene Name	logFC	Adjusted p-value
A0A286YES1	IGHG3	6.26002032	1.19E-09
TOPK	PBK	6.10755585	4.89E-09
INCE	INCENP	5.31399728	4.89E-09
IGHG1	IGHG1	5.35227481	5.45E-09
PP14A	PPP1R14A	-4.9902239	1.18E-08
FBX5	FBXO5	4.51936601	2.19E-08
SEM4A	SEMA4A	4.37703944	2.37E-08
AURKB	AURKB	4.70523681	2.89E-08
NDC80	NDC80	4.20887789	4.68E-08
CND1	NCAPD2	4.46118167	4.86E-08
KI67	MKI67	4.54424362	5.48E-08
H3BNQ7	ABAT	-3.9395198	5.48E-08
CDK1	CDK1	4.03820967	5.84E-08
MDR1	ABCB1	-4.4701889	6.51E-08
KIF4B	KIF4B	4.33987304	7.87E-08
TOP2A	TOP2A	3.76753852	1.02E-07
MX2	MX2	-3.692184	1.02E-07
SNX18	SNX18	-3.6029007	1.33E-07
HV270	IGHV2-70	3.58332715	1.51E-07
LV861	IGLV8-61	3.53152155	1.53E-07
SERA	PHGDH	3.53635171	1.90E-07
ANXA4	ANXA4	-3.6759248	2.22E-07
CND2	NCAPH	3.47212323	2.22E-07
SCMC1	SLC25A24	-3.8571863	2.39E-07
TOX3	TOX3	3.65689599	2.39E-07
A0A286YEY1	IGHA1	3.4628902	2.39E-07
CAF1A	CHAF1A	4.34393303	2.39E-07
SLIP	NUGGC	5.20688333	2.39E-07
AHNK	AHNAK	-3.295372	3.13E-07
MECP2	MECP2	-3.3128208	3.13E-07
A0A0B4J1V9	HELLS	3.34093444	3.30E-07
KMO	KMO	-3.2514154	3.30E-07
LHPP	LHPP	-3.5748439	3.30E-07
CAPG	CAPG	-3.6715997	4.97E-07
KIF2C	KIF2C	4.17124235	5.65E-07
A0A087X279	IFIT2	-3.8067094	5.89E-07
SMC2	SMC2	3.59081701	6.03E-07
SMC4	SMC4	3.17560231	6.46E-07
VIME	VIM	-3.2637174	6.89E-07
WDR76	WDR76	3.30925824	7.16E-07
PDCD4	PDCD4	-2.9877913	7.42E-07
H0YBH7	SARAF	-3.0597637	7.47E-07
RIR1	RRM1	3.10782304	7.80E-07
PTTG3	PTTG3P	3.02016431	7.87E-07
A0A087X1N8	SERPINB6	-2.9846098	7.87E-07
DDX60	DDX60	-2.9601042	8.40E-07
SIAS	NANS	2.91537428	9.14E-07
M3K5	MAP3K5	-2.9051848	9.14E-07
A0A087X211	CIP2A	2.97123641	9.14E-07
KPCB	PRKCB	-3.1035319	1.00E-06
B7ZKQ9	SCARB1	3.48986462	1.01E-06
BACH	ACOT7	3.57351709	1.02E-06
I2BPL	IRF2BPL	-2.8775104	1.05E-06
MCM7	MCM7	3.2484246	1.13E-06
HVCN1	HVCN1	-2.7910771	1.39E-06
DTX3L	DTX3L	-2.8024526	1.40E-06
CKAP2	CKAP2	2.78465333	1.40E-06
PML	PML	-2.749663	1.62E-06
RAB7L	RAB29	-2.8709336	1.77E-06
VAV3	VAV3	2.74197143	1.86E-06
TBCD4	TBC1D4	3.78651946	1.97E-06
Q5VV89	MGST3	-2.9688145	2.05E-06
TMM43	TMEM43	-2.662143	2.30E-06
PCNA	PCNA	2.76811677	2.41E-06
IF44L	IFI44L	-4.5559744	2.45E-06
T3JAM	TRAF3IP3	-2.6377253	3.25E-06
HSP72	HSPA2	2.92804537	3.33E-06
CD38	CD38	2.71375923	4.18E-06
ANXA1	ANXA1	-2.491194	4.88E-06
A0A5F9ZHB6	PRIM1	2.45467828	5.80E-06
MCM6	MCM6	2.58284736	5.84E-06
KLHL6	KLHL6	2.66427429	6.44E-06
A0A3B3IT92	MCM4	2.4270185	6.44E-06
NIBA1	NIBAN1	2.50430867	6.83E-06
MCM2	MCM2	2.59109046	7.04E-06
RRBP1	RRBP1	2.96725143	7.34E-06
EDRF1	EDRF1	3.03733315	7.44E-06
DPOD3	POLD3	2.38653136	7.44E-06
RED1	ADARB1	-2.3625682	8.63E-06
HLAE	HLA-E	-2.7725911	8.63E-06
FND3A	FNDC3A	2.3359189	9.47E-06
ANXA6	ANXA6	-2.935576	9.71E-06
ADK	ADK	-2.319207	1.00E-05
ENPL	HSP90B1	2.39033275	1.00E-05
LEG9C	LGALS9C	-2.4133108	1.00E-05
A0A499FI48	PDIA4	2.34251843	1.09E-05
F8W930	IGF2BP2	2.32765945	1.13E-05
STMN1	STMN1	2.27452298	1.34E-05
DDX58	DDX58	-2.2595755	1.34E-05
H0Y6A7	GDAP1L1	-2.4475821	1.37E-05
CBPM	CPM	2.24732884	1.43E-05
NUSAP	NUSAP1	2.18805624	1.93E-05
VIGLN	HDLBP	2.19132959	2.05E-05
ARL3	ARL3	2.1688911	2.05E-05
LV321	IGLV3-21	2.65409571	2.26E-05
UBP1	USP1	2.2180949	2.29E-05
IGLC3	IGLC3	2.65598359	2.43E-05
SQOR	SQOR	-2.2263851	2.51E-05
CO3	C3	-2.1239435	2.53E-05
CUTC	CUTC	-2.1772665	2.64E-05

Table S13, Human Proteomics, Gene Ontology, Memory vs Naïve
Up in Memory
FDR < 0.25

Name	FDR q value
ALPHA AMINO ACID BIOSYNTHETIC PROCESS	0.01059989
CELLULAR AMINO ACID BIOSYNTHETIC PROCESS	0.04044202
MEIOTIC CELL CYCLE PROCESS	0.04191775
DNA REPLICATION	0.05002333
MICROTUBULE CYTOSKELETON ORGANIZATION	0.05408017
NEGATIVE REGULATION OF PROTEIN COMPLEX DISASSEMBLY	0.11206458
NEGATIVE REGULATION OF ORGANELLE ORGANIZATION	0.11728625
CELL RECOGNITION	0.13640952
ALPHA AMINO ACID METABOLIC PROCESS	0.13750018
ESTABLISHMENT OF CELL POLARITY	0.13756353
NEGATIVE REGULATION OF DNA REPLICATION	0.13945413
MITOTIC DNA INTEGRITY CHECKPOINT	0.1451286
MICROTUBULE BASED PROCESS	0.16051607
DNA DEPENDENT DNA REPLICATION	0.17025676
NEGATIVE REGULATION OF CYTOSKELETON ORGANIZATION	0.17501712
RESPONSE TO TOPOLOGICALLY INCORRECT PROTEIN	0.17659397
MITOTIC SPINDLE ORGANIZATION	0.18946256
ORGAN REGENERATION	0.20159166
ORGANELLE FISSION	0.20281057
ESTABLISHMENT OR MAINTENANCE OF CELL POLARITY	0.20337868
DETECTION OF STIMULUS	0.2052254
CYTOSKELETON ORGANIZATION	0.23372863
DICARBOXYLIC ACID METABOLIC PROCESS	0.23660754
MEIOTIC CELL CYCLE	0.23838721
RESPONSE TO UV	0.24269181
NEGATIVE REGULATION OF DNA METABOLIC PROCESS	0.24298537

Down in Memory

Name	FDR q value
DEFENSE RESPONSE TO VIRUS	0.00141876
RESPONSE TO VIRUS	0.00738445
VACUOLAR TRANSPORT	0.04288827
REGULATION OF CELLULAR AMINO ACID METABOLIC PROCESS	0.04586278
TUMOR NECROSIS FACTOR MEDIATED SIGNALING PATHWAY	0.05288686
RESPONSE TO TUMOR NECROSIS FACTOR	0.05892983
NIK NF KAPPAB SIGNALING	0.07292286
REGULATION OF CELLULAR KETONE METABOLIC PROCESS	0.09513432
PROTEIN SECRETION	0.09554245
ANTIGEN PROCESSING AND PRESENTATION OF PEPTIDE ANTIGEN VIA MHC CLASS I	0.10348595
POSITIVE REGULATION OF CANONICAL WNT SIGNALING PATHWAY	0.10622323
NEGATIVE REGULATION OF IMMUNE EFFECTOR PROCESS	0.13218252
NEGATIVE REGULATION OF IMMUNE SYSTEM PROCESS	0.13362081
VESICLE ORGANIZATION	0.13460933
REGULATION OF T CELL PROLIFERATION	0.13643983
CYTOKINE MEDIATED SIGNALING PATHWAY	0.137765
NEGATIVE REGULATION OF CANONICAL WNT SIGNALING PATHWAY	0.13847394
SENSORY ORGAN MORPHOGENESIS	0.13956307
POSITIVE REGULATION OF HEMOPOIESIS	0.14014795
NEGATIVE REGULATION OF CYTOKINE PRODUCTION	0.14037243
NEGATIVE REGULATION OF CELL PROLIFERATION	0.14080656
REGULATION OF MYELOID CELL DIFFERENTIATION	0.14100657
POSITIVE REGULATION OF T CELL PROLIFERATION	0.14249402
REGULATION OF CANONICAL WNT SIGNALING PATHWAY	0.14489283
REGULATION OF ESTABLISHMENT OF PLANAR POLARITY	0.14496142
NON CANONICAL WNT SIGNALING PATHWAY	0.14965124
DEFENSE RESPONSE TO OTHER ORGANISM	0.15135172
INNATE IMMUNE RESPONSE	0.1513755

NEGATIVE REGULATION OF VIRAL GENOME REPLICATION	0.15194663
POSITIVE REGULATION OF WNT SIGNALING PATHWAY	0.15307596
MEMBRANE DOCKING	0.15360418
ANTIGEN PROCESSING AND PRESENTATION OF EXOGENOUS PEPTIDE ANTIGEN VIA MHC CLASS I	0.16733111
EPIDERMIS DEVELOPMENT	0.16870366
RESPONSE TO TYPE I INTERFERON	0.17076936
REGULATION OF LEUKOCYTE PROLIFERATION	0.18854608
REGULATION OF CARBOHYDRATE METABOLIC PROCESS	0.1888046
PROTEIN ACETYLATION	0.18969165
MEMBRANE BUDDING	0.19097921
REGULATION OF ORGAN MORPHOGENESIS	0.19249676
REGULATION OF RESPONSE TO BIOTIC STIMULUS	0.19310822
PROTEIN ACYLATION	0.19440052
RETROGRADE TRANSPORT ENDOSOME TO GOLGI	0.19542782
REGULATION OF MULTI ORGANISM PROCESS	0.20190795
EMBRYONIC ORGAN DEVELOPMENT	0.22305699
DEFENSE RESPONSE	0.22951418
POSITIVE REGULATION OF GENE EXPRESSION EPIGENETIC	0.23025267
T CELL DIFFERENTIATION	0.23168012
POSITIVE REGULATION OF BINDING	0.23188424
REGULATION OF MUSCLE SYSTEM PROCESS	0.23524946
REGULATION OF HORMONE SECRETION	0.23940374
NEGATIVE REGULATION OF VIRAL PROCESS	0.23997541
REGULATION OF DEFENSE RESPONSE	0.24004187
LYMPHOCYTE DIFFERENTIATION	0.24326873
ENDOSOME ORGANIZATION	0.24479869
NEGATIVE REGULATION OF IMMUNE RESPONSE	0.24583708
REGULATION OF HEMOPOIESIS	0.24597998
LEUKOCYTE DIFFERENTIATION	0.24850686

Table S14, Human Proteomics, Gene Ontology, Germinal Center vs Memory

Up in GC

FDR < 0.25, top 100 by FDR

Name	FDR q value
TRANSLATIONAL INITIATION	0
MITOTIC SISTER CHROMATID SEGREGATION	0
MULTI ORGANISM METABOLIC PROCESS	0
NUCLEAR TRANSCRIBED MRNA CATABOLIC PROCESS NONSENSE MEDIATED DECAY	0
DNA PACKAGING	1.21E-05
SISTER CHROMATID SEGREGATION	1.39E-05
DNA DEPENDENT DNA REPLICATION	1.62E-05
ESTABLISHMENT OF PROTEIN LOCALIZATION TO ENDOPLASMIC RETICULUM	1.94E-05
DNA REPLICATION	2.11E-05
PROTEIN LOCALIZATION TO ENDOPLASMIC RETICULUM	3.69E-05
NUCLEAR CHROMOSOME SEGREGATION	0.00016475
MEIOTIC CELL CYCLE PROCESS	0.00047728
RNA CATABOLIC PROCESS	0.00094217
PROTEIN TARGETING TO MEMBRANE	0.00152027
CHROMOSOME SEGREGATION	0.00153157
MITOTIC RECOMBINATION	0.00274821
B CELL MEDIATED IMMUNITY	0.00332687
DNA CONFORMATION CHANGE	0.00389146
VIRAL LIFE CYCLE	0.0039867
MEIOTIC CELL CYCLE	0.00408225
POSITIVE REGULATION OF LIGASE ACTIVITY	0.00416344
ANAPHASE PROMOTING COMPLEX DEPENDENT CATABOLIC PROCESS	0.00423934
POSITIVE REGULATION OF B CELL ACTIVATION	0.00424385
REGULATION OF LIGASE ACTIVITY	0.00460058
ORGAN REGENERATION	0.0046582
MACROMOLECULE CATABOLIC PROCESS	0.00474834
TELOMERE MAINTENANCE VIA RECOMBINATION	0.00648458
AMIDE BIOSYNTHETIC PROCESS	0.00658687
PROTEASOMAL PROTEIN CATABOLIC PROCESS	0.00684583
CELL CYCLE G1 S PHASE TRANSITION	0.00757163
HUMORAL IMMUNE RESPONSE MEDIATED BY CIRCULATING IMMUNOGLOBULIN	0.00818699
ORGANELLE FISSION	0.00824549
CELL DIVISION	0.00837352
PROTEIN UBIQUITINATION	0.00893645
REGULATION OF B CELL ACTIVATION	0.00910767
PROTEOLYSIS	0.0091702
MEMBRANE INVAGINATION	0.010078
DNA METABOLIC PROCESS	0.01036766
POSTTRANSCRIPTIONAL REGULATION OF GENE EXPRESSION	0.01055969
CHROMOSOME ORGANIZATION	0.01094323
TRANSCRIPTION COUPLED NUCLEOTIDE EXCISION REPAIR	0.01109343
CELL CYCLE PHASE TRANSITION	0.01112185
SEX DIFFERENTIATION	0.0112996
PROTEIN UBIQUITINATION INVOLVED IN UBIQUITIN DEPENDENT PROTEIN CATABOLIC PROCESS	0.01130155
RIBONUCLEOPROTEIN COMPLEX BIOGENESIS	0.01130997
ADAPTIVE IMMUNE RESPONSE BASED ON SOMATIC RECOMBINATION OF IMMUNE RECEPTORS BUILT FROM IMMUNOGLOBULIN SUPERFAMILY DOMAINS	0.01141952
CELL RECOGNITION	0.01143574
POSTREPLICATION REPAIR	0.01145132
B CELL RECEPTOR SIGNALING PATHWAY	0.01164851
DNA RECOMBINATION	0.01277509
REGULATION OF TRANSLATIONAL INITIATION	0.01282203
MITOTIC CELL CYCLE	0.0128257
POSITIVE REGULATION OF PROTEIN MODIFICATION BY SMALL PROTEIN CONJUGATION OR REMOVAL	0.01303744
DEFENSE RESPONSE TO BACTERIUM	0.01305889

CELLULAR RESPONSE TO UV	0.01371861
HUMORAL IMMUNE RESPONSE	0.01441866
REGULATION OF CELLULAR AMIDE METABOLIC PROCESS	0.01450024
CELLULAR RESPONSE TO LIGHT STIMULUS	0.01524624
RIBOSOME ASSEMBLY	0.01526411
ORGANIC CYCLIC COMPOUND CATABOLIC PROCESS	0.01527052
RIBONUCLEOPROTEIN COMPLEX SUBUNIT ORGANIZATION	0.01543544
MITOTIC NUCLEAR DIVISION	0.01546049
CYTOPLASMIC TRANSLATION	0.01548587
ESTABLISHMENT OF PROTEIN LOCALIZATION TO MEMBRANE	0.01555745
SISTER CHROMATID COHESION	0.01599557
PROTEIN ACTIVATION CASCADE	0.01673671
RIBOSOME BIOGENESIS	0.01743159
CELL CYCLE PROCESS	0.01808002
DEVELOPMENT OF PRIMARY SEXUAL CHARACTERISTICS	0.01822586
CELL CYCLE	0.0213718
PEPTIDE METABOLIC PROCESS	0.02498539
POSITIVE REGULATION OF PROTEIN CATABOLIC PROCESS	0.02499857
DETECTION OF STIMULUS	0.02741158
DNA DAMAGE RESPONSE DETECTION OF DNA DAMAGE	0.02759891
CELL PROLIFERATION	0.02813284
LYMPHOCYTE MEDIATED IMMUNITY	0.0287014
RRNA METABOLIC PROCESS	0.02898854
CELLULAR AMIDE METABOLIC PROCESS	0.02921609
LEUKOCYTE MEDIATED IMMUNITY	0.02934568
POSITIVE REGULATION OF CANONICAL WNT SIGNALING PATHWAY	0.02952155
ANTIGEN RECEPTOR MEDIATED SIGNALING PATHWAY	0.02957775
RESPONSE TO UV	0.03023103
PROTEIN MODIFICATION BY SMALL PROTEIN CONJUGATION OR REMOVAL	0.03165005
POSITIVE REGULATION OF CELLULAR PROTEIN CATABOLIC PROCESS	0.03338699
DNA SYNTHESIS INVOLVED IN DNA REPAIR	0.03359369
REPRODUCTIVE SYSTEM DEVELOPMENT	0.03390475
PROTEIN CATABOLIC PROCESS	0.03409009
DNA REPAIR	0.03489686
CELLULAR PROTEIN COMPLEX DISASSEMBLY	0.04109561
RETROGRADE VESICLE MEDIATED TRANSPORT GOLGI TO ER	0.04280585
CELLULAR RESPONSE TO DNA DAMAGE STIMULUS	0.04374087
TELOMERE ORGANIZATION	0.04464912
NUCLEOTIDE EXCISION REPAIR	0.04576841
RESPONSE TO BACTERIUM	0.04879524
NUCLEIC ACID PHOSPHODIESTER BOND HYDROLYSIS	0.04949153
REGULATION OF CELLULAR AMINO ACID METABOLIC PROCESS	0.05248792
NIK NF KAPPAB SIGNALING	0.05917221
REPRODUCTION	0.06590674
RNA SECONDARY STRUCTURE UNWINDING	0.06610991
GERM CELL DEVELOPMENT	0.06667494

Down in GC vs Memory
FDR < 0.25, top 100 by FDR

Name	FDR q-value
MONOCARBOXYLIC ACID CATABOLIC PROCESS	0.00018608
ENERGY DERIVATION BY OXIDATION OF ORGANIC COMPOUNDS	0.00027912
CELLULAR RESPIRATION	0.00033771
AEROBIC RESPIRATION	0.00190518
ORGANIC ACID CATABOLIC PROCESS	0.00216286
FATTY ACID CATABOLIC PROCESS	0.00304013
TRICARBOXYLIC ACID METABOLIC PROCESS	0.00314425
FATTY ACID BETA OXIDATION	0.00358497
DEFENSE RESPONSE TO VIRUS	0.00525758
LIPID OXIDATION	0.00759908
OXIDATION REDUCTION PROCESS	0.00800992
NEGATIVE REGULATION OF CYTOKINE PRODUCTION	0.00801924
SMALL MOLECULE CATABOLIC PROCESS	0.00877248
ION TRANSPORT	0.01412171
ACTIN FILAMENT BASED PROCESS	0.0219407

ELECTRON TRANSPORT CHAIN	0.02352414
POSITIVE REGULATION OF SEQUENCE SPECIFIC DNA BINDING TRANSCRIPTION FACTOR ACTIVITY	0.02900108
REGULATION OF GLUCOSE TRANSPORT	0.02993347
GENERATION OF PRECURSOR METABOLITES AND ENERGY	0.03315501
CELL JUNCTION ORGANIZATION	0.03529506
INTERFERON GAMMA MEDIATED SIGNALING PATHWAY	0.03781014
CELLULAR AMINO ACID CATABOLIC PROCESS	0.04245888
TRANSMEMBRANE RECEPTOR PROTEIN SERINE THREONINE KINASE SIGNALING PATHWAY	0.04324364
REGULATION OF CYTOKINE PRODUCTION	0.0436535
ANION TRANSPORT	0.04390565
REGULATION OF ACTIN FILAMENT LENGTH	0.04611156
REGULATION OF IMMUNE EFFECTOR PROCESS	0.05040627
RESPONSE TO VIRUS	0.05705569
REGULATION OF PROTEIN SECRETION	0.057107
CELLULAR LIPID CATABOLIC PROCESS	0.05720759
POSITIVE REGULATION OF IMMUNE EFFECTOR PROCESS	0.05852078
POSITIVE REGULATION OF NF KAPPAB TRANSCRIPTION FACTOR ACTIVITY	0.05995789
REGULATION OF SEQUENCE SPECIFIC DNA BINDING TRANSCRIPTION FACTOR ACTIVITY	0.0600939
RESPONSE TO INTERFERON GAMMA	0.06132324
G PROTEIN COUPLED RECEPTOR SIGNALING PATHWAY	0.06610736
POSITIVE REGULATION OF T CELL PROLIFERATION	0.06875299
CELLULAR RESPONSE TO INTERFERON GAMMA	0.06941062
NEGATIVE REGULATION OF IMMUNE RESPONSE	0.06950474
NEGATIVE REGULATION OF SECRETION	0.07347221
REGULATION OF T CELL PROLIFERATION	0.07738648
RESPONSE TO TYPE I INTERFERON	0.0799296
CALCIUM ION TRANSPORT	0.08043854
REGULATION OF HOMOTYPIC CELL CELL ADHESION	0.08172958
REGULATION OF ION TRANSPORT	0.09392521
NEGATIVE REGULATION OF VIRAL PROCESS	0.09435217
REGULATION OF ACTIN FILAMENT BASED PROCESS	0.09670254
RNA MODIFICATION	0.10994986
NEGATIVE REGULATION OF MULTICELLULAR ORGANISMAL PROCESS	0.11020558
LIPID METABOLIC PROCESS	0.11211693
ION TRANSMEMBRANE TRANSPORT	0.11960704
DIVALENT INORGANIC CATION TRANSPORT	0.12028571
FATTY ACID METABOLIC PROCESS	0.12594505
ORGANONITROGEN COMPOUND CATABOLIC PROCESS	0.13020843
NEGATIVE REGULATION OF CELL DIFFERENTIATION	0.13067234
NEGATIVE REGULATION OF IMMUNE SYSTEM PROCESS	0.13866794
NEGATIVE REGULATION OF CELL DEVELOPMENT	0.14039317
REGULATED EXOCYTOSIS	0.14324693
EXOCYTOSIS	0.14581802
REGULATION OF CALCIUM ION TRANSPORT	0.14760438
CATION TRANSPORT	0.15028992
CELLULAR LIPID METABOLIC PROCESS	0.15877154
REGULATION OF SECRETION	0.16300242
NEGATIVE REGULATION OF DEVELOPMENTAL PROCESS	0.16428532
MONOCARBOXYLIC ACID METABOLIC PROCESS	0.16499864
MAINTENANCE OF LOCATION IN CELL	0.16624904
ORGANIC ANION TRANSPORT	0.1665203
ACTIN FILAMENT ORGANIZATION	0.16703796
SENSORY PERCEPTION	0.16837431
LIPID MODIFICATION	0.17080584
CELLULAR ALDEHYDE METABOLIC PROCESS	0.17638475
NEGATIVE REGULATION OF MULTI ORGANISM PROCESS	0.18091351
REGULATION OF BODY FLUID LEVELS	0.18911366
NEGATIVE REGULATION OF CELL PROJECTION ORGANIZATION	0.19019228
REGULATION OF ADAPTIVE IMMUNE RESPONSE	0.19096623
POSITIVE REGULATION OF CELL DEVELOPMENT	0.19148275
REGULATION OF ION HOMEOSTASIS	0.19171928
REGULATION OF CELL PROJECTION ORGANIZATION	0.19590302
REGULATION OF GTPASE ACTIVITY	0.1968257
MONOVALENT INORGANIC CATION TRANSPORT	0.19882411
METAL ION TRANSPORT	0.19903187

REGULATION OF RESPONSE TO BIOTIC STIMULUS	0.20029566
ORGANIC ACID METABOLIC PROCESS	0.20124382
OXIDATIVE PHOSPHORYLATION	0.20128526
LIPID CATABOLIC PROCESS	0.20276308
TRANSMEMBRANE TRANSPORT	0.20414343
POSITIVE REGULATION OF CELL CELL ADHESION	0.20438962
NUCLEAR ENVELOPE ORGANIZATION	0.20511219
MITOCHONDRIAL RESPIRATORY CHAIN COMPLEX ASSEMBLY	0.20522113
GLYCEROLIPID METABOLIC PROCESS	0.2053369
MUSCLE SYSTEM PROCESS	0.20570666
HEMOSTASIS	0.20638551
VACUOLE ORGANIZATION	0.20651393
SMALL MOLECULE METABOLIC PROCESS	0.20651907
CYTOKINE MEDIATED SIGNALING PATHWAY	0.20655821
PLATELET ACTIVATION	0.20660132
REGULATION OF CELL CELL ADHESION	0.20706874
NEGATIVE REGULATION OF IMMUNE EFFECTOR PROCESS	0.20833392
DEFENSE RESPONSE	0.21756282
REGULATION OF PROTEIN POLYMERIZATION	0.22745416
REGULATION OF LYMPHOCYTE DIFFERENTIATION	0.22940885

Table S15, Human Proteomics, Gene Ontology, Germinal Center vs Naive
Up in GC
FDR < 0.25, top 100 by FDR

Name	FDR q-value
NUCLEAR CHROMOSOME SEGREGATION	0
SISTER CHROMATID SEGREGATION	0
DNA REPLICATION	0
MITOTIC SISTER CHROMATID SEGREGATION	3.08E-05
DNA DEPENDENT DNA REPLICATION	3.70E-05
TRANSLATIONAL INITIATION	3.88E-05
CHROMOSOME SEGREGATION	4.01E-05
MEIOTIC CELL CYCLE	4.52E-05
MEIOTIC CELL CYCLE PROCESS	4.62E-05
ORGANELLE FISSION	0.00028662
NUCLEAR TRANSCRIBED MRNA CATABOLIC PROCESS NONSENSE MEDIATED DECAY	0.00120252
CELL DIVISION	0.00134814
MITOTIC NUCLEAR DIVISION	0.00171964
MEMBRANE INVAGINATION	0.00218291
SISTER CHROMATID COHESION	0.00222093
MITOTIC RECOMBINATION	0.00236298
DNA PACKAGING	0.00248529
ESTABLISHMENT OF PROTEIN LOCALIZATION TO ENDOPLASMIC RETICULUM	0.00269839
DNA CONFORMATION CHANGE	0.00278896
CELL RECOGNITION	0.00280236
ADAPTIVE IMMUNE RESPONSE BASED ON SOMATIC RECOMBINATION OF IMMUNE RECEPTORS BUILT FROM IMMUNOGLOBULIN SUPERFAMILY DOMAINS	0.00315958
POSITIVE REGULATION OF B CELL ACTIVATION	0.00317337
MULTI ORGANISM METABOLIC PROCESS	0.0041053
CELL CYCLE G1 S PHASE TRANSITION	0.00702617
TELOMERE MAINTENANCE VIA RECOMBINATION	0.00707723
REGULATION OF TRANSLATIONAL INITIATION	0.00710246
REGULATION OF CELLULAR AMIDE METABOLIC PROCESS	0.00710248
B CELL MEDIATED IMMUNITY	0.00723693
MITOTIC CELL CYCLE	0.00723902
LYMPHOCYTE MEDIATED IMMUNITY	0.0082895
REGULATION OF B CELL ACTIVATION	0.00833836
PROTEIN LOCALIZATION TO ENDOPLASMIC RETICULUM	0.00834936
DNA METABOLIC PROCESS	0.00879423
CHROMOSOME ORGANIZATION	0.00973284
MICROTUBULE CYTOSKELETON ORGANIZATION	0.01233159
CELL CYCLE PROCESS	0.01246234
RECEPTOR MEDIATED ENDOCYTOSIS	0.01432414
CELL CYCLE	0.01741899
DETECTION OF STIMULUS	0.01752374
POSTREPLICATION REPAIR	0.01791395
CYTOKINESIS	0.01815836
ORGAN REGENERATION	0.01817497
NUCLEIC ACID PHOSPHODIESTER BOND HYDROLYSIS	0.01833975
LEUKOCYTE MEDIATED IMMUNITY	0.0198853
TRANSCRIPTION COUPLED NUCLEOTIDE EXCISION REPAIR	0.01994876
RNA CATABOLIC PROCESS	0.02026633
RESPONSE TO TEMPERATURE STIMULUS	0.02039151
HUMORAL IMMUNE RESPONSE MEDIATED BY CIRCULATING IMMUNOGLOBULIN	0.02200099
AMIDE BIOSYNTHETIC PROCESS	0.02678694
B CELL RECEPTOR SIGNALING PATHWAY	0.02848602
POSTTRANSCRIPTIONAL REGULATION OF GENE EXPRESSION	0.02990405
DNA DAMAGE RESPONSE DETECTION OF DNA DAMAGE	0.0310914
RESPONSE TO HEAT	0.03139398
CELL CYCLE PHASE TRANSITION	0.03153661
CELLULAR RESPONSE TO UV	0.03285559
DNA SYNTHESIS INVOLVED IN DNA REPAIR	0.03311695
RESPONSE TO TOPOLOGICALLY INCORRECT PROTEIN	0.03767011
NEGATIVE REGULATION OF MITOTIC CELL CYCLE	0.03767316

PHAGOCYTOSIS	0.03792055
CELLULAR RESPONSE TO LIGHT STIMULUS	0.03801395
PROTEIN UBIQUITINATION INVOLVED IN UBIQUITIN DEPENDENT PROTEIN CATABOLIC PROCESS	0.03966924
NEGATIVE REGULATION OF CELL CYCLE PROCESS	0.04273081
REGULATION OF CHROMOSOME SEGREGATION	0.04404879
DNA RECOMBINATION	0.04430691
TELOMERE ORGANIZATION	0.04455445
MITOTIC SPINDLE ORGANIZATION	0.04459376
CELLULAR RESPONSE TO DNA DAMAGE STIMULUS	0.04569341
HUMORAL IMMUNE RESPONSE	0.04573321
PROTEIN ACTIVATION CASCADE	0.04632481
MICROTUBULE BASED PROCESS	0.0492546
PROTEIN TARGETING TO MEMBRANE	0.06295092
MITOTIC DNA INTEGRITY CHECKPOINT	0.06310792
DEFENSE RESPONSE TO BACTERIUM	0.06628687
REGULATION OF MICROTUBULE POLYMERIZATION OR DEPOLYMERIZATION	0.06990311
ENDOCYTOSIS	0.07066567
FC GAMMA RECEPTOR SIGNALING PATHWAY	0.07158091
MITOTIC CELL CYCLE CHECKPOINT	0.07166812
REPRODUCTION	0.07219257
PROTEASOMAL PROTEIN CATABOLIC PROCESS	0.07242162
RESPONSE TO UV	0.07245036
MACROMOLECULE CATABOLIC PROCESS	0.07267588
POSITIVE REGULATION OF CELLULAR AMIDE METABOLIC PROCESS	0.07608307
RIBOSOME ASSEMBLY	0.08194646
PROTEIN SUMOYLATION	0.08484436
DNA REPAIR	0.08495148
POSITIVE REGULATION OF PROTEIN MODIFICATION BY SMALL PROTEIN CONJUGATION OR REMOVAL	0.0860921
DNA GEOMETRIC CHANGE	0.08702855
POSITIVE REGULATION OF LIGASE ACTIVITY	0.08718187
DNA BIOSYNTHETIC PROCESS	0.08769614
NUCLEOTIDE EXCISION REPAIR	0.08908057
ESTABLISHMENT OF PROTEIN LOCALIZATION TO MEMBRANE	0.08919804
PROTEOLYSIS	0.09204457
ANATOMICAL STRUCTURE HOMEOSTASIS	0.09363035
REGULATION OF LIGASE ACTIVITY	0.09385732
CELLULAR AMIDE METABOLIC PROCESS	0.09891792
CHAPERONE MEDIATED PROTEIN FOLDING	0.09984819
DEVELOPMENT OF PRIMARY SEXUAL CHARACTERISTICS	0.09987207
PROTEIN MODIFICATION BY SMALL PROTEIN CONJUGATION OR REMOVAL	0.10327409
PROTEIN FOLDING	0.10458512
POSITIVE REGULATION OF DNA REPLICATION	0.10460006

Down in GC

Name	FDR q-value
DEFENSE RESPONSE TO VIRUS	0.00581776
NEGATIVE REGULATION OF CYTOKINE PRODUCTION	0.01702166
REGULATION OF PROTEIN SECRETION	0.03593558
CELLULAR RESPIRATION	0.03603397
REGULATION OF IMMUNE EFFECTOR PROCESS	0.04027752
ENERGY DERIVATION BY OXIDATION OF ORGANIC COMPOUNDS	0.04106582
NEGATIVE REGULATION OF MULTI ORGANISM PROCESS	0.05158291
NEGATIVE REGULATION OF CELL DIFFERENTIATION	0.05167595
NEGATIVE REGULATION OF VIRAL PROCESS	0.05311067
RESPONSE TO TYPE I INTERFERON	0.05501264
ION TRANSPORT	0.05562511
G PROTEIN COUPLED RECEPTOR SIGNALING PATHWAY	0.05613982
NEGATIVE REGULATION OF IMMUNE SYSTEM PROCESS	0.05619909
REGULATION OF CYTOKINE PRODUCTION	0.05867169
RESPONSE TO VIRUS	0.06029249
REGULATION OF SEQUENCE SPECIFIC DNA BINDING TRANSCRIPTION FACTOR ACTIVITY	0.07155809
NEGATIVE REGULATION OF CELL DEVELOPMENT	0.07725427

REGULATION OF RESPONSE TO BIOTIC STIMULUS	0.08097497
REGULATION OF T CELL PROLIFERATION	0.08444148
CYTOKINE MEDIATED SIGNALING PATHWAY	0.08910913
NEGATIVE REGULATION OF VIRAL GENOME REPLICATION	0.09613399
NEGATIVE REGULATION OF IMMUNE RESPONSE	0.10340639
REGULATION OF HORMONE SECRETION	0.10406661
EXOCYTOSIS	0.11165727
TRICARBOXYLIC ACID METABOLIC PROCESS	0.11219546
NEGATIVE REGULATION OF SECRETION	0.1141409
TRANSMEMBRANE RECEPTOR PROTEIN SERINE THREONINE KINASE SIGNALING PATHWAY	0.11512402
POSITIVE REGULATION OF T CELL PROLIFERATION	0.11662753
RNA MODIFICATION	0.11699017
REGULATION OF SECRETION	0.1180061
POSITIVE REGULATION OF IMMUNE EFFECTOR PROCESS	0.12074847
AEROBIC RESPIRATION	0.12392357
NEGATIVE REGULATION OF MULTICELLULAR ORGANISMAL PROCESS	0.13177761
CALCIUM ION TRANSPORT	0.13182627
REGULATION OF LEUKOCYTE DIFFERENTIATION	0.13185024
POSITIVE REGULATION OF CELL CELL ADHESION	0.13269286
DIVALENT INORGANIC CATION TRANSPORT	0.13383722
POSITIVE REGULATION OF SEQUENCE SPECIFIC DNA BINDING TRANSCRIPTION FACTOR ACTIVITY	0.13391061
ACTIN FILAMENT BASED PROCESS	0.13653012
CATION TRANSPORT	0.13694458
REGULATION OF ADAPTIVE IMMUNE RESPONSE	0.14007032
NEGATIVE REGULATION OF IMMUNE EFFECTOR PROCESS	0.14341427
REGULATION OF ACTIN FILAMENT BASED PROCESS	0.14518823
REGULATION OF HOMOTYPIC CELL CELL ADHESION	0.146538
NEGATIVE REGULATION OF DEVELOPMENTAL PROCESS	0.14707647
POSITIVE REGULATION OF LEUKOCYTE DIFFERENTIATION	0.16122915
REGULATION OF LYMPHOCYTE DIFFERENTIATION	0.16272594
ELECTRON TRANSPORT CHAIN	0.1633138
REGULATION OF HEMOPOIESIS	0.16332772
POSITIVE REGULATION OF HEMOPOIESIS	0.16420725
MONOCARBOXYLIC ACID CATABOLIC PROCESS	0.16436976
ION TRANSMEMBRANE TRANSPORT	0.16531222
DEFENSE RESPONSE	0.16534518
CELL JUNCTION ORGANIZATION	0.1655438
GENERATION OF PRECURSOR METABOLITES AND ENERGY	0.16611557
REGULATION OF DEFENSE RESPONSE TO VIRUS	0.16718888
REGULATION OF LYMPHOCYTE MEDIATED IMMUNITY	0.16839166
REGULATION OF LEUKOCYTE MEDIATED IMMUNITY	0.16850032
SECRETION BY CELL	0.16892795
REGULATED EXOCYTOSIS	0.17138441
POSITIVE REGULATION OF CELL DIFFERENTIATION	0.17788425
POSITIVE REGULATION OF CELL ADHESION	0.1787687
ANION TRANSPORT	0.17878711
ORGANIC ACID CATABOLIC PROCESS	0.17979252
REGULATION OF TRANSPORT	0.18070179
FATTY ACID CATABOLIC PROCESS	0.18080062
INTERFERON GAMMA MEDIATED SIGNALING PATHWAY	0.18089426
LIPID OXIDATION	0.18253638
FATTY ACID BETA OXIDATION	0.18276219
NEGATIVE REGULATION OF NERVOUS SYSTEM DEVELOPMENT	0.18290196
REGULATION OF ACTIN FILAMENT LENGTH	0.18404002
SECRETION	0.19455227
OXIDATION REDUCTION PROCESS	0.19544575
VACUOLAR TRANSPORT	0.20054874
REGULATION OF GTPASE ACTIVITY	0.20315766
REGULATION OF SMALL GTPASE MEDIATED SIGNAL TRANSDUCTION	0.22088918
REGULATION OF PEPTIDE SECRETION	0.22424538
POSITIVE REGULATION OF NF KAPPAB TRANSCRIPTION FACTOR ACTIVITY	0.22687973
ORGANONITROGEN COMPOUND CATABOLIC PROCESS	0.23496588

Table S16, Human RNAseq vs Human Proteomics, Individual Hits,
Memory vs Naïve
Up in memory in both RNA and protein
RNAseq FDR < 0.1, protein adjusted p-value < 0.05

Name
NIBAN1
IGHA1
NUGGC
ZFP92
AHNAK
THEMIS2
KLHL6
IGHG1
VIM
TARBP1
ANKRD13A

Down in memory in both RNA and protein

Name
ABCB1
IFI44L
CAMK2D
SNX18
SARAF
TAPT1
PLEKHA2
BACH2
IRF2BPL
ZNF318
IGHD
TMSB10
CD79B
ADARB1
TMEM263

Table S17, Human RNAseq vs Human Proteomics

Germinal Center vs Memory

Up in GC in both RNA and protein

RNA FDR < 0.1, protein FDR < 0.1

Name
IGHG1
RRBP1
IGHV2-70
CD38
IGLV3-21
AURKB
CDK1
IGHV3-43
CIP2A
IGHV3-33
NUGGC
NCAPD2
PBK
NDC80
IGLC3
IGLL5
IGKV3D-7
IGKV1D-39
SEMA4A
STMN1
CKAP2
MCM6
HMGB2
MKI67
IGLV8-61
HDLBP
FNDC3A
HSP90B1
CHAF1A
EAF2
MCM2
WDR76
IDE
AARS1
TOP2A
NCAPH
RPN1
PDIA4
IGKC
SCARB1
LRRC59
ARFGAP3
FEN1
FANCI
INCENP
BACH2
RFC1

Down in GC in both RNA and protein

FDR < 0.1, protein FDR < 0.1

Name
AHNAK
VIM
CAPG
MX2
PML
RAB29
SERPINB6
DTX3L
DDX60
IFIT2
MAP3K5
KMO
ANXA4
NMI
SNX18
ZADH2
PRKCB
MGST3
EML4
PTPN1
DDX58
MARCKS
FMNL1
TRAF3IP3
RHOF
RPS6KA5
RESF1
SEMA7A
PDLIM1
GBP1
PPP1R9B
PLEKHO1

Table S18, Human RNAseq vs Human Proteomics, Germinal Center vs Naïve

N/A: data not obtained

Table S19, Human RNAseq GSEA vs Human Proteomics Gene Ontology
Memory vs Naïve

Up in both = None

Down in both = None

Table S20, Human RNAseq GSEA vs Human Proteomics Gene Ontology

Germinal Center vs Memory

Up in GC in both RNA and protein

RNA FDR < 0.1, protein FDR < 0.1

Name
GO MITOTIC SISTER CHROMATID SEGREGATION
GO DNA DEPENDENT DNA REPLICATION
GO SISTER CHROMATID SEGREGATION
GO DNA PACKAGING
GO NUCLEAR CHROMOSOME SEGREGATION
GO MEIOTIC CELL CYCLE PROCESS
GO CHROMOSOME SEGREGATION
GO B CELL MEDIATED IMMUNITY
GO MEIOTIC CELL CYCLE
GO DNA CONFORMATION CHANGE
GO PROTEASOMAL PROTEIN CATABOLIC PROCESS
GO HUMORAL IMMUNE RESPONSE MEDIATED BY CIRCULATING IMMUNOGLOBULIN
GO CELL DIVISION
GO ORGANELLE FISSION
GO MEMBRANE INVAGINATION
GO CHROMOSOME ORGANIZATION
GO B CELL RECEPTOR SIGNALING PATHWAY
GO PROTEIN UBIQUITINATION INVOLVED IN UBIQUITIN DEPENDENT PROTEIN CATABOLIC PROCESS
GO MITOTIC CELL CYCLE
GO DNA RECOMBINATION
GO CELLULAR RESPONSE TO UV
GO MITOTIC NUCLEAR DIVISION
GO SISTER CHROMATID COHESION
GO PROTEIN ACTIVATION CASCADE
GO CELL CYCLE PROCESS
GO CELL CYCLE
GO LYMPHOCYTE MEDIATED IMMUNITY
GO LEUKOCYTE MEDIATED IMMUNITY
GO RETROGRADE VESICLE MEDIATED TRANSPORT GOLGI TO ER
GO REGULATION OF CHROMOSOME SEGREGATION
GO NEGATIVE REGULATION OF CELL CYCLE PROCESS
GO RESPONSE TO TOPOLOGICALLY INCORRECT PROTEIN
GO MITOTIC DNA INTEGRITY CHECKPOINT
GO CELL CYCLE CHECKPOINT
GO MITOTIC CELL CYCLE CHECKPOINT
GO CHROMATIN ASSEMBLY OR DISASSEMBLY
GO MICROTUBULE CYTOSKELETON ORGANIZATION
GO MITOTIC SPINDLE ORGANIZATION
GO DNA INTEGRITY CHECKPOINT
GO REGULATION OF MICROTUBULE POLYMERIZATION OR DEPOLYMERIZATION
GO REGULATION OF CELL CYCLE PROCESS
GO PROTEIN DNA COMPLEX SUBUNIT ORGANIZATION
GO REGULATION OF CELL DIVISION
GO REGULATION OF SISTER CHROMATID SEGREGATION

Down in Germinal Center in both RNA and protein

RNA FDR < 0.1, protein FDR < 0.1

Name
GO INTERFERON GAMMA MEDIATED SIGNALING PATHWAY
GO RESPONSE TO INTERFERON GAMMA

Table S21, Human RNAseq GSEA vs Human Proteomics Gene Ontology
Germinal Center vs Naïve
Up in GC in both RNA and protein
RNA FDR < 0.1, protein FDR < 0.1

Name
GO NUCLEAR CHROMOSOME SEGREGATION
GO SISTER CHROMATID SEGREGATION
GO DNA REPLICATION
GO MEIOTIC CELL CYCLE PROCESS
GO DNA DEPENDENT DNA REPLICATION
GO MITOTIC SISTER CHROMATID SEGREGATION
GO MEIOTIC CELL CYCLE
GO CHROMOSOME SEGREGATION
GO ORGANELLE FISSION
GO CELL DIVISION
GO MITOTIC NUCLEAR DIVISION
GO DNA PACKAGING
GO SISTER CHROMATID COHESION
GO MEMBRANE INVAGINATION
GO DNA CONFORMATION CHANGE
GO CELL RECOGNITION
GO POSITIVE REGULATION OF B CELL ACTIVATION
GO ADAPTIVE IMMUNE RESPONSE BASED ON SOMATIC RECOMBINATION OF IMMUNE RECEPTORS BUILT FROM IMMUNOGLOBULIN SUPERFAMILY DOMAINS
GO MITOTIC CELL CYCLE
GO CELL CYCLE G1 S PHASE TRANSITION
GO B CELL MEDIATED IMMUNITY
GO LYMPHOCYTE MEDIATED IMMUNITY
GO REGULATION OF B CELL ACTIVATION
GO CHROMOSOME ORGANIZATION
GO MICROTUBULE CYTOSKELETON ORGANIZATION
GO CELL CYCLE PROCESS
GO RECEPTOR MEDIATED ENDOCYTOSIS
GO CELL CYCLE
GO LEUKOCYTE MEDIATED IMMUNITY
GO HUMORAL IMMUNE RESPONSE MEDIATED BY CIRCULATING IMMUNOGLOBULIN
GO B CELL RECEPTOR SIGNALING PATHWAY
GO CELL CYCLE PHASE TRANSITION
GO RESPONSE TO TOPOLOGICALLY INCORRECT PROTEIN
GO PHAGOCYTOSIS
GO NEGATIVE REGULATION OF CELL CYCLE PROCESS
GO MITOTIC SPINDLE ORGANIZATION
GO REGULATION OF CHROMOSOME SEGREGATION
GO DNA RECOMBINATION
GO HUMORAL IMMUNE RESPONSE
GO PROTEIN ACTIVATION CASCADE
GO MICROTUBULE BASED PROCESS
GO MITOTIC DNA INTEGRITY CHECKPOINT
GO DEFENSE RESPONSE TO BACTERIUM
GO REGULATION OF MICROTUBULE POLYMERIZATION OR DEPOLYMERIZATION
GO FC GAMMA RECEPTOR SIGNALING PATHWAY
GO MITOTIC CELL CYCLE CHECKPOINT
GO DNA GEOMETRIC CHANGE
GO ADAPTIVE IMMUNE RESPONSE
GO ALPHA AMINO ACID BIOSYNTHETIC PROCESS
GO REGULATION OF MICROTUBULE BASED PROCESS
GO CELL CYCLE CHECKPOINT
GO CELLULAR RESPONSE TO TOPOLOGICALLY INCORRECT PROTEIN
GO DNA INTEGRITY CHECKPOINT
GO RETROGRADE VESICLE MEDIATED TRANSPORT GOLGI TO ER

Down in GC in both RNA and protein
RNA FDR < 0.1, protein FDR < 0.1

Name
GO DEFENSE RESPONSE TO VIRUS
GO NEGATIVE REGULATION OF VIRAL PROCESS
GO RESPONSE TO VIRUS
GO RESPONSE TO TYPE I INTERFERON
GO REGULATION OF T CELL PROLIFERATION
GO NEGATIVE REGULATION OF VIRAL GENOME REPLICATION
GO NEGATIVE REGULATION OF IMMUNE RESPONSE
GO POSITIVE REGULATION OF T CELL PROLIFERATION
GO POSITIVE REGULATION OF CELL CELL ADHESION
GO INTERFERON GAMMA MEDIATED SIGNALING PATHWAY
GO POSITIVE REGULATION OF CELL ADHESION

REFERENCES

1. Bujold, L. M. & DLC, C. P. C. L. O. C. *Barrayar*. (New York, N.Y. : Baen Publishing Enterprises, 1991).
2. Pilcher, C. D. *et al.* Brief but efficient: acute HIV infection and the sexual transmission of HIV. *Journal of Infectious Diseases* **189,** 1785–1792 (2004).
3. Sterling, T. R. *et al.* Initial plasma HIV-1 RNA levels and progression to AIDS in women and men. *N. Engl. J. Med.* **344,** 720–725 (2001).
4. World Health Organization. *WHO case definitions of HIV for surveillance and revised clinical staging and immunological classification of HIV-related disease in adults and children*. (2007).
5. Mangal, T. D.UNAIDS Working Group on CD4 Progression and Mortality Amongst HIV Seroconverters including the CASCADE Collaboration in EuroCoord. Joint estimation of CD4+ cell progression and survival in untreated individuals with HIV-1 infection. *AIDS* **31,** 1073–1082 (2017).
6. 2013. *Fields Virology*. (Lippincott Williams & Wilkins).
7. Franzusoff, A., Volpe, A. M., Josse, D., Pichuantes, S. & Wolf, J. R. Biochemical and genetic definition of the cellular protease required for HIV-1 gp160 processing. *Journal of Biological Chemistry* **270,** 3154–3159 (1995).
8. Decroly, E. *et al.* The convertases furin and PC1 can both cleave the human immunodeficiency virus (HIV)-1 envelope glycoprotein gp160 into gp120 (HIV-1 SU) and gp41 (HIV-I TM). *Journal of Biological Chemistry* **269,** 12240–12247 (1994).
9. Roberts, J. D., Bebenek, K. & Kunkel, T. A. The accuracy of reverse transcriptase from HIV-1. *Science* **242,** 1171–1173 (1988).
10. Zhang, L. Q. *et al.* Selection for specific sequences in the external envelope protein of human immunodeficiency virus type 1 upon primary infection. *J. Virol.* **67,** 3345–3356 (1993).
11. Keele, B. F. *et al.* Identification and characterization of transmitted and early founder virus envelopes in primary HIV-1 infection. *Proc. Natl. Acad. Sci. U.S.A.* **105,** 7552–7557 (2008).
12. Wolfs, T. F., Zwart, G., Bakker, M. & Goudsmit, J. HIV-1 genomic RNA diversification following sexual and parenteral virus transmission. *Virology* **189,** 103–110 (1992).
13. Pejchal, R. *et al.* A potent and broad neutralizing antibody recognizes and penetrates the HIV glycan shield. *Science* **334,** 1097–1103 (2011).
14. Bonsignori, M. *et al.* HIV-1 antibodies from infection and vaccination: insights for guiding vaccine design. *Trends Microbiol.* **20,** 532–539 (2012).
15. Wu, X. *et al.* Focused evolution of HIV-1 neutralizing antibodies revealed by structures and deep sequencing. *Science* **333,** 1593–1602 (2011).
16. Haynes, B. F. *et al.* Cardiolipin polyspecific autoreactivity in two broadly neutralizing HIV-1 antibodies. *Science* **308,** 1906–1908 (2005).
17. Liu, M. *et al.* Polyreactivity and autoreactivity among HIV-1 antibodies. *J. Virol.* **89,** 784–798 (2015).

18. Derdeyn, C. A., Moore, P. L. & Morris, L. Development of broadly neutralizing antibodies from autologous neutralizing antibody responses in HIV infection. *Curr Opin HIV AIDS* **9,** 210–216 (2014).
19. Shingai, M. *et al.* Passive transfer of modest titers of potent and broadly neutralizing anti-HIV monoclonal antibodies block SHIV infection in macaques. *J. Exp. Med.* **211,** 2061–2074 (2014).
20. Piantadosi, A. *et al.* Breadth of neutralizing antibody response to human immunodeficiency virus type 1 is affected by factors early in infection but does not influence disease progression. *J. Virol.* **83,** 10269–10274 (2009).
21. Gray, E. S. *et al.* The neutralization breadth of HIV-1 develops incrementally over four years and is associated with CD4+ T cell decline and high viral load during acute infection. *J. Virol.* **85,** 4828–4840 (2011).
22. Mishra, N. *et al.* A Rare Mutation in an Infant-Derived HIV-1 Envelope Glycoprotein Alters Interprotomer Stability and Susceptibility to Broadly Neutralizing Antibodies Targeting the Trimer Apex. *J. Virol.* **94,** (2020).
23. Goo, L., Chohan, V., Nduati, R. & Overbaugh, J. Early development of broadly neutralizing antibodies in HIV-1-infected infants. *Nat. Med.* **20,** 655–658 (2014).
24. Simonich, C. A. *et al.* HIV-1 Neutralizing Antibodies with Limited Hypermutation from an Infant. *Cell* **166,** 77–87 (2016).
25. Kumar, S. *et al.* An HIV-1 Broadly Neutralizing Antibody from a Clade C-Infected Pediatric Elite Neutralizer Potently Neutralizes the Contemporaneous and Autologous Evolving Viruses. *J. Virol.* **93,** 487 (2019).
26. Sather, D. N. *et al.* Emergence of broadly neutralizing antibodies and viral coevolution in two subjects during the early stages of infection with human immunodeficiency virus type 1. *J. Virol.* **88,** 12968–12981 (2014).
27. Wibmer, C. K. *et al.* Viral escape from HIV-1 neutralizing antibodies drives increased plasma neutralization breadth through sequential recognition of multiple epitopes and immunotypes. *PLoS Pathog.* **9,** e1003738 (2013).
28. van Gils, M. J., Euler, Z., Schweighardt, B., Wrin, T. & Schuitemaker, H. Prevalence of cross-reactive HIV-1-neutralizing activity in HIV-1-infected patients with rapid or slow disease progression. *AIDS* **23,** 2405–2414 (2009).
29. Jardine, J. G. *et al.* Minimally Mutated HIV-1 Broadly Neutralizing Antibodies to Guide Reductionist Vaccine Design. *PLoS Pathog.* **12,** e1005815 (2016).
30. Liao, H.-X. *et al.* Initial antibodies binding to HIV-1 gp41 in acutely infected subjects are polyreactive and highly mutated. *J. Exp. Med.* **208,** 2237–2249 (2011).
31. Trama, A. M. *et al.* HIV-1 envelope gp41 antibodies can originate from terminal ileum B cells that share cross-reactivity with commensal bacteria. *Cell Host Microbe* **16,** 215–226 (2014).
32. Song, L. *et al.* Broadly neutralizing anti-HIV-1 antibodies disrupt a hinge-related function of gp41 at the membrane interface. *Proc. Natl. Acad. Sci. U.S.A.* **106,** 9057–9062 (2009).
33. Kim, M. *et al.* Antibody mechanics on a membrane-bound HIV segment essential for GP41-targeted viral neutralization. *Nat. Struct. Mol. Biol.* **18,** 1235–1243 (2011).

34. Irimia, A., Sarkar, A., Stanfield, R. L. & Wilson, I. A. Crystallographic Identification of Lipid as an Integral Component of the Epitope of HIV Broadly Neutralizing Antibody 4E10. *Immunity* **44,** 21–31 (2016).
35. Diskin, R., Marcovecchio, P. M. & Bjorkman, P. J. Structure of a clade C HIV-1 gp120 bound to CD4 and CD4-induced antibody reveals anti-CD4 polyreactivity. *Nat. Struct. Mol. Biol.* **17,** 608–613 (2010).
36. Liao, H.-X. *et al.* Co-evolution of a broadly neutralizing HIV-1 antibody and founder virus. *Nature* **496,** 469–476 (2013).
37. Knipe, D. M. & Cliffe, A. Chromatin control of herpes simplex virus lytic and latent infection. *Nat. Rev. Microbiol.* **6,** 211–221 (2008).
38. Wherry, E. J. *et al.* Molecular signature of CD8+ T cell exhaustion during chronic viral infection. *Immunity* **27,** 670–684 (2007).
39. Fainboim, L. *et al.* Protracted, but not acute, hepatitis A virus infection is strongly associated with HLA-DRB*1301, a marker for pediatric autoimmune hepatitis. *Hepatology* **33,** 1512–1517 (2001).
40. McFarlane, B. M. *et al.* Autoimmune mechanisms in chronic hepatitis B and delta virus infections. *Eur J Gastroenterol Hepatol* **7,** 615–621 (1995).
41. Roughan, J. E. *et al.* Chronic hepatitis C virus infection breaks tolerance and drives polyclonal expansion of autoreactive B cells. *Clin. Vaccine Immunol.* **19,** 1027–1037 (2012).
42. Verkoczy, L. & Diaz, M. Autoreactivity in HIV-1 broadly neutralizing antibodies: implications for their function and induction by vaccination. *Curr Opin HIV AIDS* **9,** 224–234 (2014).
43. Hunziker, L. *et al.* Hypergammaglobulinemia and autoantibody induction mechanisms in viral infections. *Nat. Immunol.* **4,** 343–349 (2003).
44. Soulas, P. *et al.* Autoantigen, innate immunity, and T cells cooperate to break B cell tolerance during bacterial infection. *J. Clin. Invest.* **115,** 2257–2267 (2005).
45. Jung, S. *et al.* Chronic bacterial infection activates autoreactive B cells and induces isotype switching and autoantigen-driven mutations. *Eur. J. Immunol.* **46,** 131–146 (2016).
46. Garcia-De La Torre, I. Autoimmune phenomena in leprosy, particularly antinuclear antibodies and rheumatoid factor. *J Rheumatol* **20,** 900–903 (1993).
47. Kroumpouzos, G. *et al.* Evaluation of the autoimmune response in leprosy. *Lepr Rev* **64,** 199–207 (1993).
48. Leadbetter, E. A. *et al.* Chromatin-IgG complexes activate B cells by dual engagement of IgM and Toll-like receptors. *Nature* **416,** 603–607 (2002).
49. Marshak-Rothstein, A. Toll-like receptors in systemic autoimmune disease. *Nature Reviews Immunology* **6,** 823–835 (2006).
50. Moir, S. & Fauci, A. S. Pathogenic mechanisms of B-lymphocyte dysfunction in HIV disease. *J Allergy Clin Immunol* **122,** 12–9– quiz 20–1 (2008).
51. Moir, S. *et al.* Evidence for HIV-associated B cell exhaustion in a dysfunctional memory B cell compartment in HIV-infected viremic individuals. *J. Exp. Med.* **205,** 1797–1805 (2008).
52. Ehrhardt, G. R. A. *et al.* Expression of the immunoregulatory molecule FcRH4 defines a distinctive tissue-based population of memory B cells. *J. Exp. Med.* **202,** 783–791 (2005).

53. Ferreira, C. B. *et al.* Evolution of broadly cross-reactive HIV-1-neutralizing activity: therapy-associated decline, positive association with detectable viremia, and partial restoration of B-cell subpopulations. *J. Virol.* **87,** 12227–12236 (2013).
54. Knox, J. J. *et al.* T-bet+ B cells are induced by human viral infections and dominate the HIV gp140 response. *JCI Insight* **2,** (2017).
55. Lane, H. C. *et al.* Abnormalities of B-cell activation and immunoregulation in patients with the acquired immunodeficiency syndrome. *N. Engl. J. Med.* **309,** 453–458 (1983).
56. Moir, S. *et al.* HIV-1 induces phenotypic and functional perturbations of B cells in chronically infected individuals. *Proc Natl Acad Sci USA* **98,** 10362–10367 (2001).
57. Shirai, A., Cosentino, M., Leitman-Klinman, S. F. & Klinman, D. M. Human immunodeficiency virus infection induces both polyclonal and virus-specific B cell activation. *J. Clin. Invest.* **89,** 561–566 (1992).
58. Morris, L. *et al.* HIV-1 antigen-specific and -nonspecific B cell responses are sensitive to combination antiretroviral therapy. *J. Exp. Med.* **188,** 233–245 (1998).
59. Moir, S. *et al.* Decreased survival of B cells of HIV-viremic patients mediated by altered expression of receptors of the TNF superfamily. *J. Exp. Med.* **200,** 587–599 (2004).
60. Kovacs, J. A. *et al.* Identification of dynamically distinct subpopulations of T lymphocytes that are differentially affected by HIV. *J. Exp. Med.* **194,** 1731–1741 (2001).
61. Nagase, H. *et al.* Mechanism of hypergammaglobulinemia by HIV infection: circulating memory B-cell reduction with plasmacytosis. *Clin Immunol* **100,** 250–259 (2001).
62. Conge, A. M. *et al.* Impairment of B-lymphocyte differentiation induced by dual triggering of the B-cell antigen receptor and CD40 in advanced HIV-1-disease. *AIDS* **12,** 1437–1449 (1998).
63. Notermans, D. W. *et al.* Potent antiretroviral therapy initiates normalization of hypergammaglobulinemia and a decline in HIV type 1-specific antibody responses. *AIDS Res. Hum. Retroviruses* **17,** 1003–1008 (2001).
64. Shearer, W. T. *et al.* Prospective 5-year study of peripheral blood CD4, CD8, and CD19/CD20 lymphocytes and serum Igs in children born to HIV-1 women. The P(2)C(2) HIV Study Group. *J Allergy Clin Immunol* **106,** 559–566 (2000).
65. Lane, H. C. *et al.* Abnormalities of B-cell activation and immunoregulation in patients with the acquired immunodeficiency syndrome. *N. Engl. J. Med.* **309,** 453–458 (1983).
66. Wright, B. R., Warrington, A. E., Edberg, D. D., Edberg, D. E. & Rodriguez, M. Cellular mechanisms of central nervous system repair by natural autoreactive monoclonal antibodies. *Arch Neurol* **66,** 1456–1459 (2009).
67. Nishio, N., Ito, S., Suzuki, H. & Isobe, K.-I. Antibodies to wounded tissue enhance cutaneous wound healing. *Immunology* **128,** 369–380 (2009).
68. Abbas, A. K., Lichtman, A. H. & Pillai, S. *Cellular and molecular immunology*. (Philadelphia : Elsevier/Saunders, 2012).

69. Iordache, L. *et al.* Autoimmune diseases in HIV-infected patients: 52 cases and literature review. *Autoimmun Rev* **13,** 850–857 (2014).
70. Wu, C.-Y. *et al.* Association between nucleoside analogues and risk of hepatitis B virus–related hepatocellular carcinoma recurrence following liver resection. *JAMA* **308,** 1906–1914 (2012).
71. Yen, Y.-F. *et al.* Incidence of autoimmune diseases in a nationwide HIV/AIDS patient cohort in Taiwan, 2000-2012. *Ann. Rheum. Dis.* **76,** 661–665 (2017).
72. Tiemessen, C. T. & Kuhn, L. Immune pathogenesis of pediatric HIV-1 infection. *Curr HIV/AIDS Rep* **3,** 13–19 (2006).
73. Tobin, N. H. & Aldrovandi, G. M. Immunology of pediatric HIV infection. *Immunol. Rev.* **254,** 143–169 (2013).
74. Goulder, P. J., Lewin, S. R. & Leitman, E. M. Paediatric HIV infection: the potential for cure. *Nat. Rev. Immunol.* **16,** 259–271 (2016).
75. Bonsignori, M. *et al.* An autoreactive antibody from an SLE/HIV-1 individual broadly neutralizes HIV-1. *J. Clin. Invest.* **124,** 1835–1843 (2014).
76. Sather, D. N. *et al.* Factors associated with the development of cross-reactive neutralizing antibodies during human immunodeficiency virus type 1 infection. *J. Virol.* **83,** 757–769 (2009).
77. Wardemann, H. *et al.* Predominant autoantibody production by early human B cell precursors. *Science* **301,** 1374–1377 (2003).
78. Roskin, K. M. *et al.* Aberrant B cell repertoire selection associated with HIV neutralizing antibody breadth. *Nat. Immunol.* **28,** 163 (2020).
79. Moody, M. A. *et al.* Immune perturbations in HIV-1–infected individuals who make broadly neutralizing antibodies. *Science Immunology* **1,** aag0851–aag0851 (2016).
80. Hoot, S. *et al.* Recombinant HIV envelope proteins fail to engage germline versions of anti-CD4bs bNAbs. *PLoS Pathog.* **9,** e1003106 (2013).
81. Scheid, J. F. *et al.* Sequence and structural convergence of broad and potent HIV antibodies that mimic CD4 binding. *Science* **333,** 1633–1637 (2011).
82. Zhou, T. *et al.* Structural basis for broad and potent neutralization of HIV-1 by antibody VRC01. *Science* **329,** 811–817 (2010).
83. Jardine, J. *et al.* Rational HIV immunogen design to target specific germline B cell receptors. *Science* **340,** 711–716 (2013).
84. Jardine, J. G. *et al.* HIV-1 VACCINES. Priming a broadly neutralizing antibody response to HIV-1 using a germline-targeting immunogen. *Science* **349,** 156–161 (2015).
85. Pillai, S. & Baltimore, D. Formation of disulphide-linked mu 2 omega 2 tetramers in pre-B cells by the 18K omega-immunoglobulin light chain. *Nature* **329,** 172–174 (1987).
86. Mayer, C. T. *et al.* The microanatomic segregation of selection by apoptosis in the germinal center. *Science* **358,** (2017).
87. McHeyzer-Williams, M. G., Nossal, G. J. & Lalor, P. A. Molecular characterization of single memory B cells. *Nature* **350,** 502–505 (1991).
88. Anderson, S. M., Tomayko, M. M. & Shlomchik, M. J. Intrinsic properties of human and murine memory B cells. *Immunol. Rev.* **211,** 280–294 (2006).

89. Tangye, S. G., Avery, D. T., Deenick, E. K. & Hodgkin, P. D. Intrinsic differences in the proliferation of naive and memory human B cells as a mechanism for enhanced secondary immune responses. *The Journal of Immunology* **170,** 686–694 (2003).
90. Good, K. L., Avery, D. T. & Tangye, S. G. Resting human memory B cells are intrinsically programmed for enhanced survival and responsiveness to diverse stimuli compared to naive B cells. *J. Immunol.* **182,** 890–901 (2009).
91. Bernasconi, N. L., Onai, N. & Lanzavecchia, A. A role for Toll-like receptors in acquired immunity: up-regulation of TLR9 by BCR triggering in naive B cells and constitutive expression in memory B cells. *Blood* **101,** 4500–4504 (2003).
92. Klein, U., Küppers, R. & Rajewsky, K. Evidence for a large compartment of IgM-expressing memory B cells in humans. *Blood* **89,** 1288–1298 (1997).
93. Tangye, S. G., Liu, Y. J., Aversa, G., Phillips, J. H. & de Vries, J. E. Identification of functional human splenic memory B cells by expression of CD148 and CD27. *J. Exp. Med.* **188,** 1691–1703 (1998).
94. Bar-Or, A. *et al.* Immunological memory: contribution of memory B cells expressing costimulatory molecules in the resting state. *The Journal of Immunology* **167,** 5669–5677 (2001).
95. Fecteau, J. F., Côté, G. & Néron, S. A new memory CD27-IgG+ B cell population in peripheral blood expressing VH genes with low frequency of somatic mutation. *The Journal of Immunology* **177,** 3728–3736 (2006).
96. Wei, C. *et al.* A new population of cells lacking expression of CD27 represents a notable component of the B cell memory compartment in systemic lupus erythematosus. *The Journal of Immunology* **178,** 6624–6633 (2007).
97. Rakhmanov, M. *et al.* CD21low B cells in common variable immunodeficiency do not show defects in receptor editing, but resemble tissue-like memory B cells. *Blood* **116,** 3682–3683 (2010).
98. Moir, S. *et al.* Evidence for HIV-associated B cell exhaustion in a dysfunctional memory B cell compartment in HIV-infected viremic individuals. *J. Exp. Med.* **205,** 1797–1805 (2008).
99. Isnardi, I. *et al.* Complement receptor 2/CD21- human naive B cells contain mostly autoreactive unresponsive clones. *Blood* **115,** 5026–5036 (2010).
100. Weller, S. *et al.* Human blood IgM 'memory' B cells are circulating splenic marginal zone B cells harboring a prediversified immunoglobulin repertoire. *Blood* **104,** 3647–3654 (2004).
101. Weill, J.-C. & Reynaud, C.-A. IgM memory B cells: specific effectors of innate-like and adaptive responses. *Curr. Opin. Immunol.* **63,** 1–6 (2020).
102. McWilliams, L. *et al.* The human fetal lymphocyte lineage: identification by CD27 and LIN28B expression in B cell progenitors. *J. Leukoc. Biol.* **94,** 991–1001 (2013).
103. Dogan, I. *et al.* Multiple layers of B cell memory with different effector functions. *Nat. Immunol.* **10,** 1292–1299 (2009).
104. Anderson, S. M., Hannum, L. G. & Shlomchik, M. J. Memory B cell survival and function in the absence of secreted antibody and immune complexes on follicular dendritic cells. *The Journal of Immunology* **176,** 4515–4519 (2006).

105. Tomayko, M. M., Steinel, N. C., Anderson, S. M. & Shlomchik, M. J. Cutting edge: Hierarchy of maturity of murine memory B cell subsets. *J. Immunol.* **185,** 7146–7150 (2010).
106. Anderson, S. M., Tomayko, M. M., Ahuja, A., Haberman, A. M. & Shlomchik, M. J. New markers for murine memory B cells that define mutated and unmutated subsets. *J. Exp. Med.* **204,** 2103–2114 (2007).
107. Zuccarino-Catania, G. V. *et al.* CD80 and PD-L2 define functionally distinct memory B cell subsets that are independent of antibody isotype. *Nat. Immunol.* **15,** 631–637 (2014).
108. Inamine, A. *et al.* Two waves of memory B-cell generation in the primary immune response. *Int. Immunol.* **17,** 581–589 (2005).
109. Weisel, F. J., Zuccarino-Catania, G. V., Chikina, M. & Shlomchik, M. J. A Temporal Switch in the Germinal Center Determines Differential Output of Memory B and Plasma Cells. *Immunity* **44,** 116–130 (2016).
110. Viant, C. *et al.* Antibody Affinity Shapes the Choice between Memory and Germinal Center B Cell Fates. *Cell* **183,** 1298–1311.e11 (2020).
111. Weisel, F. J., Zuccarino-Catania, G. V., Chikina, M. & Shlomchik, M. J. A Temporal Switch in the Germinal Center Determines Differential Output of Memory B and Plasma Cells. *Immunity* **44,** 116–130 (2016).
112. Anderson, S. M., Hannum, L. G. & Shlomchik, M. J. Memory B cell survival and function in the absence of secreted antibody and immune complexes on follicular dendritic cells. *The Journal of Immunology* **176,** 4515–4519 (2006).
113. Di Niro, R. *et al.* Salmonella Infection Drives Promiscuous B Cell Activation Followed by Extrafollicular Affinity Maturation. *Immunity* **43,** 120–131 (2015).
114. Takahashi, Y., Ohta, H. & Takemori, T. Fas is required for clonal selection in germinal centers and the subsequent establishment of the memory B cell repertoire. *Immunity* **14,** 181–192 (2001).
115. Toyama, H. *et al.* Memory B cells without somatic hypermutation are generated from Bcl6-deficient B cells. *Immunity* **17,** 329–339 (2002).
116. Taylor, J. J., Pape, K. A. & Jenkins, M. K. A germinal center-independent pathway generates unswitched memory B cells early in the primary response. *J. Exp. Med.* **209,** 597–606 (2012).
117. Stewart, I., Radtke, D., Phillips, B., McGowan, S. J. & Bannard, O. Germinal Center B Cells Replace Their Antigen Receptors in Dark Zones and Fail Light Zone Entry when Immunoglobulin Gene Mutations are Damaging. *Immunity* **49,** 477–489.e7 (2018).
118. Kuo, T. C. *et al.* Repression of BCL-6 is required for the formation of human memory B cells in vitro. *J. Exp. Med.* **204,** 819–830 (2007).
119. Saito, M. *et al.* BCL6 suppression of BCL2 via Miz1 and its disruption in diffuse large B cell lymphoma. *Proc. Natl. Acad. Sci. U.S.A.* **106,** 11294–11299 (2009).
120. Hatzi, K. *et al.* A hybrid mechanism of action for BCL6 in B cells defined by formation of functionally distinct complexes at enhancers and promoters. *Cell Rep* **4,** 578–588 (2013).
121. Laidlaw, B. J., Duan, L., Xu, Y., Vazquez, S. E. & Cyster, J. G. The transcription factor Hhex cooperates with the corepressor Tle3 to promote memory B cell development. *Nat. Immunol.* **21,** 1082–1093 (2020).

122. Ise, W. *et al.* T Follicular Helper Cell-Germinal Center B Cell Interaction Strength Regulates Entry into Plasma Cell or Recycling Germinal Center Cell Fate. *Immunity* **48,** 702–715.e4 (2018).
123. Zhang, T.-T. *et al.* Germinal center B cell development has distinctly regulated stages completed by disengagement from T cell help. *Elife* **6,** (2017).
124. Sciammas, R. *et al.* Graded expression of interferon regulatory factor-4 coordinates isotype switching with plasma cell differentiation. *Immunity* **25,** 225–236 (2006).
125. Laidlaw, B. J. & Cyster, J. G. Transcriptional regulation of memory B cell differentiation. *Nat. Rev. Immunol.* 1–12 (2020). doi:10.1038/s41577-020-00446-2
126. Barnett, B. E. *et al.* Asymmetric B cell division in the germinal center reaction. *Science* **335,** 342–344 (2012).
127. Lin, W.-H. W. *et al.* Asymmetric PI3K Signaling Driving Developmental and Regenerative Cell Fate Bifurcation. *Cell Rep* **13,** 2203–2218 (2015).
128. Thomas, M. J., Klein, U., Lygeros, J. & Rodríguez Martínez, M. A Probabilistic Model of the Germinal Center Reaction. *Front Immunol* **10,** 689 (2019).
129. Taylor, J. J., Pape, K. A., Steach, H. R. & Jenkins, M. K. Humoral immunity. Apoptosis and antigen affinity limit effector cell differentiation of a single naïve B cell. *Science* **347,** 784–787 (2015).
130. Weinstein, J. S. *et al.* TFH cells progressively differentiate to regulate the germinal center response. *Nat. Immunol.* **17,** 1197–1205 (2016).
131. Barton, L. L. & Mets, M. B. Congenital lymphocytic choriomeningitis virus infection: decade of rediscovery. *Clin. Infect. Dis.* **33,** 370–374 (2001).
132. Barton, L. L. & Mets, M. B. Lymphocytic choriomeningitis virus: pediatric pathogen and fetal teratogen. *Pediatr Infect Dis J* **18,** 540–541 (1999).
133. Rousseau, M. C., Saron, M. F., Brouqui, P. & Bourgeade, A. Lymphocytic choriomeningitis virus in southern France: four case reports and a review of the literature. *Eur J Epidemiol* **13,** 817–823 (1997).
134. Gregg, M. B. Recent outbreaks of lymphocytic choriomeningitis in the United States of America. *Bull World Health Organ* **52,** 549–553 (1975).
135. Jamieson, D. J., Kourtis, A. P., Bell, M. & Rasmussen, S. A. Lymphocytic choriomeningitis virus: an emerging obstetric pathogen? *Am J Obstet Gynecol* **194,** 1532–1536 (2006).
136. Bonthius, D. J. *et al.* Congenital lymphocytic choriomeningitis virus infection: spectrum of disease. *Ann Neurol* **62,** 347–355 (2007).
137. Wright, R. *et al.* Congenital lymphocytic choriomeningitis virus syndrome: a disease that mimics congenital toxoplasmosis or Cytomegalovirus infection. *Pediatrics* **100,** E9 (1997).
138. Sevilla, N. *et al.* Immunosuppression and resultant viral persistence by specific viral targeting of dendritic cells. *J. Exp. Med.* **192,** 1249–1260 (2000).
139. Smelt, S. C. *et al.* Differences in affinity of binding of lymphocytic choriomeningitis virus strains to the cellular receptor alpha-dystroglycan correlate with viral tropism and disease kinetics. *J. Virol.* **75,** 448–457 (2001).

140. Matloubian, M., Concepcion, R. J. & Ahmed, R. CD4+ T cells are required to sustain CD8+ cytotoxic T-cell responses during chronic viral infection. *J. Virol.* **68,** 8056–8063 (1994).
141. Sullivan, B. M. *et al.* Point mutation in the glycoprotein of lymphocytic choriomeningitis virus is necessary for receptor binding, dendritic cell infection, and long-term persistence. *Proc. Natl. Acad. Sci. U.S.A.* **108,** 2969–2974 (2011).
142. Cao, W. *et al.* Identification of alpha-dystroglycan as a receptor for lymphocytic choriomeningitis virus and Lassa fever virus. *Science* **282,** 2079–2081 (1998).
143. Zinkernagel, R. M. & Doherty, P. C. Restriction of in vitro T cell-mediated cytotoxicity in lymphocytic choriomeningitis within a syngeneic or semiallogeneic system. *Nature* **248,** 701–702 (1974).
144. Traub, E. PERSISTENCE OF LYMPHOCYTIC CHORIOMENINGITIS VIRUS IN IMMUNE ANIMALS AND ITS RELATION TO IMMUNITY. *J. Exp. Med.* **63,** 847–861 (1936).
145. Moskophidis, D., Lechner, F., Pircher, H. & Zinkernagel, R. M. Virus persistence in acutely infected immunocompetent mice by exhaustion of antiviral cytotoxic effector T cells. *Nature* **362,** 758–761 (1993).
146. Barber, D. L. *et al.* Restoring function in exhausted CD8 T cells during chronic viral infection. *Nature* **439,** 682–687 (2006).
147. Lichterfeld, M. *et al.* Selective depletion of high-avidity human immunodeficiency virus type 1 (HIV-1)-specific CD8+ T cells after early HIV-1 infection. *J. Virol.* **81,** 4199–4214 (2007).
148. Goonetilleke, N. *et al.* The first T cell response to transmitted/founder virus contributes to the control of acute viremia in HIV-1 infection. *J. Exp. Med.* **206,** 1253–1272 (2009).
149. Klenerman, P. & Hill, A. T cells and viral persistence: lessons from diverse infections. *Nat. Immunol.* **6,** 873–879 (2005).
150. De Milito, A. *et al.* Mechanisms of hypergammaglobulinemia and impaired antigen-specific humoral immunity in HIV-1 infection. *Blood* **103,** 2180–2186 (2004).
151. Iordache, L. *et al.* Nonorgan-specific autoantibodies in HIV-infected patients in the HAART era. *Medicine (Baltimore)* **96,** e6230 (2017).
152. Schroeder, K. M. S. *et al.* Breaching peripheral tolerance promotes the production of HIV-1-neutralizing antibodies. *J. Exp. Med.* **71,** jem.20161190–2302 (2017).
153. Barouch, D. H. *et al.* Mosaic HIV-1 vaccines expand the breadth and depth of cellular immune responses in rhesus monkeys. *Nat. Med.* **16,** 319–323 (2010).
154. Tian, M. *et al.* Induction of HIV Neutralizing Antibody Lineages in Mice with Diverse Precursor Repertoires. *Cell* **166,** 1471–1484.e18 (2016).
155. Zhou, T. *et al.* Multidonor analysis reveals structural elements, genetic determinants, and maturation pathway for HIV-1 neutralization by VRC01-class antibodies. *Immunity* **39,** 245–258 (2013).
156. Zhou, T. *et al.* Structural Repertoire of HIV-1-Neutralizing Antibodies Targeting the CD4 Supersite in 14 Donors. *Cell* **161,** 1280–1292 (2015).

157. Kao, C. *et al.* Transcription factor T-bet represses expression of the inhibitory receptor PD-1 and sustains virus-specific CD8+ T cell responses during chronic infection. *Nat. Immunol.* **12,** 663–671 (2011).
158. Weaver, G. C. *et al.* In vitro reconstitution of B cell receptor-antigen interactions to evaluate potential vaccine candidates. *Nature Protocols* **11,** 193–213 (2016).
159. Kanekiyo, M. *et al.* Self-assembling influenza nanoparticle vaccines elicit broadly neutralizing H1N1 antibodies. *Nature* **499,** 102–106 (2013).
160. Yassine, H. M. *et al.* Hemagglutinin-stem nanoparticles generate heterosubtypic influenza protection. *Nat. Med.* **21,** 1065–1070 (2015).
161. Chen, X. *et al.* Vaccination induces maturation in a mouse model of diverse unmutated VRC01-class precursors to HIV-neutralizing antibodies with >50% breadth. *Immunity* **54,** 324–339.e8 (2021).
162. Rizzuto, C. D. *et al.* A conserved HIV gp120 glycoprotein structure involved in chemokine receptor binding. *Science* **280,** 1949–1953 (1998).
163. Labrijn, A. F. *et al.* Access of antibody molecules to the conserved coreceptor binding site on glycoprotein gp120 is sterically restricted on primary human immunodeficiency virus type 1. *J. Virol.* **77,** 10557–10565 (2003).
164. Madani, N. *et al.* CD4-mimetic small molecules sensitize human immunodeficiency virus to vaccine-elicited antibodies. *J. Virol.* **88,** 6542–6555 (2014).
165. Murray, R., Cohen, P. & Hardegree, M. C. Mineral oil adjuvants: biological and chemical studies. *Ann Allergy* **30,** 146–151 (1972).
166. Whitehouse, M. W., Orr, K. J., Beck, F. W. & Pearson, C. M. Freund's adjuvants: relationship of arthritogenicity and adjuvanticity in rats to vehicle composition. *Immunology* **27,** 311–330 (1974).
167. Kuroda, Y., Nacionales, D. C., Akaogi, J., Reeves, W. H. & Satoh, M. Autoimmunity induced by adjuvant hydrocarbon oil components of vaccine. *Biomed Pharmacother* **58,** 325–337 (2004).
168. Bossaller, L. *et al.* TLR9 Deficiency Leads to Accelerated Renal Disease and Myeloid Lineage Abnormalities in Pristane-Induced Murine Lupus. *J. Immunol.* **197,** 1044–1053 (2016).
169. Micera, M. *et al.* Squalene: More than a Step toward Sterols. *Antioxidants (Basel)* **9,** (2020).
170. Downing, D. T., Stewart, M. E. & Strauss, J. S. Estimation of sebum production rates in man by measurement of the squalene content of skin biopsies. *J Invest Dermatol* **77,** 358–360 (1981).
171. Satoh, M. *et al.* Induction of lupus autoantibodies by adjuvants. *J. Autoimmun.* **21,** 1–9 (2003).
172. Umotoy, J. *et al.* Rapid and Focused Maturation of a VRC01-Class HIV Broadly Neutralizing Antibody Lineage Involves Both Binding and Accommodation of the N276-Glycan. *Immunity* **51,** 141–154.e6 (2019).
173. Weill, J.-C. & Reynaud, C.-A. IgM memory B cells: specific effectors of innate-like and adaptive responses. *Curr. Opin. Immunol.* **63,** 1–6 (2020).
174. Kaji, T. *et al.* Distinct cellular pathways select germline-encoded and somatically mutated antibodies into immunological memory. *J. Exp. Med.* **209,** 2079–2097 (2012).

175. Takemori, T., Kaji, T., Takahashi, Y., Shimoda, M. & Rajewsky, K. Generation of memory B cells inside and outside germinal centers. *Eur. J. Immunol.* **44,** 1258–1264 (2014).
176. Shinnakasu, R. *et al.* Regulated selection of germinal-center cells into the memory B cell compartment. *Nat. Immunol.* **17,** 861–869 (2016).
177. Laidlaw, B. J. *et al.* The Eph-related tyrosine kinase ligand Ephrin-B1 marks germinal center and memory precursor B cells. *J. Exp. Med.* **214,** 639–649 (2017).
178. Toboso-Navasa, A. *et al.* Restriction of memory B cell differentiation at the germinal center B cell positive selection stage. *J. Exp. Med.* **217,** 943 (2020).
179. Bannard, O. *et al.* Germinal center centroblasts transition to a centrocyte phenotype according to a timed program and depend on the dark zone for effective selection. *Immunity* **39,** 912–924 (2013).
180. Ligorio, M. *et al.* Stromal Microenvironment Shapes the Intratumoral Architecture of Pancreatic Cancer. *Cell* **178,** 160–175.e27 (2019).
181. Rieckmann, J. C. *et al.* Social network architecture of human immune cells unveiled by quantitative proteomics. *Nat. Immunol.* **18,** 583–593 (2017).
182. Hipp, N. *et al.* IL-2 imprints human naive B cell fate towards plasma cell through ERK/ELK1-mediated BACH2 repression. *Nat Commun* **8,** 1443 (2017).
183. Straight, A. F. *et al.* Dissecting temporal and spatial control of cytokinesis with a myosin II Inhibitor. *Science* **299,** 1743–1747 (2003).
184. Tan, F. *et al.* Role of TXNDC5 in tumorigenesis of colorectal cancer cells: In vivo and in vitro evidence. *Int J Mol Med* **42,** 935–945 (2018).
185. Wu, X. & Levine, A. J. p53 and E2F-1 cooperate to mediate apoptosis. *Proc Natl Acad Sci USA* **91,** 3602–3606 (1994).
186. Farmer, J. R. *et al.* Induction of metabolic quiescence defines the transitional to follicular B cell switch. *Sci Signal* **12,** (2019).
187. Zhang, Y. *et al.* Histone Loaders CAF1 and HIRA Restrict Epstein-Barr Virus B-Cell Lytic Reactivation. *MBio* **11,** (2020).
188. Suzuki, K. *et al.* Semaphorin 7A initiates T-cell-mediated inflammatory responses through alpha1beta1 integrin. *Nature* **446,** 680–684 (2007).
189. Scott, G. A., McClelland, L. A. & Fricke, A. F. Semaphorin 7a promotes spreading and dendricity in human melanocytes through beta1-integrins. *J Invest Dermatol* **128,** 151–161 (2008).
190. Pasterkamp, R. J., Peschon, J. J., Spriggs, M. K. & Kolodkin, A. L. Semaphorin 7A promotes axon outgrowth through integrins and MAPKs. *Nature* **424,** 398–405 (2003).
191. Richter, K. *et al.* Speckled-like pattern in the germinal center (SLIP-GC), a nuclear GTPase expressed in activation-induced deaminase-expressing lymphomas and germinal center B cells. *J. Biol. Chem.* **284,** 30652–30661 (2009).
192. Shankar, J. *et al.* Pseudopodial actin dynamics control epithelial-mesenchymal transition in metastatic cancer cells. *Cancer Res.* **70,** 3780–3790 (2010).
193. Bertocci, B. *et al.* Klhl6 Deficiency Impairs Transitional B Cell Survival and Differentiation. *J. Immunol.* **199,** 2408–2420 (2017).

194. Gupta-Rossi, N. *et al.* Specific over-expression of deltex and a new Kelch-like protein in human germinal center B cells. *Mol. Immunol.* **39,** 791–799 (2003).
195. Majima, S., Kajino, K., Fukuda, T., Otsuka, F. & Hino, O. A novel gene 'Niban' upregulated in renal carcinogenesis: cloning by the cDNA-amplified fragment length polymorphism approach. *Jpn J Cancer Res* **91,** 869–874 (2000).
196. Matsumoto, F. *et al.* A novel tumor marker, Niban, is expressed in subsets of thyroid tumors and Hashimoto's thyroiditis. *Hum Pathol* **37,** 1592–1600 (2006).
197. Tang, S. *et al.* Niban protein regulates apoptosis in HK-2 cells via caspase-dependent pathway. *Ren Fail* **41,** 455–466 (2019).
198. Edwards, A. & Haas, W. Multiplexed Quantitative Proteomics for High-Throughput Comprehensive Proteome Comparisons of Human Cell Lines. *Methods Mol. Biol.* **1394,** 1–13 (2016).
199. Erickson, B. K. *et al.* Evaluating multiplexed quantitative phosphopeptide analysis on a hybrid quadrupole mass filter/linear ion trap/orbitrap mass spectrometer. *Anal Chem* **87,** 1241–1249 (2015).
200. McAlister, G. C. *et al.* MultiNotch MS3 enables accurate, sensitive, and multiplexed detection of differential expression across cancer cell line proteomes. *Anal Chem* **86,** 7150–7158 (2014).
201. Ting, L., Rad, R., Gygi, S. P. & Haas, W. MS3 eliminates ratio distortion in isobaric multiplexed quantitative proteomics. *Nat. Methods* **8,** 937–940 (2011).
202. Eng, J. K., McCormack, A. L. & Yates, J. R. An approach to correlate tandem mass spectral data of peptides with amino acid sequences in a protein database. *J Am Soc Mass Spectrom* **5,** 976–989 (1994).
203. Huttlin, E. L. *et al.* A tissue-specific atlas of mouse protein phosphorylation and expression. *Cell* **143,** 1174–1189 (2010).
204. Elias, J. E. & Gygi, S. P. Target-decoy search strategy for increased confidence in large-scale protein identifications by mass spectrometry. *Nat. Methods* **4,** 207–214 (2007).
205. Ritchie, M. E. *et al.* limma powers differential expression analyses for RNA-sequencing and microarray studies. *Nucl. Acids Res.* **43,** e47 (2015).
206. Subramanian, A. *et al.* Gene set enrichment analysis: a knowledge-based approach for interpreting genome-wide expression profiles. *Proc Natl Acad Sci USA* **102,** 15545–15550 (2005).
207. Liberzon, A. *et al.* Molecular signatures database (MSigDB) 3.0. *Bioinformatics* **27,** 1739–1740 (2011).
208. Love, M. I., Huber, W. & Anders, S. Moderated estimation of fold change and dispersion for RNA-seq data with DESeq2. *Genome Biol.* **15,** 550 (2014).
209. Merico, D., Isserlin, R., Stueker, O., Emili, A. & Bader, G. D. Enrichment map: a network-based method for gene-set enrichment visualization and interpretation. *PLoS ONE* **5,** e13984 (2010).
210. Shannon, P. *et al.* Cytoscape: a software environment for integrated models of biomolecular interaction networks. *Genome Res.* **13,** 2498–2504 (2003).
211. Reed, J. H., Jackson, J., Christ, D. & Goodnow, C. C. Clonal redemption of autoantibodies by somatic hypermutation away from self-reactivity during human immunization. *J. Exp. Med.* **213,** 1255–1265 (2016).

212. Yau, I. W. *et al.* Censoring of self-reactive B cells by follicular dendritic cell-displayed self-antigen. *J. Immunol.* **191,** 1082–1090 (2013).
213. Gitlin, A. D. *et al.* Independent Roles of Switching and Hypermutation in the Development and Persistence of B Lymphocyte Memory. *Immunity* **44,** 769–781 (2016).
214. Degn, S. E. *et al.* Clonal Evolution of Autoreactive Germinal Centers. *Cell* **170,** 913–926.e19 (2017).
215. Freitas, E. C., de Oliveira, M. S. & Monticielo, O. A. Pristane-induced lupus: considerations on this experimental model. *Clin Rheumatol* **36,** 2403–2414 (2017).
216. Mitchell, T. C. & Casella, C. R. No pain no gain? Adjuvant effects of alum and monophosphoryl lipid A in pertussis and HPV vaccines. *Curr. Opin. Immunol.* **47,** 17–25 (2017).
217. Di Pasquale, A., Preiss, S., Tavares Da Silva, F. & Garçon, N. Vaccine Adjuvants: from 1920 to 2015 and Beyond. *Vaccines (Basel)* **3,** 320–343 (2015).
218. Ismaili, J. *et al.* Monophosphoryl lipid A activates both human dendritic cells and T cells. *The Journal of Immunology* **168,** 926–932 (2002).
219. Del Cornò, M. *et al.* HIV-1 gp120 signaling through TLR4 modulates innate immune activation in human macrophages and the biology of hepatic stellate cells. *J. Leukoc. Biol.* **100,** 599–606 (2016).
220. Ishikawa, E. *et al.* Direct recognition of the mycobacterial glycolipid, trehalose dimycolate, by C-type lectin Mincle. *J. Exp. Med.* **206,** 2879–2888 (2009).
221. Schoenen, H. *et al.* Cutting edge: Mincle is essential for recognition and adjuvanticity of the mycobacterial cord factor and its synthetic analog trehalose-dibehenate. *J. Immunol.* **184,** 2756–2760 (2010).
222. Miyake, Y. *et al.* C-type lectin MCL is an FcRγ-coupled receptor that mediates the adjuvanticity of mycobacterial cord factor. *Immunity* **38,** 1050–1062 (2013).
223. Verkoczy, L. *et al.* Autoreactivity in an HIV-1 broadly reactive neutralizing antibody variable region heavy chain induces immunologic tolerance. *Proc. Natl. Acad. Sci. U.S.A.* **107,** 181–186 (2010).
224. Zhang, R. *et al.* Initiation of immune tolerance-controlled HIV gp41 neutralizing B cell lineages. *Sci Transl Med* **8,** 336ra62–336ra62 (2016).
225. Verkoczy, L. *et al.* Induction of HIV-1 broad neutralizing antibodies in 2F5 knock-in mice: selection against membrane proximal external region-associated autoreactivity limits T-dependent responses. *J. Immunol.* **191,** 2538–2550 (2013).
226. McGuire, A. T. *et al.* Specifically modified Env immunogens activate B-cell precursors of broadly neutralizing HIV-1 antibodies in transgenic mice. *Nat Commun* **7,** 10618 (2016).
227. Doyle-Cooper, C. *et al.* Immune tolerance negatively regulates B cells in knock-in mice expressing broadly neutralizing HIV antibody 4E10. *J. Immunol.* **191,** 3186–3191 (2013).
228. Alam, S. M. *et al.* Differential reactivity of germ line allelic variants of a broadly neutralizing HIV-1 antibody to a gp41 fusion intermediate conformation. *J. Virol.* **85,** 11725–11731 (2011).

229. Malbec, M. *et al.* Broadly neutralizing antibodies that inhibit HIV-1 cell to cell transmission. *J. Exp. Med.* **210,** 2813–2821 (2013).